Chapter 3

From 1879 to 2018: Indophenine to Indophenine Polymers

Table of Contents

Introduction

High performing small molecules and polymers have gained considerable interest of researchers, in the field of organic electronics for potential applications such as polymer solar cells (PSCs), organic light emitting diodes (OLEDs), organic field effect transistors (OFETs) and organic thin film transistors (OTFTs).[1,2] Conjugated small molecules and polymers exhibit solution processability and compatibility with flexible substrates, which enable them to be fabricated conveniently in large areas at much lower temperature, lower cost and at high throughput compared to the conventional devices using inorganic semiconductors such as silicon.[3–6] These tempting features, offered by organic small molecules and polymers have unveiled the opportunities for the development of the next generation electronic products. The higher charge carrier mobility of the organic semiconducting materials (small molecules and polymers) is the most importantly required characteristic to realize many of the target applications.[7–11] The charge carrier mobility of the organic material is greatly influenced by the molecular conformation and the thin film morphology.[3] The efficient charge transport can be achieved by understanding and controlling the molecular features that impart a favourable backbone orientation and facilitate close intermolecular interactions, which are required for optimisation of morphology and long range order. Compared to the inorganic semiconductors, where ions and/or atoms are connected by the much stronger and shorter primary bonds such as ionic and covalent bonds, organic semiconductors are better at charge transport because of the nature of the weak secondary bonds (eg. the van der Waals force). Moreover, the proper alignment of the frontier energy levels with the Fermi energy (E_F) of the electrode is also important in order to minimize the charge injection barrier.[4–6,12–14]

Over the past decades and specially within the last few years, the development of the new materials, improved materials processing and device optimisation studies have led to the remarkable enhancement in the charge carrier mobilities of the organic semiconductors.[6,14–17] Single crystals[18,19] and aligned small molecules[20] based OFETs have achieved high mobilities of up to ~40 $cm^2V^{-1}s^{-1}$, while the well aligned polymers[21] based OFETs have demonstrated high mobilities of up to ~50 $cm^2V^{-1}s^{-1}$. The solution processible polymeric semiconductors' hole mobilities have exceeded 10 $cm^2V^{-1}s^{-1}$, which are far better than that of amorphous silicon (0.1−1 $cm^2V^{-1}s^{-1}$).[22–25]

In the past few years, several molecules have been reported, which can induce dipole-dipole interactions that facilitates close intermolecular packing and shorten π-π distances. A few of such examples are rylene diimide-based small molecules and polymers, *N*-heteroacenes, azulene derivatives, diketopyrrolopyrrole (DPP)-based polymers, isoindigo (IIG) and its derivatives-based small molecules and polymers, indigo-based polymers, phenyl-flanked and thiophene-flanked benzodipyrrolidone (BDPDP and BDPDT)-based polymers, etc. Researchers have explored naphthalene diimide-based small molecules[26–29] and polymers[30–33] as well as perylene diimide-based small molecules[34] and polymers[35,36] for its n-type semiconducting properties, due to their extended π-face and strong dipole-dipole interactions. *N*-heteroacenes[37–39] and azulene derivatives[40–42] have also been studied as semiconducting materials owing to its close intermolecular packing and shorter π-π interaction distances.

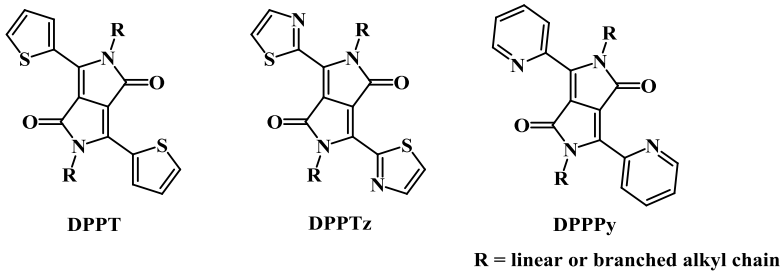

Figure 3.1 Structures of different DPP-based scaffolds

Another strong electron acceptor building block, which can induce dipole-dipole interactions, is diketopyrrolopyrrole (DPP) and some DPP-based polymers have exhibited the best polymeric semiconductor performance[19,23] owing to the presence of two polar lactam rings in DPP scaffold. Thiophene is the most widely used as flanking unit to DPP (**DPPT**), owing to its small steric effect which facilitates DPP to hold coplanar structure, a desirable feature for achieving high carrier mobility. Besides thiophene, thiazole[43] and pyridine[44] flanking units have also been reported to the **DPP**, **DPPTz** and **DPPPy** (Figure 3.1). A wide variety of DPP-based conjugated polymers with different donor and acceptor units, like thiophene,[45] dithiophene,[44] 2,1,3-benzothiadiazole,[46] azine (−C=N−N=C−),[47] dithiazole,[43] etc. have been extensively studied for its semiconductor characteristics with moderate to good electron and/or hole mobilities. Apart from DPP, the electron deficient isoindigo (IIG) and its derivatives based building blocks have recently been explored extensively for high charge carrier mobility materials. Isoindigo and its π-extended derivatives based small molecules like

terminal benzothiophene and benzofuran fused isoindigo (**BTIIG** and **BFIIG**; Figure 3.2),[48] central benzodifurandione fused isoindigo and its peripheral hexafluoro-substituted derivative (**BDOPV** and **F_6-BDOPV**; Figure 3.2)[49] have exhibited low lying LUMO energy levels and have been studied broadly for their semiconducting characteristics.

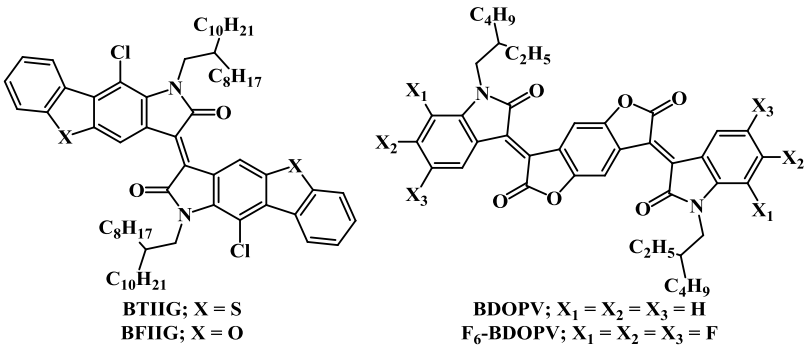

Figure 3.2 IIG-based conjugated molecules

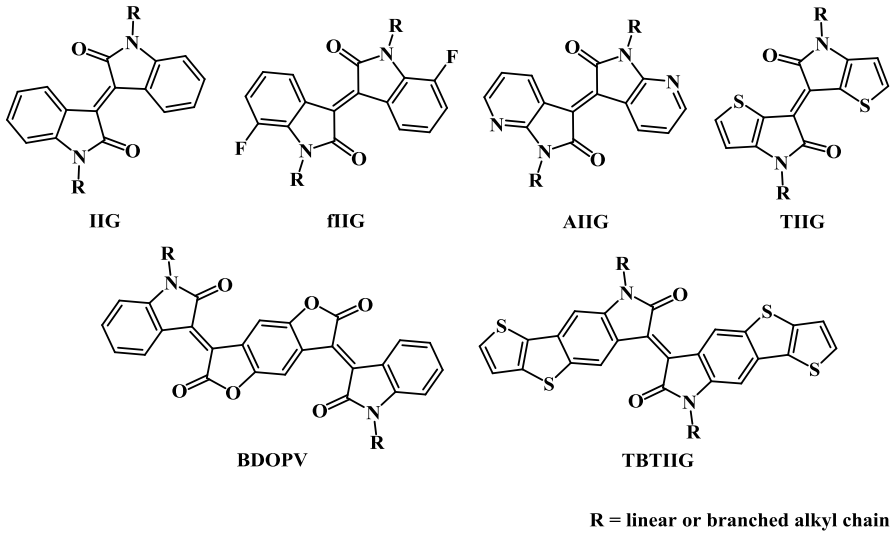

Figure 3.3 Structures of various IIG-based scaffolds

The electron-accepting building block, isoindigo (**IIG**) and its derivatives like 7,7-difluoroisoindigo (**fIIG**),[50] 7,7-diazaisoindigo (**AIIG**),[51] central benzodifurandione fused isoindigo (**BDOPV**),[25,52] thienoisoindigo (**TIIG**),[24,53,54] π-extended terminal thieno[3,2-*b*]thiophene fused isoindigo (**TBTIIG**),[55] etc. (Figure 3.3) have also been explored to develop various IIG-based D-A polymers with varied donor or acceptor building blocks like thiophene,[55–57] dithiophene,[25,50,51,56] selenophene,[58] thieno[3,2-*b*]thiophene,[52] naphthalene,[24] 2,1,3-benzothiadiazole,[52,58] bisthiophenylbenzodithiophene,[53] etc. and these IIG-based polymers have showed high charge carrier mobilities.

As one of the much valued and oldest of the vegetable dyes, indigo, a structural isomer of isoindigo, has a long recorded history, going back to the 7th century BC.[59] The indigo is an intensely blue coloured dye and the non substituted indigo can form intramolecular hydrogen bonding between the oxygen and the hydrogen atoms of the two 1*H*-indol-3-one units, which results in a highly coplanar geometry.[60–63] Recently, indigo and its derivative, tyrian purple (6,6′-dibromoindigo) were reported to exhibit ambipolar semiconductor properties with hole mobilities of up to 0.40 $cm^2V^{-1}s^{-1}$.[64–67] Li *et al*. reported indigo-based polymers for the first time, with dithiophene (2T) unit. The synthesized D-A polymer **PID-2T** (Figure 3.4) showed HOMO and LUMO energy levels of −5.78 eV and −4.02 eV, respectively and unipolar n-channel charge transport behaviour with electron mobility of up to 0.0011 $cm^2V^{-1}s^{-1}$. The lower electron mobility of the polymer **PID-2T** was attributed to the twisting of the polymer backbone, caused by the solubilising *N*-acyl side chains that induced a large dihedral angle between the two lactam rings.[68]

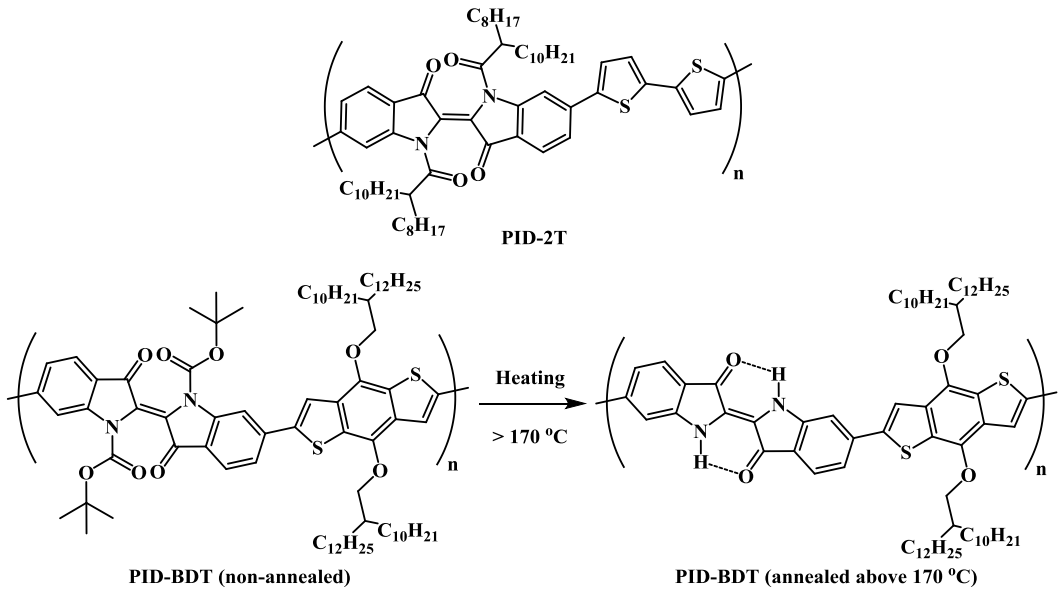

Figure 3.4 Indigo-based conjugated polymers

Later on, Li *et al*. reported another indigo-based polymer **PID-BDT** (Figure 3.4), with benzo[1,2-*b*:4,5-*b*′]dithiophene (BDT) unit. This polymer had thermo-cleavable *t*-Boc side chains, which could be easily removed by annealing the polymer films at 200 °C, thereby rendering the indigo units high planarity. The non annealed **PID-BDT** showed the HOMO and LUMO energies of −5.60 eV and −3.90 eV, respectively. However, **PID-BDT** films annealed at 200 °C for 1 h exhibited lowered HOMO and LUMO levels of −5.80 eV and −4.20 eV, respectively. After removal of *t*-

Boc groups, resultant polymer showed unipolar n-channel charge transport behaviour with electron mobility of up to 0.0057 $cm^2V^{-1}s^{-1}$.[69]

Benzodipyrrolidone, a molecule originally reported as a colourant[70], is a nitrogen analogue of the benzodifurandione, which can also be envisioned as a 'stretched' DPP. Compared to the DPP, benzodipyrrolidone exhibit extended π-conjugation and enhanced π-π stacking. Wudl *et al*. reported two benzodipyrrolidone (BDPD)-based polymers, having phenyl-flanked benzodipyrrolidone (**BDPDP**) units copolymerized with benzene (B) and thiophene (T) units (Figure 3.5). The polymer **PBDPDP-B** showed HOMO and LUMO energies of −5.39 eV and −3.35 eV, respectively and exhibited unipolar charge transport properties with electron mobility of up to 0.0024 $cm^2V^{-1}s^{-1}$. However, the polymer **PBDPDP-T** showed lower LUMO energy of −3.50 eV and slightly elevated HOMO energy of −5.25 eV, probably due to the presence of electron donating thiophene (T) unit. **PBDPDP-T** exhibited n-channel dominant ambipolar behaviour with electron mobility of up to 0.0064 $cm^2V^{-1}s^{-1}$ and hole mobility of up to 0.0035 $cm^2V^{-1}s^{-1}$.[71]

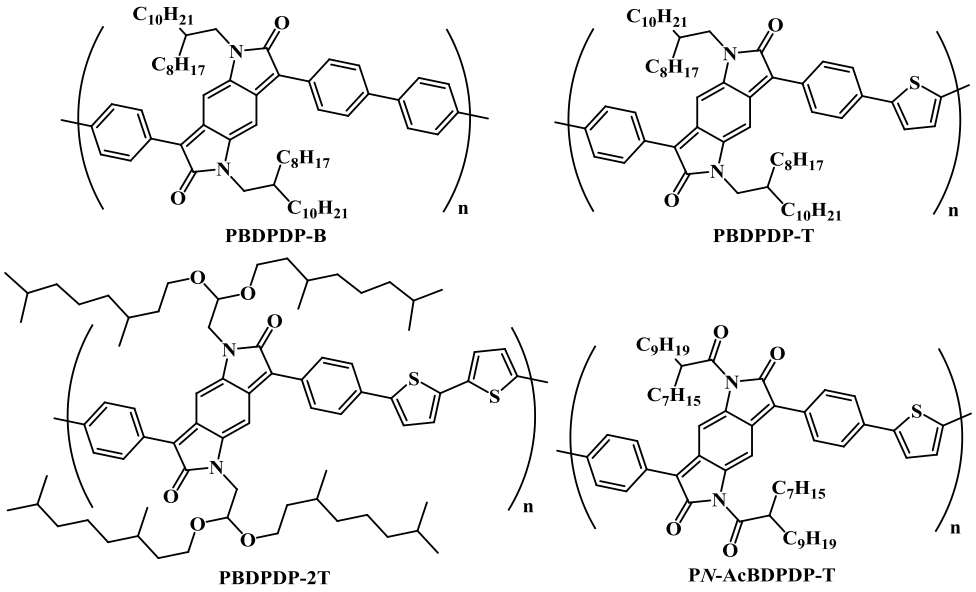

Figure 3.5 Phenyl-flanked benzodipyrrolidone (BDPDP)-based conjugated polymers

Facchetti *et al*. reported phenyl-flanked benzodipyrrolidone (BDPDP)-based polymer **PBDPDP-2T** (Figure 3.5), with dithiophene (2T) unit. The polymer **PBDPDP-2T** showed HOMO and LUMO energies of −5.62 eV and −4.03 eV, respectively and exhibited unipolar p-channel charge transport behaviour with an average hole mobility of 0.026 $cm^2V^{-1}s^{-1}$.[72] Zhang *et al*. reported phenyl-flanked

BDPD derivative, having *N*-acyl side chains, which lowered the LUMO energy of BDPDP-core. The *N*-acyl BDPDP-based polymer **P*N*-AcBDPDP-T** (Figure 3.5), with thiophene (T) unit, exhibited the HOMO and LUMO energies of −5.62 eV and −3.90 eV, respectively. The polymer showed n-channel semiconductor performance with the electron mobility of up to 0.012 $cm^2V^{-1}s^{-1}$.[73]

McCulloch *et al.* reported for the first time, thiophene-flanked benzodipyrrolidone (BDPDT), using a different synthetic methodology, involving a two-directional Pummerer-type cyclization[74,75] and a ceric ammonium nitrate (CAN) mediated oxidation to yield phenyl bisisatin, which was subjected to the two directional Grignard reaction, immediately followed by reduction using NaH_2PO_2/NaI/AcOH and selective oxidation with DDQ.

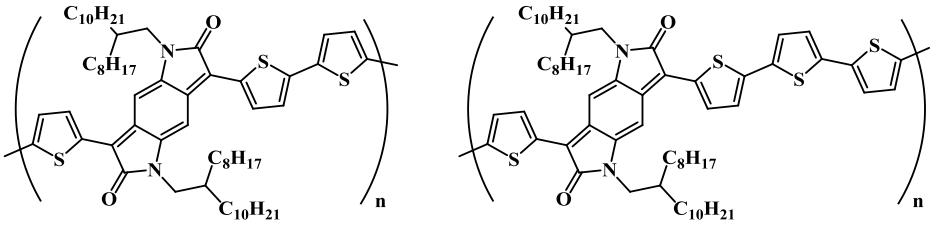

Figure 3.6 Thiophene-flanked benzodipyrrolidone (BDPDT)-based conjugated polymers

The BDPDT-based polymers **PBDPDT-T** and **PBDPDT-2T** (Figure 3.6) were obtained by copolymerizing BDPDT unit with thiophene (T) and dithiophene (2T) units. The polymers **PBDPDT-T** and **PBDPDT-2T** exhibited HOMO/LUMO energies of −5.27 eV/−4.24 eV and −5.33 eV/−4.16 eV, respectively. **PBDPDT-T** showed ambipolar semiconductor characteristics with balanced electron and hole mobilities of 0.1 $cm^2V^{-1}s^{-1}$ and 0.2 $cm^2V^{-1}s^{-1}$, while **PBDPDT-2T** showed p-channel dominant ambipolar charge transport behaviour with hole mobility of 0.08 $cm^2V^{-1}s^{-1}$ and electron mobility of 0.01 $cm^2V^{-1}s^{-1}$.[76]

Wudl *et al*. reported a series of thiophene-flanked BDPD-based polymers, with different donor units of different donating capabilities like fluorene (F), difluorene (DF), dithienosilole (DTSi) and dithienopyrrole (DTPy). The synthesized BDPDT-based D-A polymers , **PBDPDT-F**, **PBDPDT-DF**, **PBDPDT-DTSi** and **PBDPDT-DTPy** exhibited low to very low optical bandgaps (Figure 3.7).[77]

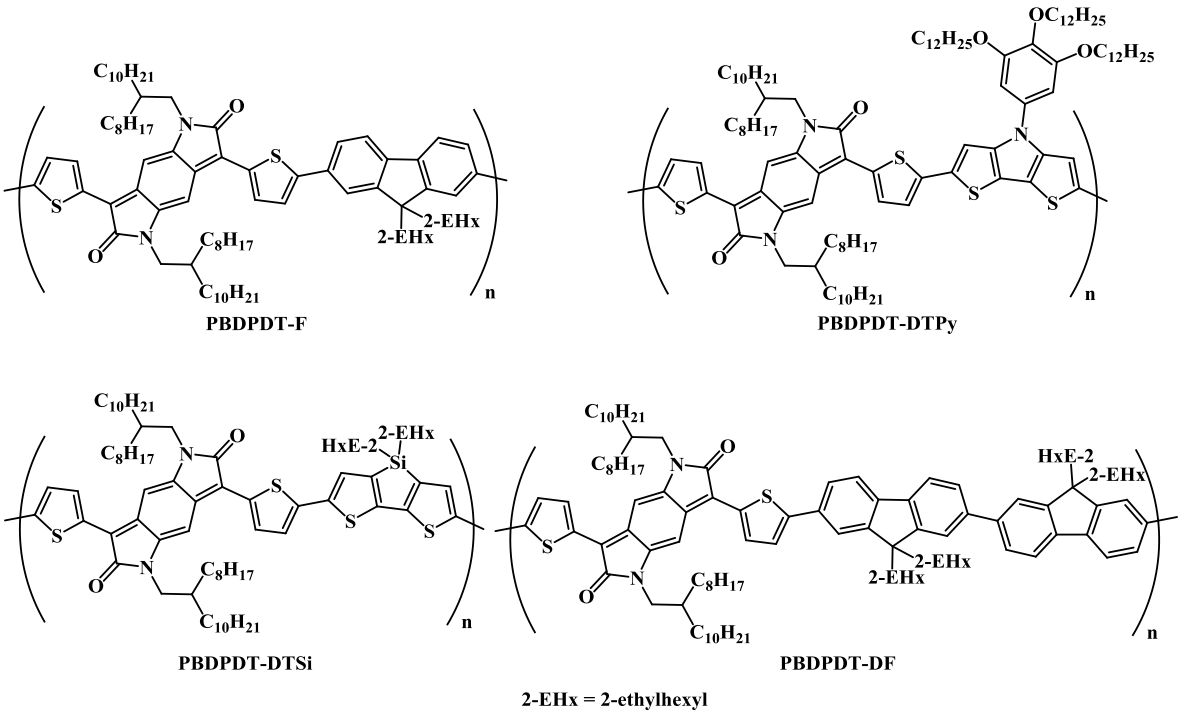

Figure 3.7 Thiophene-flanked benzodipyrrolidone (BDPDT)-based conjugated polymers

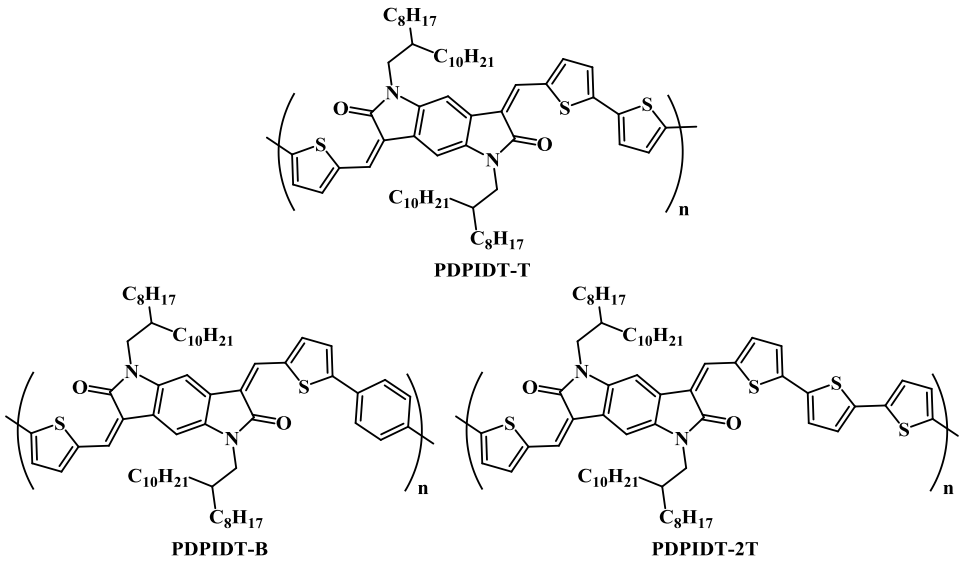

Figure 3.8 Dihydropyrroloindoledione (DPID)-based conjugated polymers

In 2013, McCulloch *et al.* reported a novel acceptor core, dihydropyrroloindoledione (DPID), which is structurally related to the DPP and BDPD, having the bislactam ring structure. To the DPID core, two electron rich thiophene (T) units were inserted *via* vinyl linkages which are directly flanking the DPID core, yielding the thiophene-flanked dihydropyrroloindoledione (DPIDT). This modified DPID core was copolymerized with thiophene (T) unit to form a D-A copolymer

PDPIDT-T (Figure 3.8), which showed HOMO and LUMO energies of −5.62 eV and −3.90 eV, respectively and a lower optical bandgap of 1.57 eV.[78] This polymer exhibited ambipolar charge transport behaviour with balanced electron and hole mobilities of 0.04 $cm^2V^{-1}s^{-1}$ and 0.05 $cm^2V^{-1}s^{-1}$, respectively.[79] Later on, McCulloch et al reported two more DPIDT-based copolymers, **PDPIDT-B** and **PDPIDT-2T** (Figure 3.8), with benzene (B) and dithiophene (2T) units. Both the polymers **PDPIDT-B** and **PDPIDT-2T** showed HOMO/LUMO energies of −5.20 eV/−3.50 eV and −5.30 eV/−3.70 eV, respectively. The polymer **PDPIDT-B** exhibited unipolar p-channel semiconductor properties with hole mobility of up to 0.08 $cm^2V^{-1}s^{-1}$, while **PDPIDT-2T** showed ambipolar charge transport behaviour with electron and hole mobilities of up to 0.04 $cm^2V^{-1}s^{-1}$ and 0.09 $cm^2V^{-1}s^{-1}$, respectively.[79]

Compared to the various conjugated molecular building blocks, quinoidal molecular building blocks offer several advantages like highly planar structure, favourable π-π staking which in turn leads to the efficient charge transport in the solid state, efficient delocalization of π-electrons resulting into the reduced band-gaps and amphoteric redox behaviour which makes them good candidates as both n-type and p-type semiconductors when properly polarized.[80–85] Till now, the most efficient strategy to obtain quinoidal molecules has been the incorporation of dicyanomethylene (DCM) groups at both termini. Quinoidal oligothiophenes (QOTs), obtained by incorporating the DCM groups at the terminals, are a class of well explored n-channel semiconductors.[86–88] However, QOTs exhibit much lower electron mobilities than 1 $cm^2V^{-1}s^{-1}$, which can be attributed to the much smaller π-face of QOTs, that negatively affects the magnitude of the transfer integral and the charge transport in organic semiconductors.[89] Moreover, DCM substituted QOTs show poor solubility in common organic solvents due to the absence of solubilising side chain groups.

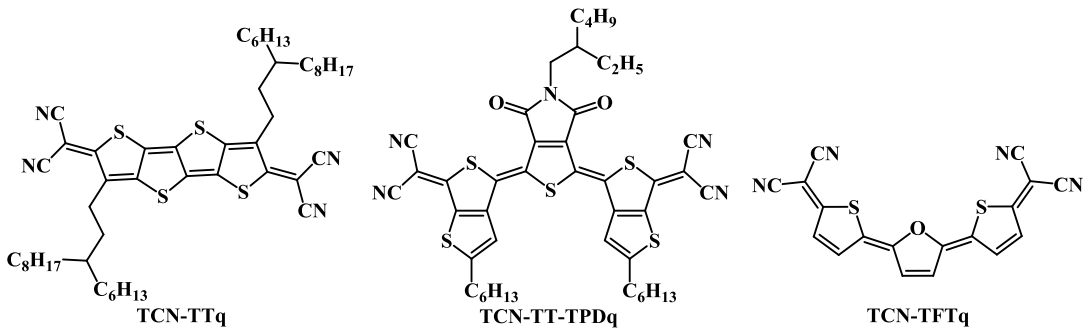

Figure 3.9 Quinoidal oligothiophenes (QOTs) having terminal dicyanomethylene (DCM) group

Zhu *et al*. reported dicyanomethylene-substituted tetrathienoquinoid (**TCN-TTq**; Figure 3.9), having four fused thiophene units and two terminal 3-hexylundecyl side chains, which enhanced intermolecular interactions owing to the wide π-face overlap. **TCN-TTq** exhibited LUMO energy of −4.30 eV and unipolar n-channel semiconducting behaviour with electron mobility of 0.9 $cm^2V^{-1}s^{-1}$ with an I_{on}/I_{off} ratio of 10^5 under ambient conditions.[90] Zhang et al reported QOT using 2-hexylthieno[3,4-*b*]thiophene and 5-(2-ethylhexyl)-4*H*-thieno[3,4-*c*]pyrrole-4,6(5*H*)-dione, having DCM groups at both terminals (Figure 3.9). The synthesized **TCN-TT-TPDq** exhibited expanded π-surface and a small optical bandgap of 1.11 eV. Moreover, **TCN-TT-TPDq** showed formation of J-type aggregates in the solid state, which favours the electron transport. It exhibited unipolar n-channel semiconducting behaviour with high electron mobility of 3.0 $cm^2V^{-1}s^{-1}$ and a high I_{on}/I_{off} ratio of 10^6.[89] Li *et al*. reported another furan and thiophene-based quinoidal molecule **TCN-TFTq** (Figure 3.9), with DCM terminal groups. The synthesized quinoidal molecule showed LUMO and HOMO energies of −4.15 eV and −5.72 eV, respectively and the unipolar n-type semiconducting properties with electron mobility of 1.1 $cm^2V^{-1}s^{-1}$.[91]

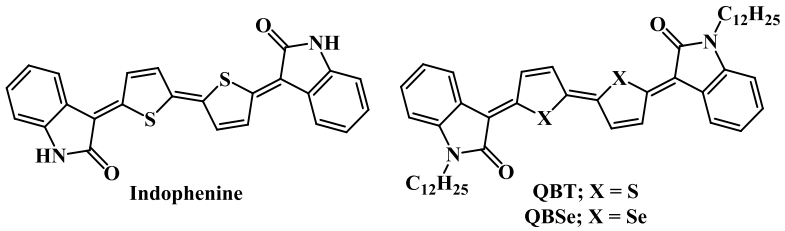

Figure 3.10 Indophenine (blue dye) and indophenine-based quinoidal molecules, QBT and QBSe

Apart from DCM-substituted quinoidal molecules, **Indophenine** (Figure 3.10), a well known blue dyestuff[92], which was first prepared by Baeyer in 1879[93], consists of quinoidal bithiophene unit. In 2015, Hwang *et al*. reported soluble *N*-dodecyl substituted indophenine (quinoidal bithiophene, **QBT**) and its biselenophene analogue (quinoidal biselenophene, **QBSe**) (Figure 3.10). Both **QBT** and **QBSe** exhibited low optical bandgaps of 1.49 eV and 1.60 eV, respectively and HOMO/LUMO energies of −5.25 eV/−3.76 eV and −5.33 eV/−3.73 eV, respectively. **QBT** showed p-channel dominant ambipolar charge transport behaviour with an average electron and hole mobilities of 0.0046 $cm^2V^{-1}s^{-1}$ and 0.029 $cm^2V^{-1}s^{-1}$, respectively, while **QBSe** showed

enhanced and balanced ambipolar semiconducting characteristics with an average electron and hole mobilities of 0.018 $cm^2V^{-1}s^{-1}$ and 0.052 $cm^2V^{-1}s^{-1}$, respectively.[94]

In 2013, McCulloch *et al.* reported for the first time, synthesis of linear **phenyl bis-isatin**, using a two-directional Pummerer-type cyclization[74,75] of *N*,*N*′-(1,4-phenylene)bis(2-hydroxy-*N*-(2-octyldodecyl)acetamide), compound **3** and a ceric ammonium nitrate (CAN) mediated oxidation of subsequently obtained 1,5-bis(2-octyldodecyl)-3,7-bis(phenylsulfanyl)-5,7-dihydropyrrolo[2,3-*f*]indole-2,6-dione, compound **4** to yield **phenyl bis-isatin** (Scheme 3.1).[76] In 2016, Kelly *et al*. reported improved synthesis of **naphthalene bis-isatin**, following the Martinet isatin synthesis reaction conditions (Scheme 3.2),[95] compared to the previously reported synthetic procedure based on the Sandmeyer isatin syntheis, by Kossmehl *et al*. in 1975.[96]

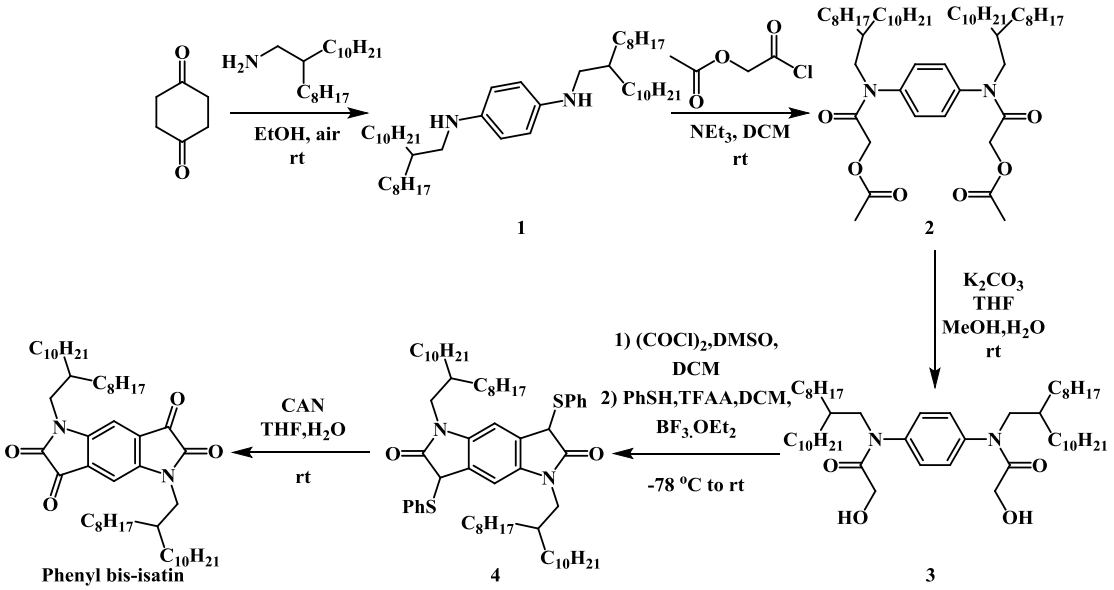

Scheme 3.1 Synthesis of linear **phenyl bis-isatin**, *via* synthetic route reported by McCulloch *et al*.[76]

1,5-diaminonaphthalene was reacted with diethylketomalonate in presence of glacial acetic acid to yield intermediate diethyl 1,6-dihydroxy-2,7-dioxo-1,2,3,6,7,8-hexahydroindolo[7,6-*g*]indole-1,6-dicarboxylate (compound **5**). The subsequent hydrolysis and de-carboxylation using aqueous NaOH under refluxing conditions, followed by the aerial oxidation yielded **naphthalene bis-isatin**.

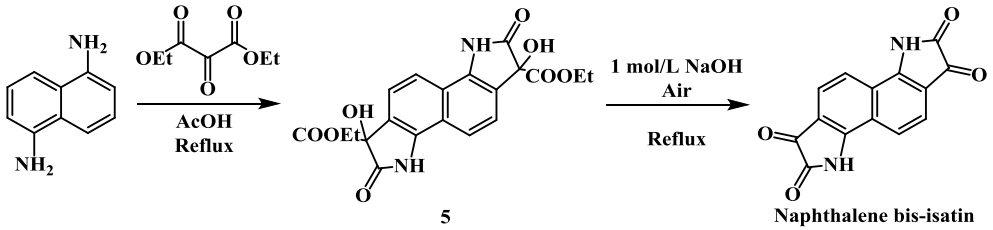

Scheme 3.2 Synthesis of **naphthalene bis-isatin**, *via* Martinet isatin synthesis reported by Kelly *et al*.[95]

In 2018, McCulloch *et al*. reported **thieno[3,2-*b*]thiophene bis-isatin** for the first time[97], by two-directional condensation-cyclisation reaction of N_3,N_6-bis(2-octyldodecyl)thieno[3,2-*b*]thiophene-3,6-diamine, compound **11**, using oxalyl chloride in anhydrous diethylether in very low yield. The synthesis of **thieno[3,2-*b*]thiophene bis-isatin** is outlined below in scheme 3.3.

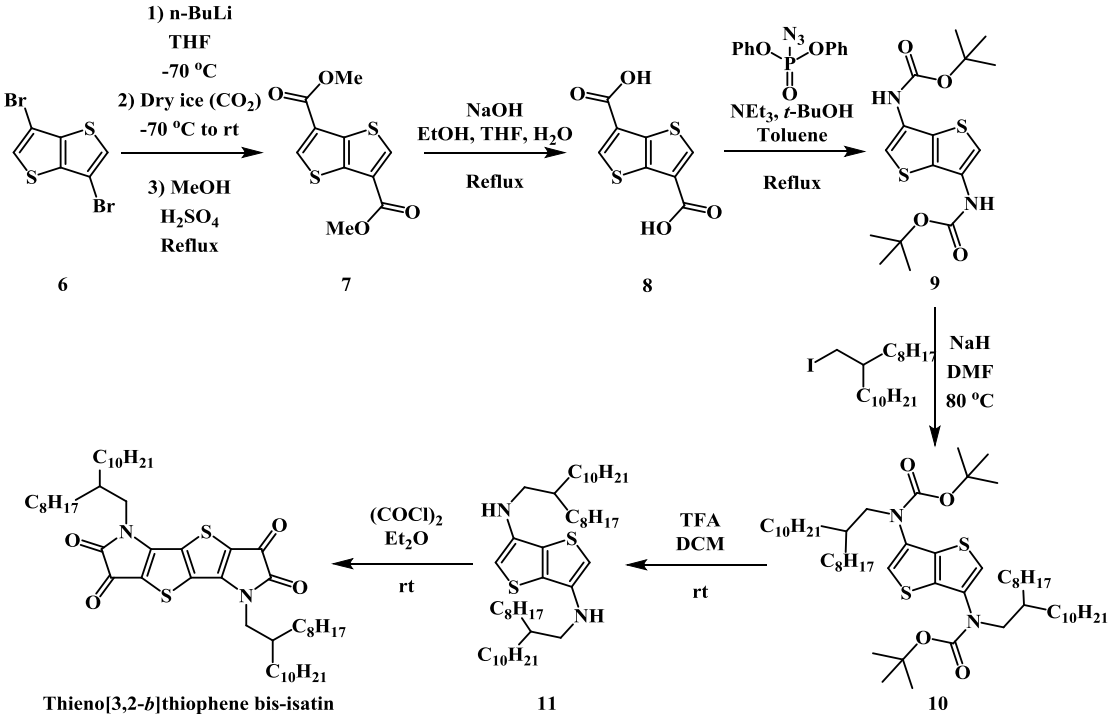

Scheme 3.3 Synthesis of **thieno[3,2-*b*]thiophene bis-isatin**, *via* synthetic route reported by McCulloch *et al*.[97]

Very recently, in 2018, McCulloch *et al*. reported a series of novel fully ladder-type conjugated polymers, utilizing the simple aldol condensation reaction of various synthesized bis-isatins like **phenyl bis-isatin**, **naphthalene bis-isatin** and **thieno[3,2-*b*]thiophene bis-isatin**, with the phenyl bis-oxindole[77,78,97] and naphthalene bis-oxindole[97,98] in presence of *p*-toluene sulphonic acid monohydrate.[97] The synthesized fully ladder-type conjugated polymers **PPBIs-PBIn-L**, **PPBIs-PBIn-B**, **PNBIs-NBIn-**

B, **PNBIs-NBIn-LB** and **PNBIn-TTBIs-LB** (Figure 3.11), required neither organometallic monomers nor transition-metal catalysts, thereby providing a more cheaper and eco-friendly synthetic route to the ladder-type semiconducting polymers. Moreover, these polymers exhibited extended NIR absorption with much lowered optical bandgaps of −1.01 eV, −1.10 eV, −1.07 eV, −1.01 eV and −0.84 eV, respectively with lower electron affinities (EA) of −4.40 eV, −4.50 eV, −4.20 eV, −4.20 eV and −4.20 eV, respectively. The lower LUMO energy levels afforded stable electron transport in air with electron mobilities as high as of 0.03 $cm^2V^{-1}s^{-1}$ for polymer **PNBIs-NBIn-LB**.

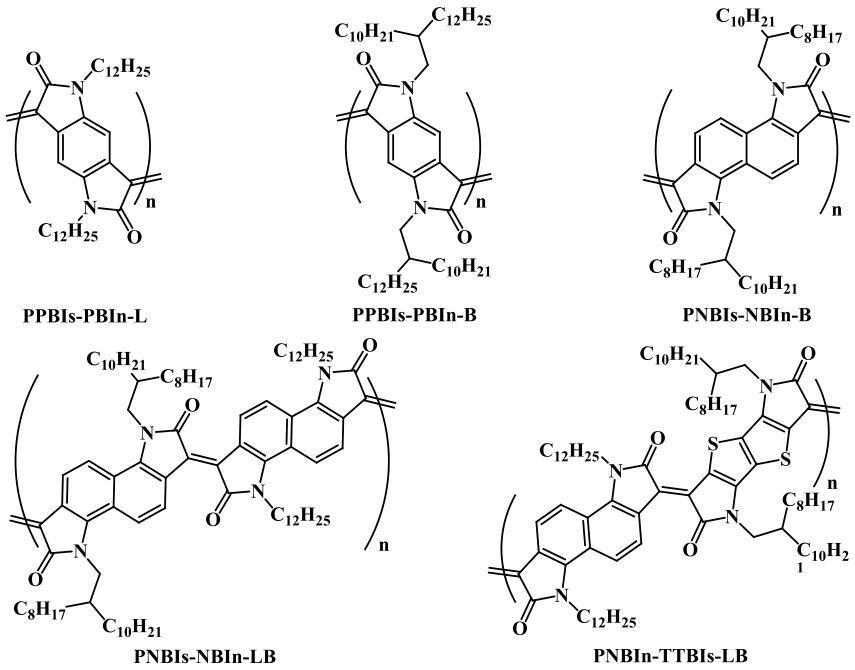

Figure 3.11 Bis-isatin-based ladder-type conjugated polymers reported by McCulloch et al.[97]

Thus, focusing the advantages of the quinoidal systems, like highly coplanar structure, favourable π-π stacking and efficient charge transport in solid state, lowered bandgaps owing to the efficient delocalization of π electrons and an amphoteric redox behaviour, we became interested in developing indophenine-based polymers, which will have highly planar and rigid quinoidal backbone, having quinoidal bithiophene units. Tormos *et al*. have reported the synthesis of soluble *N*-heptyl substituted indophenine, by reacting *N*-heptylisatin with thiophene in benzene, using concentrated sulphuric acid.[99] To synthesize indophenine polymers, we developed novel fused bi-isatyls, which would give a similar indophenine reaction, just like the isatin, when reacted with thiophene in presence of concentrated sulphuric acid. Moreover, fused

architecture of the bi-isatyls would help to retain the planarity of the quinoidal backbone.

Part-A: Development of the synthetic routes for fused bi-isatyls: Synthesis and characterization of novel fused bi-isatyls

Results and discussion

Synthetic approaches to synthesize novel fused bi-isatyls

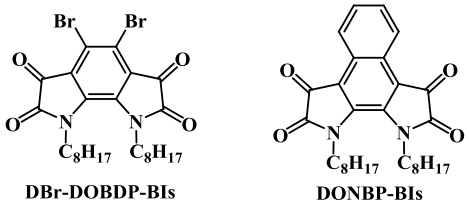

Figure 3.12 Structures of the synthesized novel fused bi-isatyls; 4,5-dibromo-1,8-dioctyl-1,8-dihydropyrrolo[3,2-*g*]indole-2,3,6,7-tetraone (**DBr-DOBDP-BIs**) and 1,10-dioctyl-1,10-dihydrobenzo[*e*]pyrrolo[3,2-*g*]indole-2,3,8,9-tetraone (**DONBP-BIs**)

The synthesis of novel fused bi-isatyls (Figure 3.12) bestowed many discrete synthetic challanges. As the most popular and obvious synthetic approach to isatin from subsequent aniline derivatives, Sandmeyer isatin synthesis was employed to synthesize fused bi-isatyl, 1,8-dihydropyrrolo[3,2-*g*]indole-2,3,6,7-tetraone (**BDP-BIs**) from 1,2-diaminobenzene using chloral hydrate and hydroxylamine hydrochloride following the literature procedure reported by Z. J. Allan in 1953[100] and by Kossmehl *et al*. in 1975[96], as shown in scheme 3.4. Following the Sandmeyer synthetic route, reaction of 1,2-diaminobenzene in aqueous hydrochloric acid with chloral hydrate ($Cl_3CCH(OH)_2$) and hydroxylamine hydrochloride ($NH_2OH.HCl$) and anhydrous sodium sulphate (Na_2SO_4) should yield 1,2-phenylenebis(2-(hydroxyimino)acetamide), compound **12**, which would undergo concentrated sulphuric acid mediated cyclization at 3- and 6- positions of the benzene ring to give novel fused bi-isatyl compound 1,8-dihydropyrrolo[3,2-*g*]indole-2,3,6,7-tetraone; **BDP-BIs**. But, instead of isolating compound **12** during the first step, quinoxalin-2(1*H*)-one (**QxN**) was isolated as the major product of first step

reaction, which probably would have generated from the acid catalyzed condensation-cyclization reaction of compound **12**.

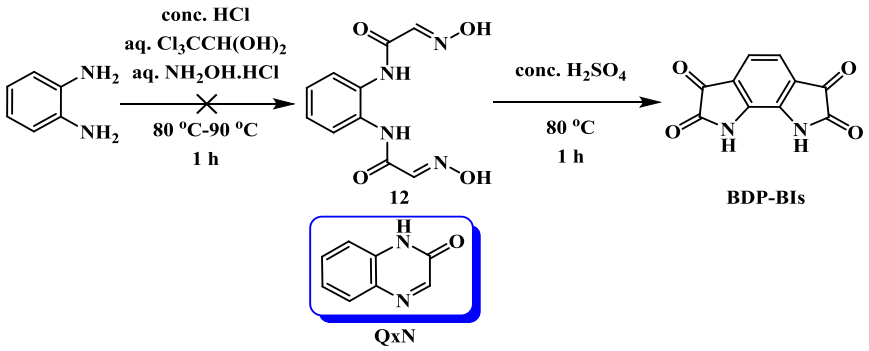

Scheme 3.4 Synthetic approach to the novel fused bi-isatyl **BDP-BIs** *via* Sandmeyer synthetic route

As an alternative approach to the novel fused bi-isatyl compound **BDP-BIs**, a new synthetic route (scheme 3.5) was devised, which involved the conversion of 1,2-diaminobenzene into the diethyl-1,2-phenylenebis(oxamato), compound **13** using ethyloxalyl chloride in dry THF. In the subsequent step, compound **2** is hydrolyzed to the 1,2-phenylenebis(oxamic acid), compound **14** using an aqueous 0.1 M sodium hydroxide solution at 60 °C.

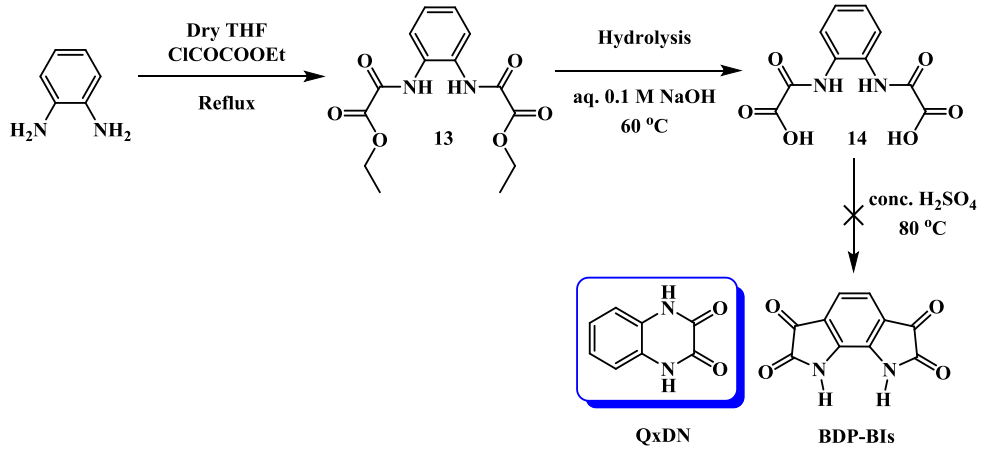

Scheme 3.5 Synthetic approach to the novel fused bi-isatyl **BDP-BIs** *via* acid catalyzed condensation-cyclization of compound **14**

The hydrolyzed product compound **14** was isolated by acidifying the reaction mass using aqueous 1.2 M hydrochloric acid solution to pH ~1 and filtering the solid product. Our synthetic strategy was to carry out the acid catalyzed condensation-cyclization reaction of 1,2-phenylenebis(oxamic acid) at 3- and 6- positions of the benzene ring under strong acidic conditions at 80 °C to yield target molecule **BDP-BIs**.

By applying this synthetic route, 1,4-dihydroquinoxalin-2,3-dione (**QxDN**) was obtained as the major product instead of **BDP-BIs**, which was characterized by ^{1}H and ^{13}C NMR spectroscopy and ESI-Mass spectroscopy.

Due to the failure of above mentioned synthetic approaches, we designed a new synthetic route, which involved the synthesis of 1,8-dihydropyrrolo[3,2-*g*]indole (**BDP**) *via* tetra-*n*-butylammonium fluoride (TBAF) promoted cyclisation of 3,6-bis((trimethylsilyl)ethynyl)-1,2-phenylene)diacetamide, compound **19** in THF (Scheme 3.6). The detailed synthesis is given in Chapter 2.

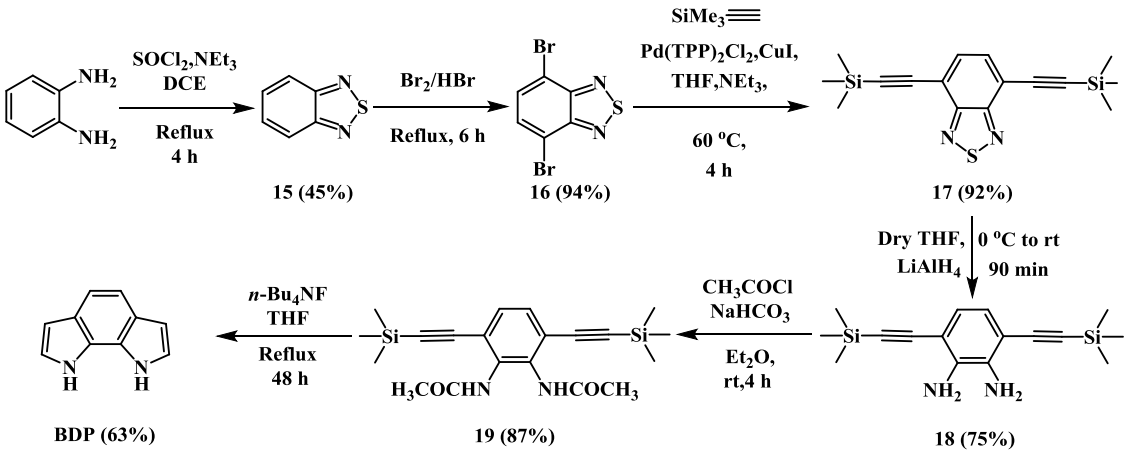

Scheme 3.6 Synthesis of 1,8-dihydropyrrolo[3,2-*g*]indole (**BDP**)

In the subsequent step, the synthesized **BDP** was further explored for oxidation reactions to yield **BDP-BIs** with the help of different oxidizing reagents. We have tried different oxidizing agents involving $AlCl_3$/pyridinium chlorochromate (PCC) supported over SiO_2,[101] polyaniline salt/PCC,[102] CrO_3/acetic acid-water-acetone,[103,104] I_2/*tert*-butyl hydroperoxide (TBHP),[105] $CeCl_3.7H_2O$/iodoxybenzoic acid (IBX),[106] *N*-bromosuccinimide (NBS)/*tert*-butanol-aqueous methanol,[107,108] etc. to convert **BDP** into **BDP-BIs**, but in all the cases, we ended up with either decomposition of starting materials or sticky side products, which could not be isolated and characterized. We believe that, **BDP**, being an unstable product couldn't withstand the oxidizing reaction conditions and decomposed during the reactions, resulting into the generation of sticky tarry mass.

To stabilize the **BDP**, *N*-Boc-protection was performed using Boc-anhydride and *N*,*N*-dimethylpyridin-4-amine (DMAP) as a catalyst in refluxing dry THF (Scheme 3.7). The di-Boc-protected **DBoc-BDP** was subjected to the subsequent oxidation

reaction using NBS/*tert*-butanol-aqueous methanol, to obtain di-Boc-protected fused bi-isatyl, di-tert-butyl 2,3,6,7-tetraoxopyrrolo[3,2-*g*]indole-1,8-dicarboxylate (**DBoc-BDP-BIs**) *via* formation of an intermediate compound **20** (Scheme 3.7). Unfortunately, following this synthetic procedure, di-tert-butyl-2,3,6,7 tetrabromopyrrolo[3,2-*g*]indole-1,8-dicarboxylate (**DBoc-TBr-BDP**) was isolated as a major product instead of getting intermediate compound **20**, due to the deactivated fused pyrrole rings[105] and hence it favoured the substitution by bromine and resulted into the formation of **DBoc-TBr-BDP**.

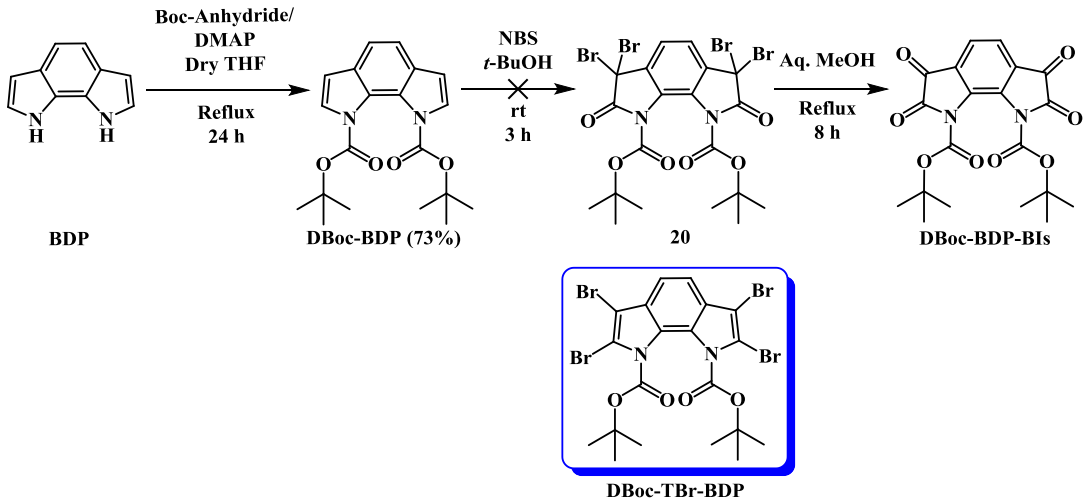

Scheme 3.7 Synthetic approach to the novel fused bi-isatyl **DBoc-BDP-BIs** from **BDP** using mild oxidizing reaction conditions, NBS/*tert*-butanol-aqueous methanol

This observation motivated us to further modify the **BDP** building block, by introducing solubilizing alkyl chains, which also activated the fused pyrrole rings of the **BDP** unit. The *N*-alkylation reaction of **BDP** was carried out using excess of *n*-octylbromide and NaOH in DMF at 80 °C for 3 h. Both the compounds 1,8-dioctyl-1,8-dihydropyrrolo[3,2-*g*]indole (**DOBDP**) and 1,3,8-trioctyl-1,8-dihydropyrrolo[3,2-*g*]indole (**TOBDP**) are being formed during the alkylation reaction and the desired compound **DOBDP** was separated using extensive column chromatography over silica gel using pet-ether as eluent.

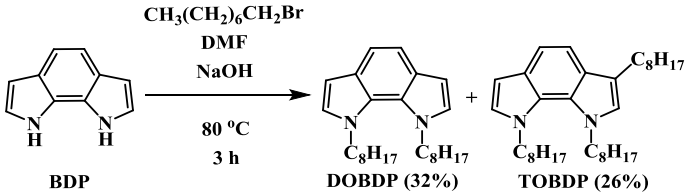

Scheme 3.8 Synthesis of alkylated **DOBDP** and **TOBDP** from **BDP**

The synthesized **DOBDP** was subjected to the oxidation reaction using NBS/*tert*-butyl hydroperoxide (TBHP) in DMF/chloroform at room temperature (Scheme 3.9). The addition of NBS to the vigorously stirred reaction mixture caused the immediate colour change from light yellow to deep red, indicating the progress of the reaction, however, the completion of the reaction required 20 h of vigorous stirring. The oxidized product 4,5-dibromo-1,8-dioctyl-1,8-dihydropyrrolo[3,2-*g*]indole-2,3,6,7-tetraone (**DBr-DOBDP-BIs**) was obtained by quenching the reaction mass in aqueous sodium thiosulphate solution and filtering the solid dark red-purple precipitates. The pure product was obtained by washing the crude material with copious amounts of petroleum ether. The bromine substitution on the 4- and 5- position of the phenyl ring takes place during the NBS/TBHP-mediated oxidation because both of these positions, being *para*- to the fused pyrrole ring nitrogen atom, are susceptible to bromination. Reducing the stoichiometric ratio of NBS used for the oxidation did not favoured the formation of unsubstituted bi-isatyl, 1,8-dioctyl-1,8-dihydropyrrolo[3,2-*g*]indole-2,3,6,7-tetraone.

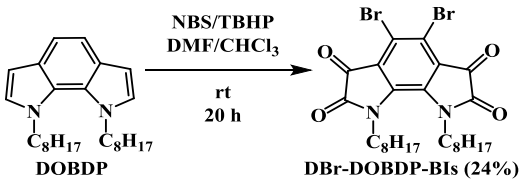

Scheme 3.9 Synthesis of **DBr-DOBDP-BIs** from **DOBDP**

The similar methodology was adopted to synthesize 1,10-dioctyl-1,10-dihydrobenzo[*e*]pyrrolo[3,2-*g*]indole (**DONBP-BIs**). 1,10-dihydrobenzo[*e*]pyrrolo[3,2-*g*]indole (**NBP**), having two fused pyrrole rings to the central naphthalene, was conveniently synthesized according to the synthetic procedure discussed in Chapter 2.

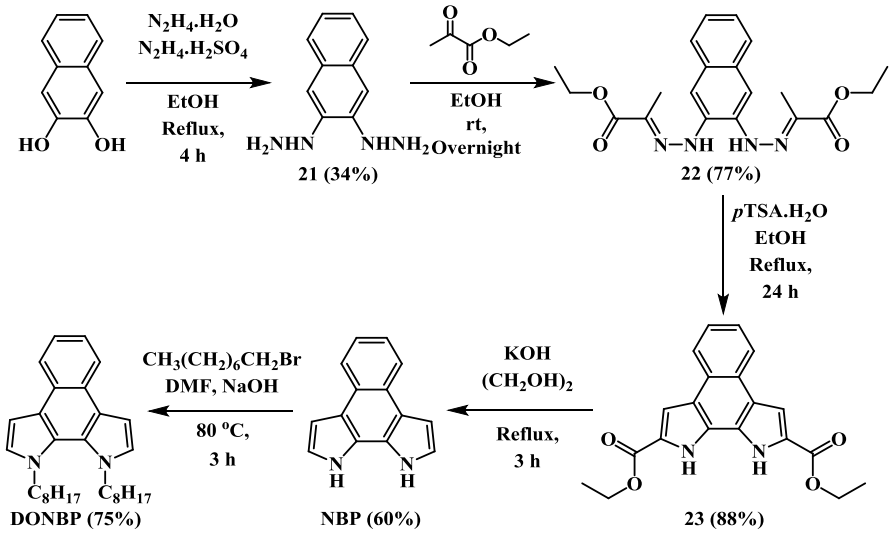

Scheme 3.10 Synthesis of polycyclic fused aromatic pyrrole-based building block **NBP** and alkylated **DONBP** from **NBP**

The *N*-alkylation reaction of **NBP** was carried out using excess of 1-bromoocatne and NaOH in DMF at 80 °C for 3 h and the desired compound 1,10-dioctyl-1,10-dihydrobenzo[*e*]pyrrolo[3,2-*g*]indole (**DONBP**) was separated using extensive column chromatography over silica gel using pet-ether as eluent. The naphthalene-based polycyclic fused aromatic pyrrole-based building block **NBP** is more stable under the ambient conditions compared to the **BDP**. The synthesized **DONBP** was subjected to the similar oxidation reaction conditions, utilized for the oxidation of **DOBDP**, using NBS/*tert*-butyl hydroperoxide in DMF/chloroform at room temperature. To our surprise, what had worked out for **DOBDP**, didn't work quiet well for **DONBP** and the reaction yielded very less amount (less than 2% yield) of the oxidized product 1,10-dioctyl-1,10-dihydrobenzo[*e*]pyrrolo[3,2-*g*]indole-2,3,8,9-tetraone (**DONBP-BIs**). Therefore, the modified synthetic procedure reported by Zi *et al*. was followed to oxidize **DONBP**, utilizing the combination of I_2/TBHP as a mild oxidizing reagent in DMSO at 80 °C (Scheme 3.11).[105] The above reaction yielded mono-oxidized product 1,10-dioctyl-1,10-dihydrobenzo[*e*]pyrrolo[3,2-*g*]indole-2,3-dione (**DONBP-MIs**). Further increasing the stoichiometric ratio of the reagents or increasing the temperature or reaction time didn't convert mono-oxidized product **DONBP-MIs** into the di-oxidized product **DONBP-BIs**.

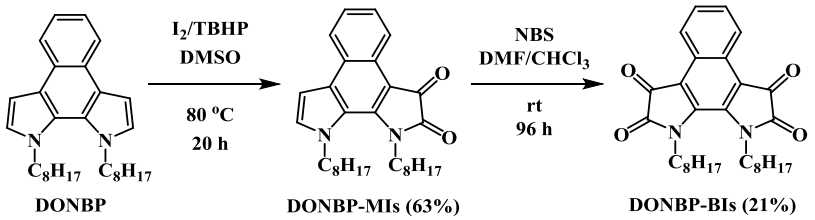

Scheme 3.11 Synthesis of mono-oxidized **DONBP-MIs** and di-oxidized **DONBP-BIs** from **DONBP**

In the subsequent step, the mono-oxidized product **DONBP-MIs** was subjected to the second oxidation reaction by using NBS as an oxidizing reagent in DMF/chloroform at room temperature, allowing the reaction mixture to stir vigorously for 96 h (Scheme 3.11). After completion of the reaction, the product **DONBP-BIs** was isolated by quenching the reaction mixture into the water and extracting the product using chloroform. The pure product was obtained by washing the crude material with copious amounts of petroleum ether, which conveniently removed the mono-oxidized product **DONBP-MIs**, leaving behind the violet-black coloured pure product **DONBP-BIs** in reasonable yield of 21%.

Conclusion

On our expedition to synthesize novel fused bi-isatyls, we have explored many synthetic routes involving sandmeyer isatin synthesis, acid catalyzed condensation-cyclization reaction of 1,2-phenylenebis(oxamic acid), synthesis and subsequent oxidation reactions of **BDP** utilizing various oxidizing agents and synthesis and subsequent oxidation reaction of Boc-protected di-tert-butyl pyrrolo[3,2-g]indole-1,8-dicarboxylate (**DBoc-BDP**) using NBS/*tert*-butanol-aqueous methanol as a mild oxidizing agent. Finally, the targeted fused bi-isatyl product **DBr-DOBDP-BIs** was synthesized by the oxidation reaction of **DOBDP** using NBS/*tert*-butyl hydroperoxide (TBHP) as a mild oxidizing agent. The synthesized **DBr-DOBDP-BIs** has been characterized by ^{1}H, ^{13}C, DEPT-135 NMR spectroscopy and High Resolution Mass Spectroscopy (HRMS). Another naphthalene-fused bi-isatyl **DONBP-BIs** has been synthesized from the *N*-alkylated naphthalene-based polycyclic fused aromatic pyrrole-based building block, **DONBP** using a two step synthetic route; first step involves the oxidation of **DONBP** using mild oxidizing agent I_2/TBHP in DMSO, affording the mono-oxidized product **DONBP-MIs**, which was isolated and characterized by the ^{1}H and ^{13}C NMR spectroscopy. In the second step, the mono-oxidized product was

converted to the di-oxidized product **DONBP-BIs** using NBS as an oxidizing reagent in DMF/chloroform. The synthesized di-oxidized product **DONBP-BIs** has been characterized by ^{1}H, ^{13}C NMR spectroscopy and High Resolution Mass Spectroscopy (HRMS).

Experimental procedures

General procedures

All the chemicals were reagent grade and used as purchased. Moisture-sensitive reactions were performed under an inert atmosphere of dry nitrogen with dried solvents. Reactions were monitored by thin-layer chromatography (TLC) using Merck 60 F_{254} aluminium-coated plates and the spots were visualized under ultraviolet (UV) light. Column chromatography was carried out on silica gel (60–120 mesh). NMR spectra were recorded on a Bruker Avance-III 400 spectrometer in $CDCl_3$ and DMSO-D_6. Mass spectra were recorded on a Thermo-Fischer DSQ II GCMS instrument. The high resolution mass spectra were recorded on Xevo G2-XS QTOF Mass Spectrometer.

Sandmeyer synthetic approach

Synthesis of **QxN**: Compound **12** was synthesized following the modified literature procedure reported by Kossmehl *et al.*[96] In a two necked round bottom flask, 1,2-diaminobenzene (1.08 g; 10 mmol), chloral hydrate (4.96 g; 30 mmol), concentrated hydrochloride acid (2 mL) and de-ionized water (150 mL) was added and kept stirring at 50 ^{o}C. To this stirred solution was added saturated solution of hydroxylamine hydrochloride (4.17 g; 60 mmol) in de-ionized water, drop wise. The resultant reaction mixture was stirred at 80 ^{o}C–90 ^{o}C for 1 h. The reaction mass was allowed to cool at room temperature and resulting precipitates were filtered and washed with copious amounts of de-ionized water till washings showed neutral *p*H. The precipitates were again dissolved in chloroform and subjected to the column chromatography over silica gel. The pure product was eluted using 50% ethyl acetate-petroleum ether as an eluent. The isolated product was proven to be quinoxalin-2(1*H*)-one (**QxN**) by characterization of the isolated pure product and comparison of that with the literature values[109] reported for quinoxalin-2(1*H*)-one, instead of the expected compound **12**.

Quinoxalin-2(1*H*)-one (**QxN**): Light yellow solid (0.73 g, 54%); ^{1}H NMR (400 MHz, $CDCl_3$): 11.99 (s, 1H), 8.39 (s, 1H), 7.92–7.94 (dd, J_1 = 7.2 Hz, J_2 = 1.6 Hz, 1H),

7.58−7.62 (t, J = 7.6 Hz, 1H), 7.39−7.43 (m, 2H), ESI-MS 146.10 [M] (76.4%), 145.31 [M−H] (64.2%).

Acid catalyzed condensation-cyclization reaction of 1,2-phenylenebis(oxamic acid)

Compound **13** was synthesized according to the literature procedure reported by Stumpf *et al*.[110] and was carried forward to the hydrolysis step without any purification. Compound **14** was synthesized according to the literature procedure reported by Souza *et al*.[111]

Compound **14**[111]: White crystalline solid; Melting point 251 ^{o}C with decomposition (literature[111] 250 ^{o}C).

Synthesis of **QxDN**: The acid catalyzed condensation-cyclization approach was utilized to synthesize targeted compound **BDP-BIs**. The synthesized compound 1,2-phenylenebis(oxamic acid) (compound **14**, 1.00 g; 3.96 mmol) was added in portions to the continuously stirred concentrated sulphuric acid (98%, 15 mL) at 60 ^{o}C over the period of 30 min. Resulting brown reaction mixture was allowed to stir at 80 ^{o}C for 1 h. Reaction mixture was cooled to the room temperature and poured into 300 mL of ice-water and resulting brown-black precipitates were filtered and washed with water till washings didn't show acidity on the litmus paper. The precipitates were re-dissolved into the hot ethyl acetate and were subjected to the column chromatography over silica gel. The pure compound was eluted from the column using 60% ethyl acetate-petroleum ether as an eluent. The isolated product was proven to be 1,4-dihyroquinoxalin-2,3-dione (**QxDN**) by characterization of the isolated pure product and comparison of that with the literature values[112] reported for 1,4-dihydroquinoxalin-2,3-dione, instead of the expected compound **BDP-BIs**.

1,4-dihydroquinoxalin-2,3-dione (**QxDN**): Yellowish white crystalline solid (0.27 g, 42%); ^{1}H NMR (400 MHz, DMSO-D_6): 11.93 (s, 1H), 7.06−7.13 (m, 2H), ^{13}C NMR (100 MHz, DMSO-D_6): 155.6, 126.0, 123.5, 115.6. ESI-MS 161.46 [M−H] (100.0%), 162.20 [M] (66.2%).

Oxidation reaction of stabilized Boc-protected polycyclic fused aromatic pyrrole-based compound di-tert-butyl pyrrolo[3,2-g]indole-1,8-dicarboxylate (DBoc-BDP)

The synthesis and the characterization of the polycyclic fused aromatic pyrrole-based building block **BDP** has been discussed thoroughly in the Chapter 2. The stabilized di-Boc-protected **BDP** derivative **DBoc-BDP** is synthesized according to the following literature procedure.

Synthesis of di-tert-butyl pyrrolo[3,2-*g*]indole-1,8-dicarboxylate (**DBoc-BDP**): **BDP** (0.405 g, 2.6 mmol) was dissolved in dry THF (30 mL) and stirred at room temperature in a two necked round bottom flask under nitrogen atmosphere. To this stirred solution was added, DMAP (0.032 g, 0.26 mmol) and Boc-anhydride (2.84 g, 13.0 mmol), portion wise and the resulting mixture was refluxed for 24 h and monitored by TLC. After completion of reaction as indicated by TLC, the reaction mixture was quenched by addition of water (50 mL) and extracted using ethyl acetate (2 X 50 mL). The combined organic layers were dried over anhydrous sodium sulphate and subjected to flash column chromatography using 30% ethyl acetate-petroleum ether as an eluent. First light yellow coloured fraction was isolated which upon evaporation gave **DBoc-BDP** as light yellow oil.

Di-tert-butyl pyrrolo[3,2-*g*]indole-1,8-dicarboxylate (**DBoc-BDP**): Light yellow oil (0.67 g, 73%); ^{1}H NMR (400 MHz, $CDCl_3$): 7.49−7.50 (d, J = 3.6 Hz, 1H), 7.45 (s, 1H), 6.63−6.64 (d, J= 4 Hz, 1H), 1.62 (s, 9H). ^{13}C NMR (100 MHz, $CDCl_3$): 150.5, 129.5, 126.7, 124.1, 116.8, 108.2, 83.2, 28.2. ESI-MS 355.81 [M−H] (100%).

Synthesis of di-tert-butyl 2,3,6,7-tetrabromopyrrolo[3,2-*g*]indole-1,8-dicarboxylate (**DBoc-TBr-BDP**): Compound **20** was synthesized following the modified literature procedure reported by Parrick *et al.*[107] The **DBoc-BDP** (0.36 g; 1 mmol) was dissolved in *tert*-butanol (30 mL) in a two necked round bottom flask and the solution was stirred at room temperature under nitrogen atmosphere. To this stirred solution was added *N*-bromosuccinimide (crystallized before use, 0.89 g; 5 mmol) portion wise over a period of 30 min. The reaction mixture was allowed to stir at room temperature under nitrogen atmosphere for 3 h. After completion of the reaction, as indicated by TLC, the reaction mixture was concentrated under reduced pressure and

the precipitated succinimide was filtered off, washed with cold diethyl ether (2 X 20 mL) and combined filtrate was evaporated to dryness and the obtained crude product was purified by column chromatography over silica gel using 20% ethyl acetate-petroleum ether as an eluent. The isolated product was proven to be **DBoc-TBr-BDP** by characterization of the isolated pure product, instead of the expected compound **20**.

Di-tert-butyl 2,3,6,7-tetrabromopyrrolo[3,2-*g*]indole-1,8-dicarboxylate (**DBoc-TBr-BDP**): Off white solid (0.21 g; 32%); ^{1}H NMR (400 MHz, $CDCl_3$): 7.49 (s, 1H), 1.62 (s, 9H). ^{13}C NMR (100 MHz, $CDCl_3$): 149.8, 126.9, 124.5, 122.5, 107.7, 95.0, 87.5, 28.2.

Oxidation reaction of N-alkylated polycyclic fused aromatic pyrrole-based compound 1,8-dioctyl-1,8-dihydropyrrolo[3,2-g]indole (DOBDP)

The synthesis and the characterization of the *N*-alkylated polycyclic fused aromatic pyrrole-based building block 1,8-dioctyl-1,8-dihydropyrrolo[3,2-*g*]indole (**DOBDP**) has been discussed thoroughly in the Chapter 2.

Synthesis of fused bi-isatyl product 4,5-dibromo-1,8-dioctyl-1,8-dihydropyrrolo[3,2-*g*]indole-2,3,6,7-tetraone (**DBr-DOBDP-BIs**): The **DOBDP** (0.14 g; 0.29 mmol) was dissolved in the mixture of chloroform (3 mL) and DMF (20 mL) and stirred at room temperature. To this stirred solution, *tert*-butyl hydroperoxide (~70% aqueous solution, 0.6 mL; 2.92 mmol) was added and reaction mixture was allowed to stir at room temperature for 5 min. NBS (0.52 g; 2.92 mmol) was added to this stirred reaction mixture and up on addition of NBS, reaction mixture immediately turned into deep red coloured solution. After stirring the reaction mixture for 2 h, additional *tert*-butyl hydroperoxide (~70% aqueous solution, 0.3 mL; 1.46 mmol) and NBS (0.26 g; 1.46 mmol) was added and reaction was allowed to continue for 20 h. After completion, the reaction mixture was poured into the 400 mL of aqueous sodium thiosulphate solution and was stirred for about 30 min at room temperature. The resulting dark red-purple precipitates were filtered and washed with water for several times to remove traces of DMF and *tert*-butanol. The pure product was obtained by washing the crude material with copious amounts of petroleum ether, leaving behind deep purple-black solid product **DBr-DOBDP-BIs**.

4,5-dibromo-1,8-dioctyl-1,8-dihydropyrrolo[3,2-g]indole-2,3,6,7-tetraone (**DBr-DOBDP-BIs**): Dark purple-black solids (0.05 g, 24%); ^{1}H NMR (400 MHz, $CDCl_3$): 3.93−3.97 (t, J = 7.6 Hz, 2H), 1.70 (br s, 2H), 1.23−1.27 (m, 10H), 0.85−0.88 (t, J = 6.8 Hz, 3H). ^{13}C NMR (100 MHz, $CDCl_3$): 179.7, 158.4, 136.1, 125.6, 122.4, 46.0, 31.6, 29.0, 28.9, 27.6, 26.6, 22.6, 14.1. HRMS (ES+): $C_{26}H_{35}N_2O_4Br_2$ requires 597.0964, found 597.0969.

Oxidation reaction of N-alkylated polycyclic fused aromatic pyrrole-based compound 1,10-dioctyl-1,10-dihydrobenzo[e]pyrrolo[3,2-g]indole (DONBP)

The synthesis and the characterization of the *N*-alkylated polycyclic fused aromatic pyrrole-based building block 1,10-dioctyl-1,10-dihydrobenzo[*e*]pyrrolo[3,2-*g*]indole (**DONBP**) has been discussed thoroughly in the Chapter 2.

Synthesis of fused mono-isatyl product 1,10-dioctyl-1,10-dihydrobenzo[*e*]pyrrolo[3,2-*g*]indole-2,3-dione (**DONBP-MIs**): The **DONBP** (0.43 g; 1 mmol) was dissolved in DMSO (12 mL) and stirred at 60 ^{o}C under nitrogen atmosphere. To this stirred solution, *tert*-butyl hydroperoxide (~70% aqueous solution, 2.0 mL; 15 mmol) was added and reaction mixture was allowed to stir at 60 ^{o}C under nitrogen atmosphere for 5 min. The solution of I_2 (0.63 g; 5 mmol) in DMSO (5 mL) was added drop wise to this stirred reaction mixture and up on addition of I_2, the colour of the reaction mixture changed from light yellow to olive green and then deep red. After stirring the reaction mixture for 8 h at 80 ^{o}C under nitrogen atmosphere, additional *tert*-butyl hydroperoxide (~70% aqueous solution, 2.0 mL; 15 mmol) and I_2 (0.63 g; 5 mmol) was added and reaction was allowed to continue at 80 ^{o}C for 12 h. After completion, the reaction mixture was poured into the 400 mL of water and was stirred for about 30 min at room temperature. The product was extracted from aqueous solution using ethyl acetate (2 X 50 mL) and combined organic layer was washed with water (2 X 100 mL), brine (1 X 100 mL), dried over anhydrous sodium sulphate and evaporated to dryness under reduced pressure to yield dark red crude product, which was subjected to the column chromatography over silica gel and the pure product **DONBP-MIs** was isolated as a dark red solids using 15% ethyl acetate-petroleum ether as an eluent.

1,10-dioctyl-1,10-dihydrobenzo[*e*]pyrrolo[3,2-*g*]indole-2,3-dione (**DONBP-MIs**): Dark red solids (0.29 g, 63%); ^{1}H NMR (400 MHz, $CDCl_3$): 8.91−8.93 (d, J = 8.0 Hz, 1H), 8.11−8.13 (d, J = 8.0 Hz, 1H), 7.56−7.60 (dt, J_1 = 8.0 Hz, J_2 = 1.2 Hz, 1H), 7.50−7.51 (d, J = 3.2 Hz, 1H), 7.46−7.50 (dt, J_1 = 8.0 Hz, J_2 = 1.2 Hz, 1H), 7.15−7.16 (d, J = 2.8 Hz, 1H), 4.30−4.34 (t, J = 7.6 Hz, 2H), 4.04−4.08 (t, J = 7.6 Hz, 2H), 1.81−1.83 (m, 2H), 1.70−1.72 (m, 2H), 1.12−1.38 (m, 20H), 0.82−0.85 (t, J = 7.2 Hz, 6H). ^{13}C NMR (100 MHz, $CDCl_3$): 180.1, 164.6, 146.6, 138.3, 137.2, 128.1, 125.5, 125.5, 124.8, 124.0, 123.0, 121.4, 109.2, 104.8, 51.2, 46.0, 31.6, 31.6, 29.0, 29.0, 29.0, 28.4, 26.8, 26.5, 22.6, 14.1.

Synthesis of 1,10-dioctyl-1,10-dihydrobenzo[*e*]pyrrolo[3,2-*g*]indole-2,3,8,9-tetraone (**DONBP-BIs**): The **DONBP-MIs** (0.23 g; 0.5 mmol) was dissolved in the mixture of anhydrous DMF (140 mL) and chloroform (40 mL) and stirred at room temperature. To this stirred solution, NBS (1.33 g; 7.5 mmol) was added in a single portion and the reaction mixture was allowed to stir at room temperature for 96 h. After completion, the reaction mixture was poured into the 400 mL of water and was stirred for about 2 h at room temperature. The product was extracted from aqueous solution using chloroform (2 X 50 mL) and combined organic layer was washed with water (2 X 100 mL), brine (1 X 100 mL), dried over anhydrous sodium sulphate and evaporated to dryness under reduced pressure to yield dark red-purple crude product, which was washed with copious amounts of petroleum ether to remove impurities and the pure product **DONBP-BIs** was isolated as purple solids.

1,10-dioctyl-1,10-dihydrobenzo[*e*]pyrrolo[3,2-*g*]indole-2,3,8,9-tetraone (**DONBP-BIs**): Purple solids (0.05 g, 21%); ^{1}H NMR (400 MHz, $CDCl_3$): 8.75−8.78 (dd, J_1 = 6.4 Hz, J_2 = 3.2 Hz, 1H), 7.64−7.66 (dd, J_1 = 6.4 Hz, J_2 = 3.2 Hz, 1H), 3.94−3.98 (t, J = 7.6 Hz, 2H), 1.70−1.76 (m, 2H), 1.20−1.27 (m, 10H), 0.82−0.86 (t, J = 6.8 Hz, 3H). ^{13}C NMR (100 MHz, $CDCl_3$): 183.0, 160.5, 141.1, 130.8, 127.2, 123.7, 120.4, 46.3, 31.6, 29.0, 28.9, 27.8, 26.6, 22.6, 14.0. HRMS (ES+): $C_{30}H_{39}N_2O_4$ requires 491.2910, found 491.2907.

Spectral data

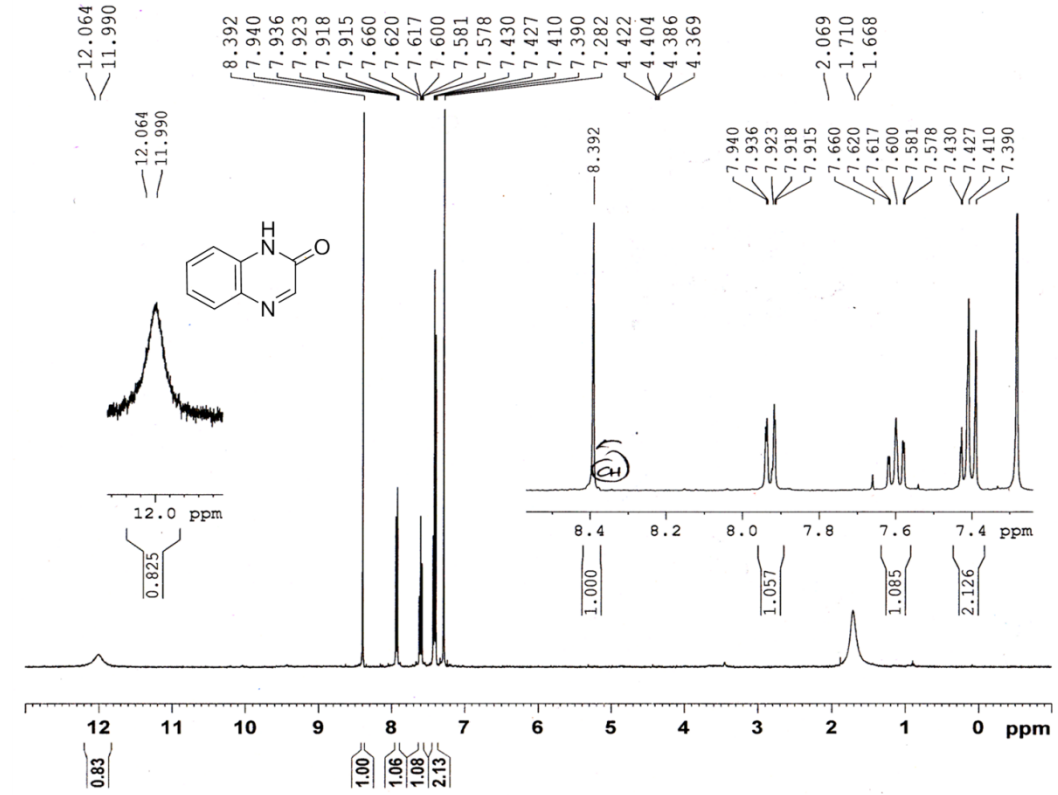

Figure 3.13 ^{1}H NMR spectrum of **QxN**

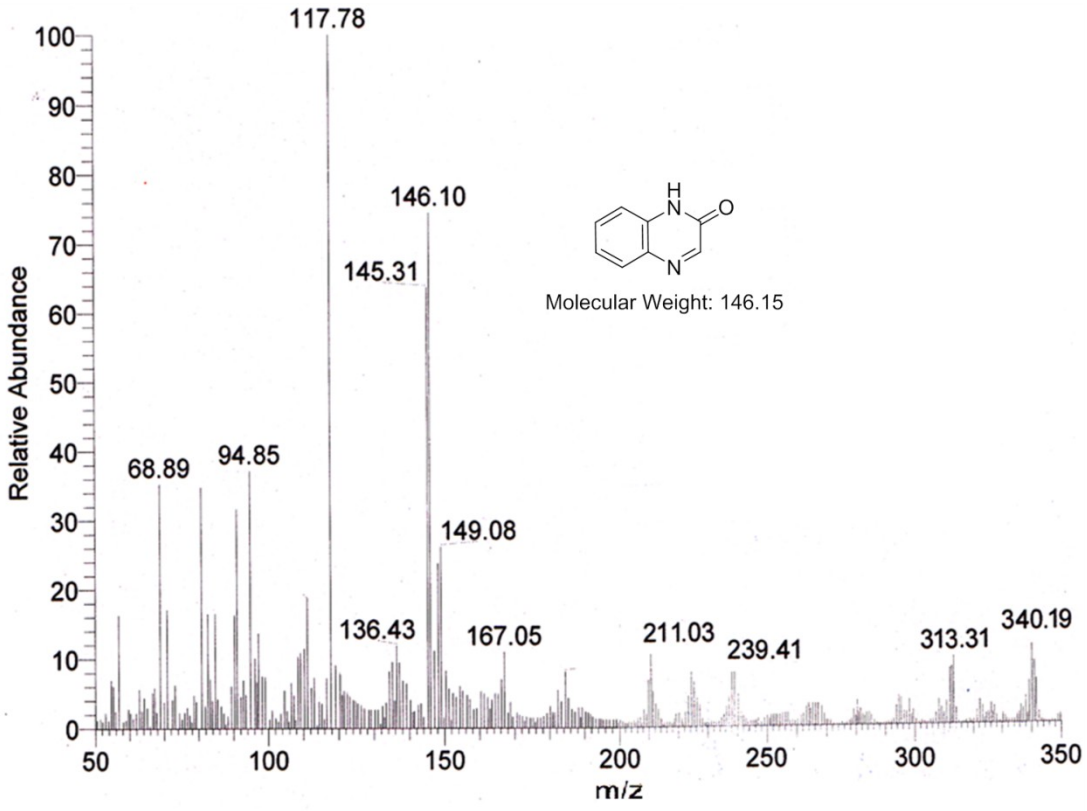

Figure 3.14 ESI-Mass spectrum of **QxN**

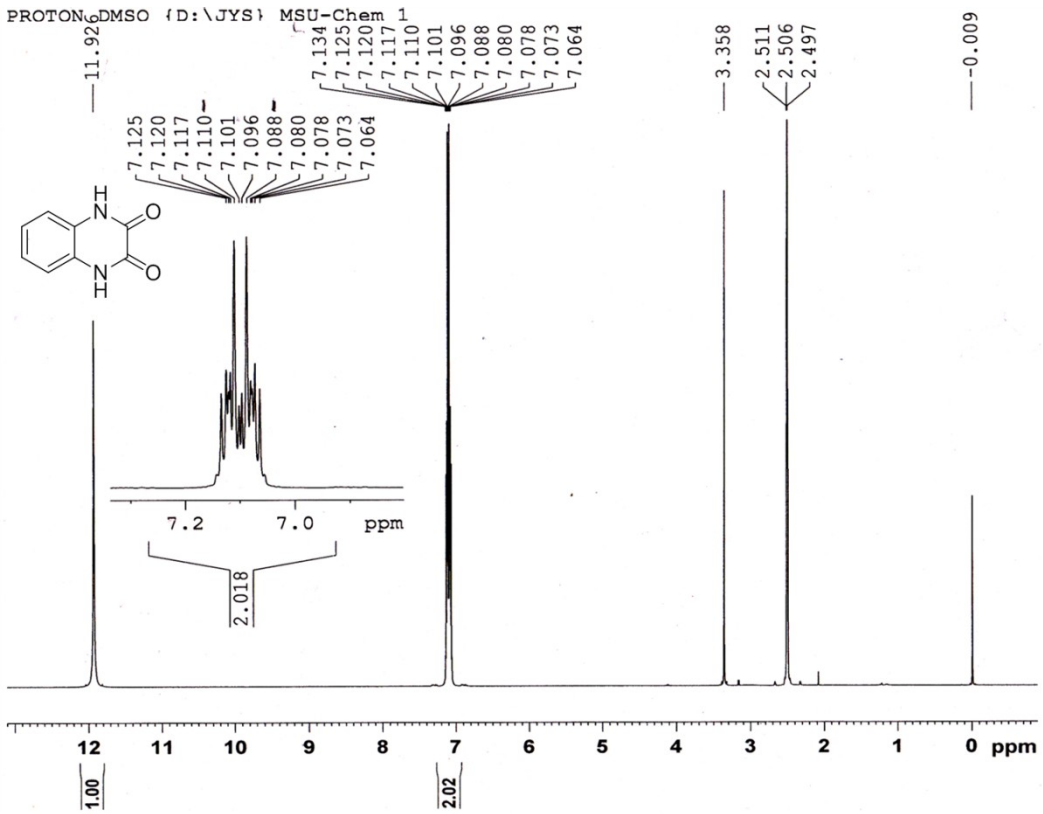

Figure 3.15 ^{1}H NMR spectrum of **QxDN**

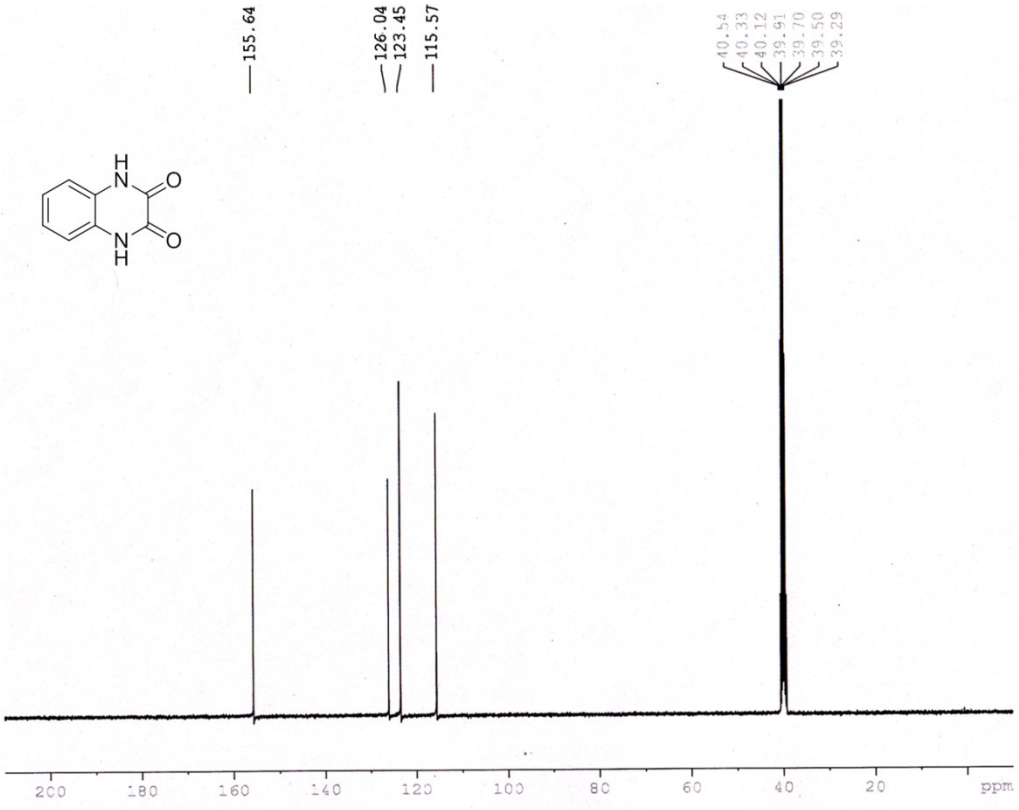

Figure 3.16 ^{13}C NMR spectrum of **QxDN**

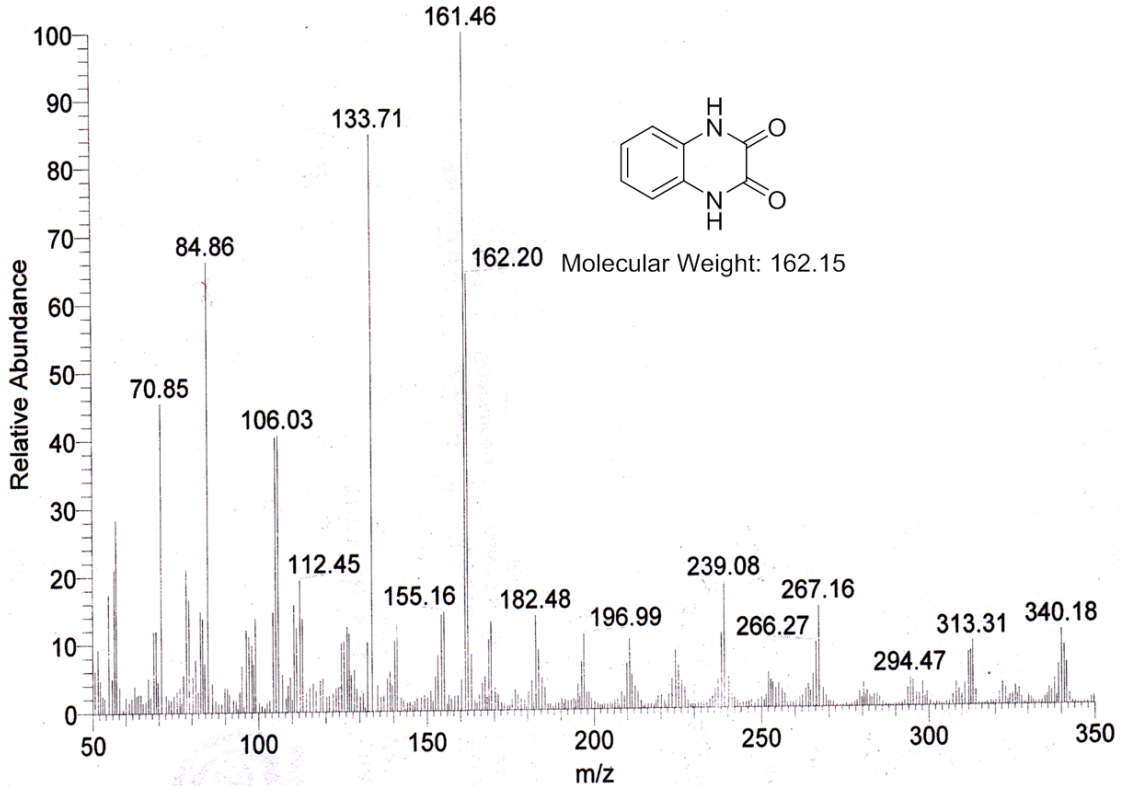

Figure 3.17 ESI-Mass spectrum of **QxDN**

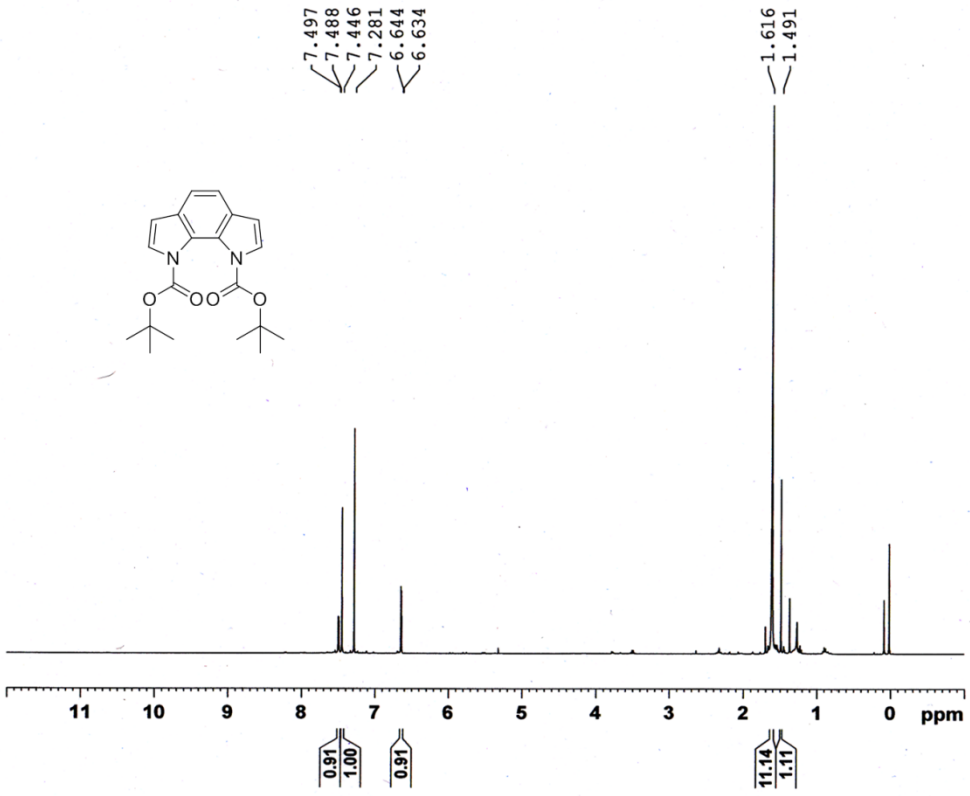

Figure 3.18 ^{1}H NMR spectrum of **DBoc-BDP**

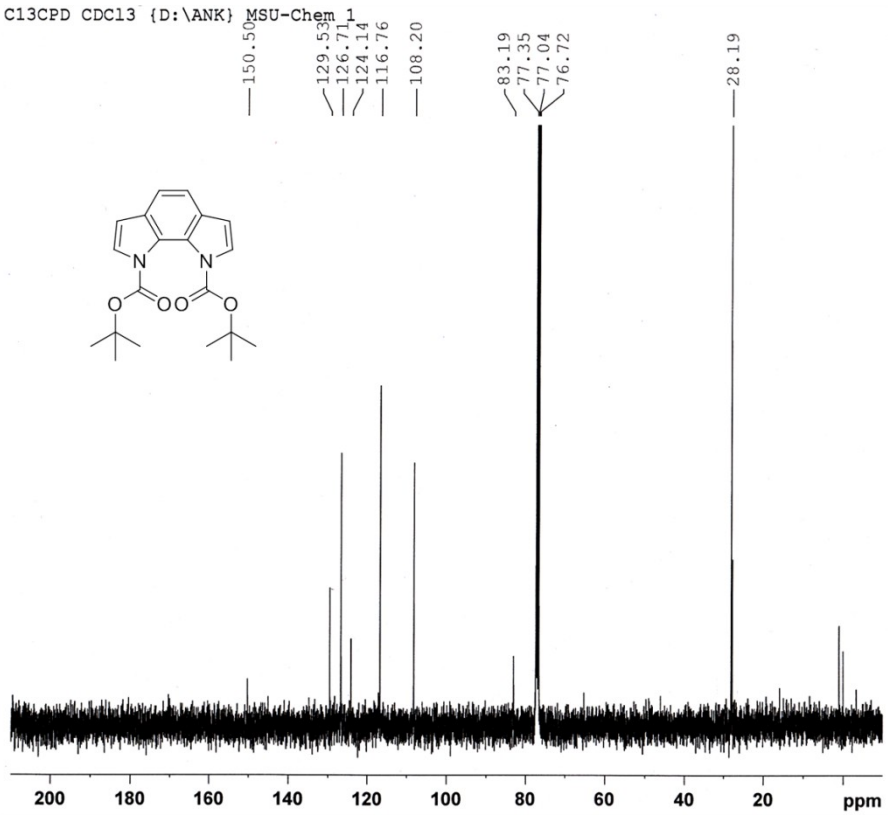

Figure 3.19 ^{13}C NMR spectrum of **DBoc-BDP**

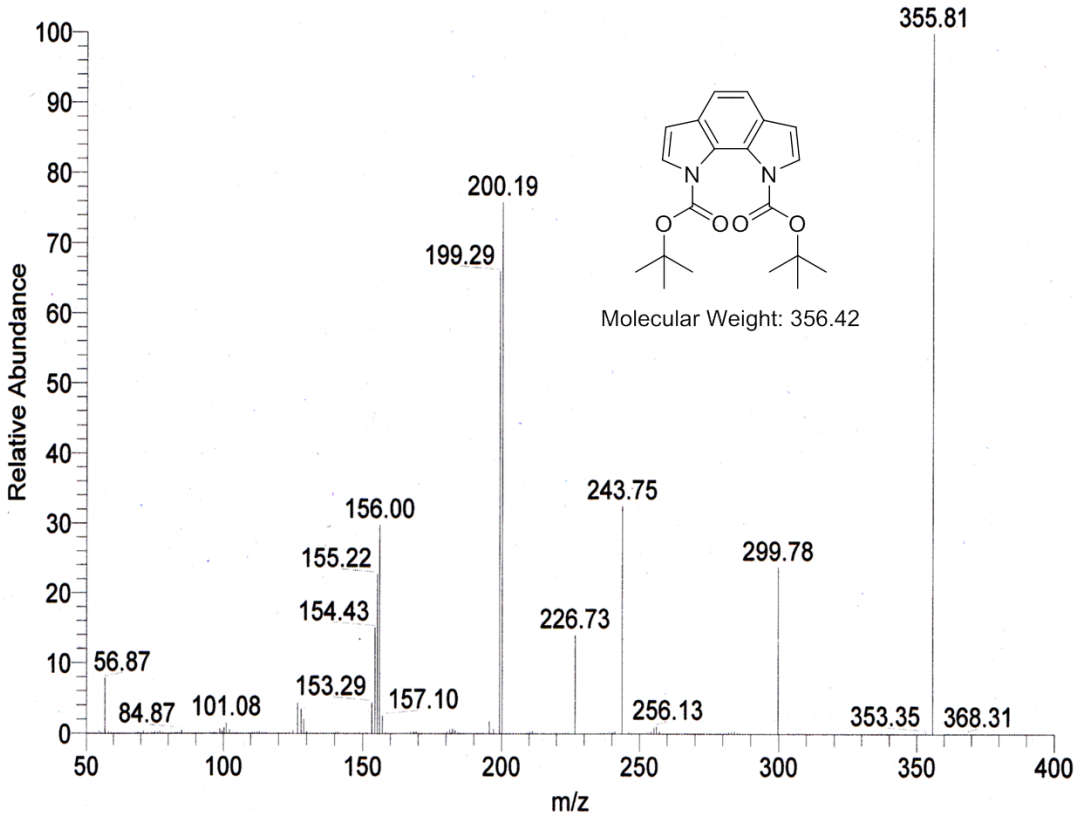

Figure 3.20 ESI-Mass spectrum of **DBoc-BDP**

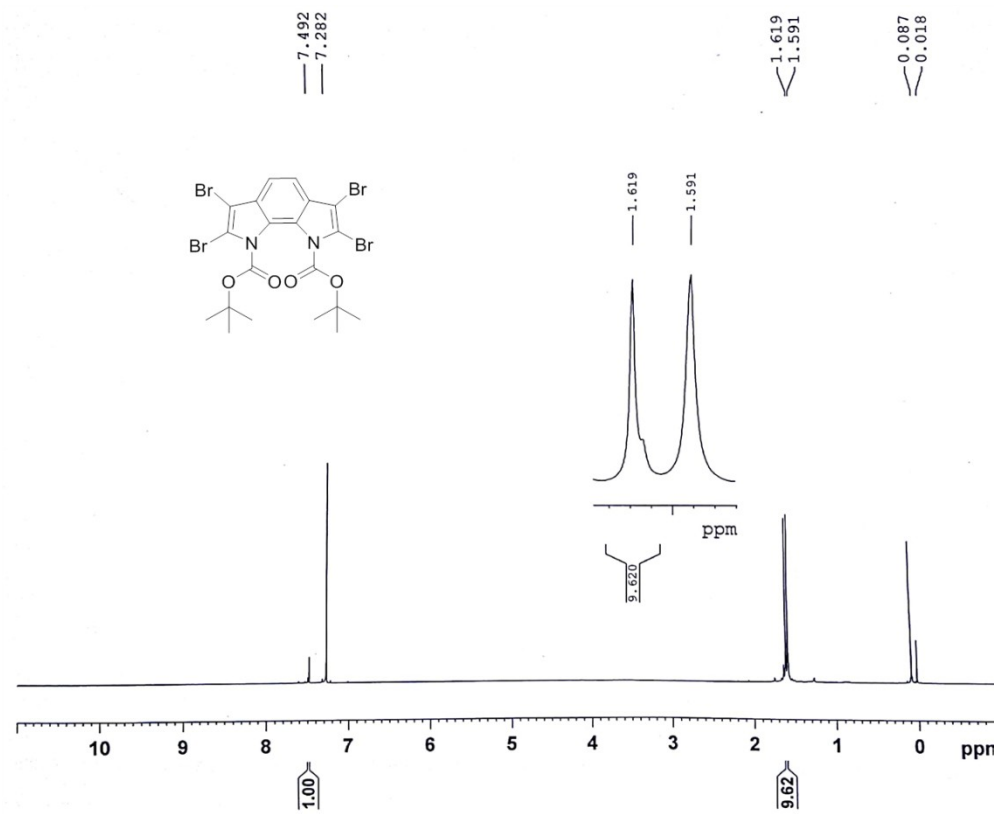

Figure 3.21 ^{1}H NMR spectrum of **DBoc-TBr-BDP**

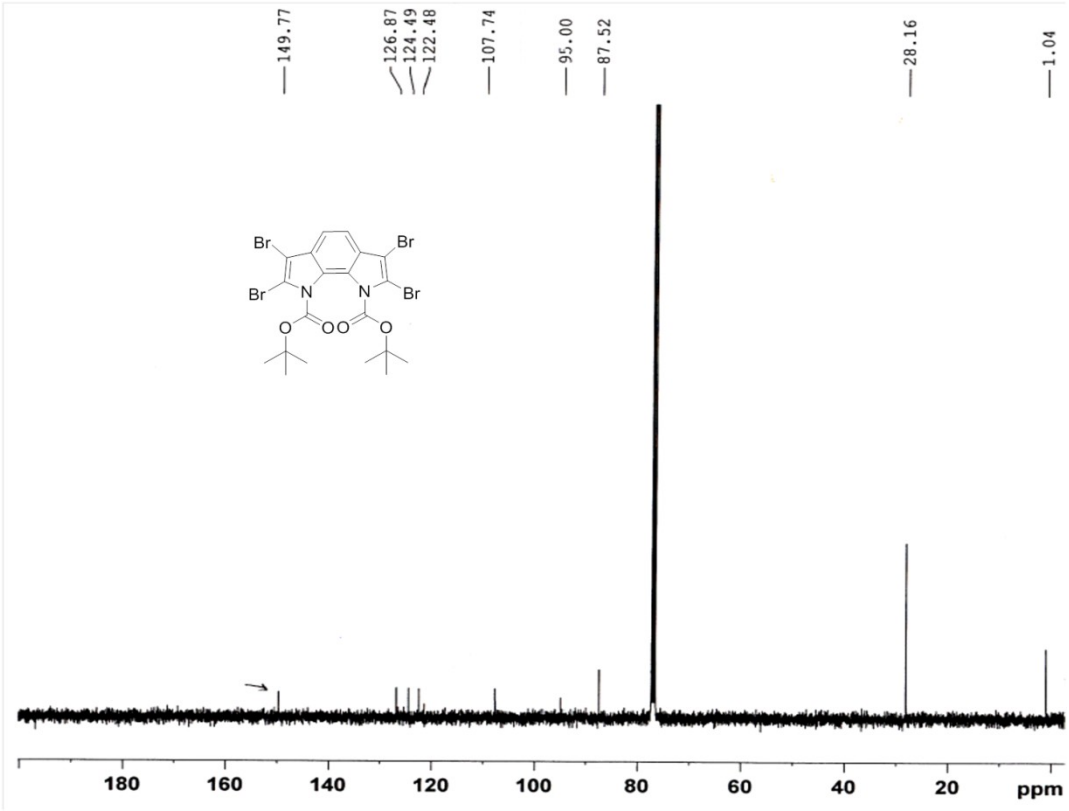

Figure 3.22 ^{13}C NMR spectrum of **DBoc-TBr-BDP**

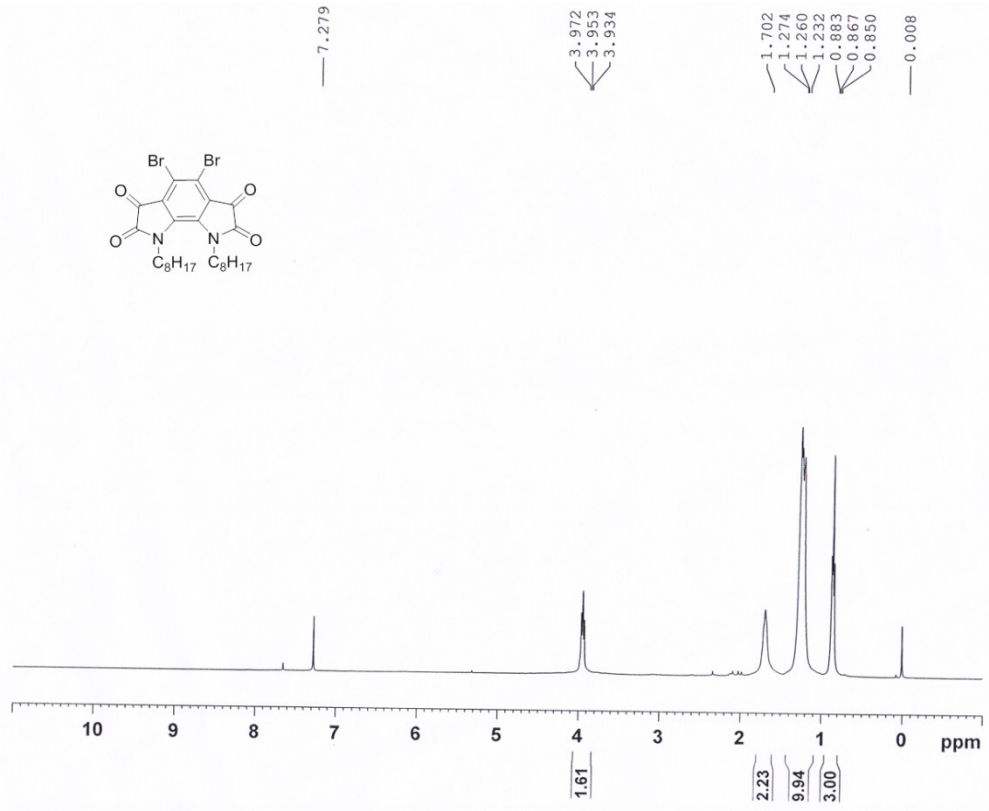

Figure 3.23 ^{1}H NMR spectrum of **DBr-DOBDP-BIs**

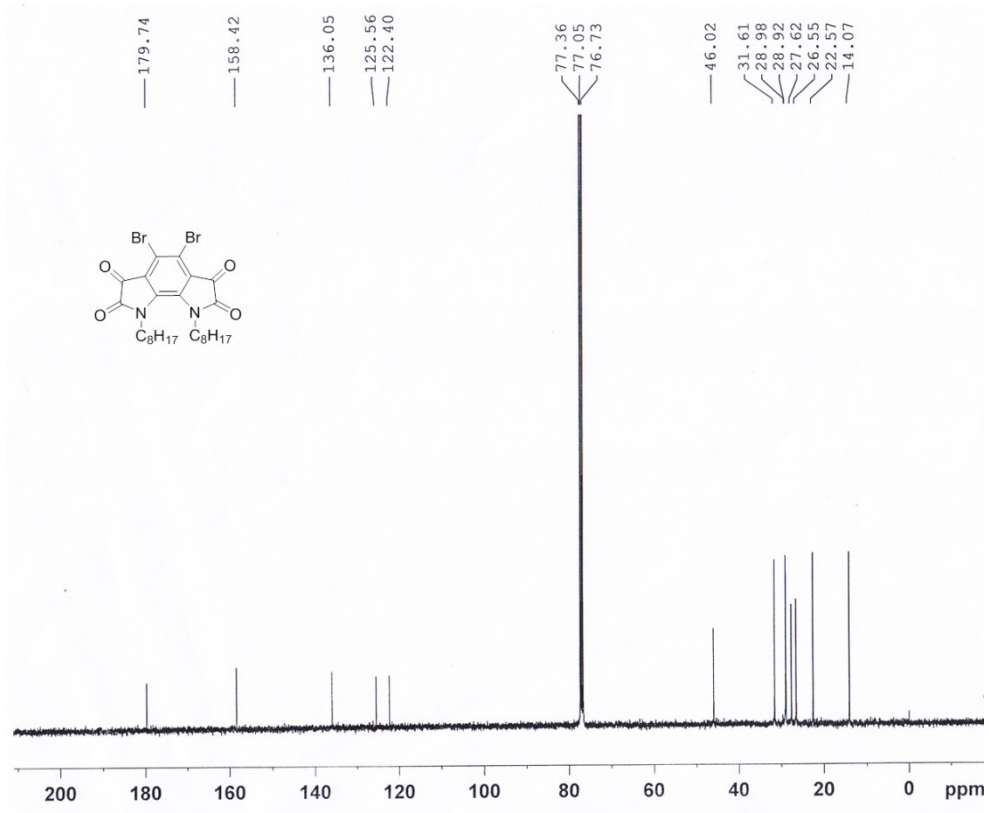

Figure 3.24 ^{13}C NMR spectrum of **DBr-DOBDP-BIs**

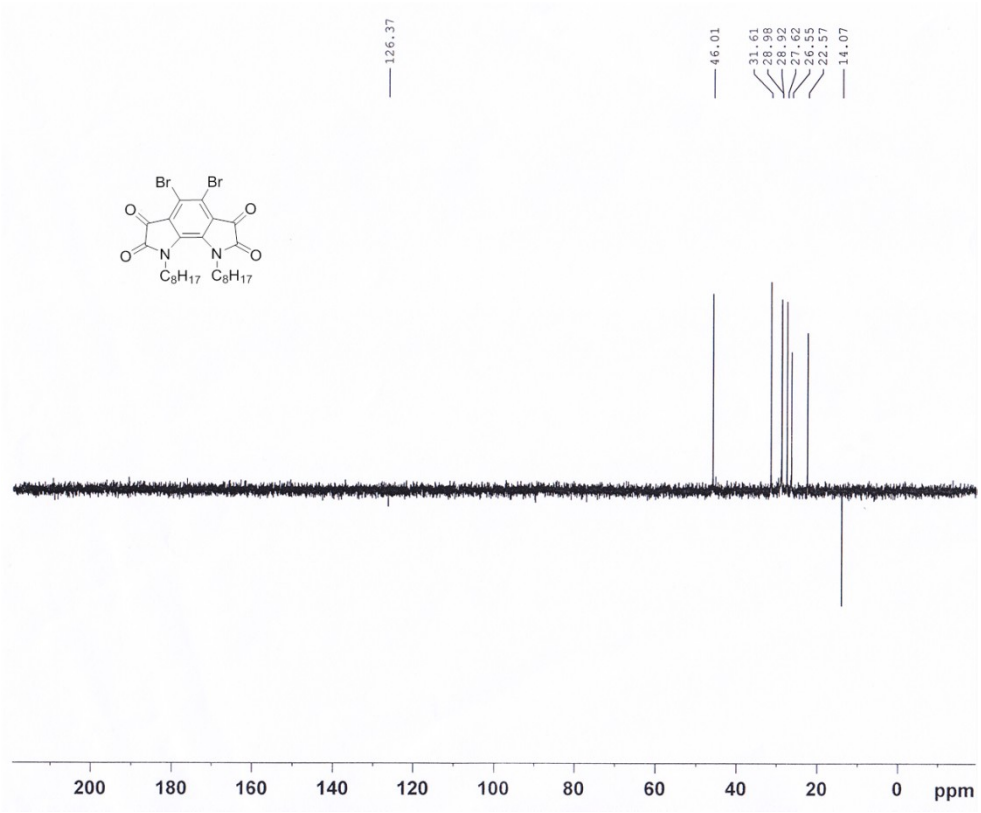

Figure 3.25 DEPT-135 NMR spectrum of **DBr-DOBDP-BIs**

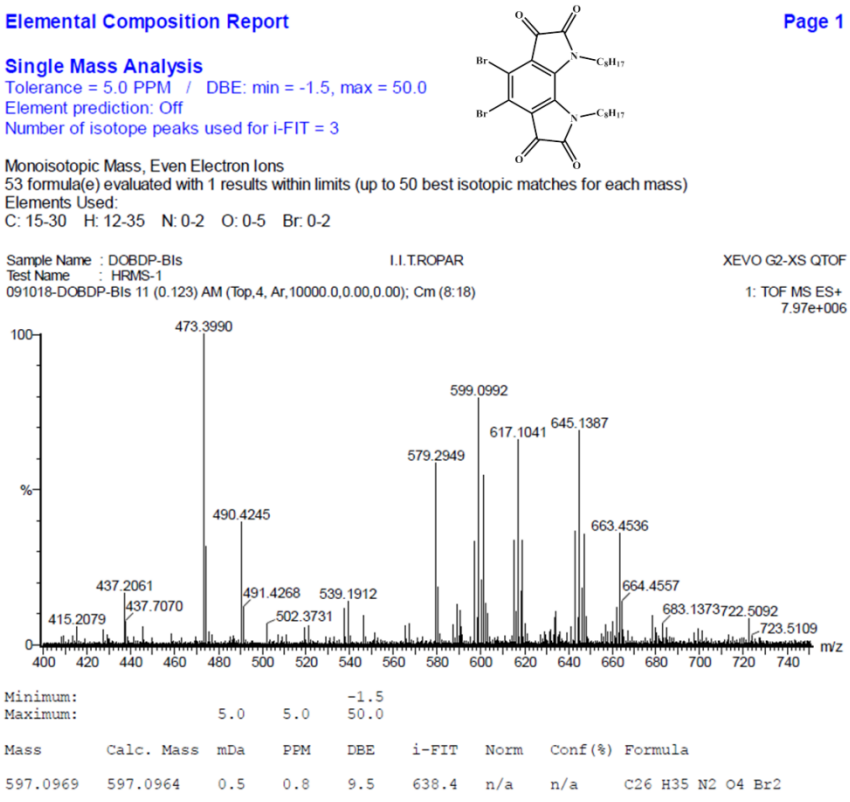

Figure 3.26 HRMS spectrum of **DBr-DOBDP-BIs**

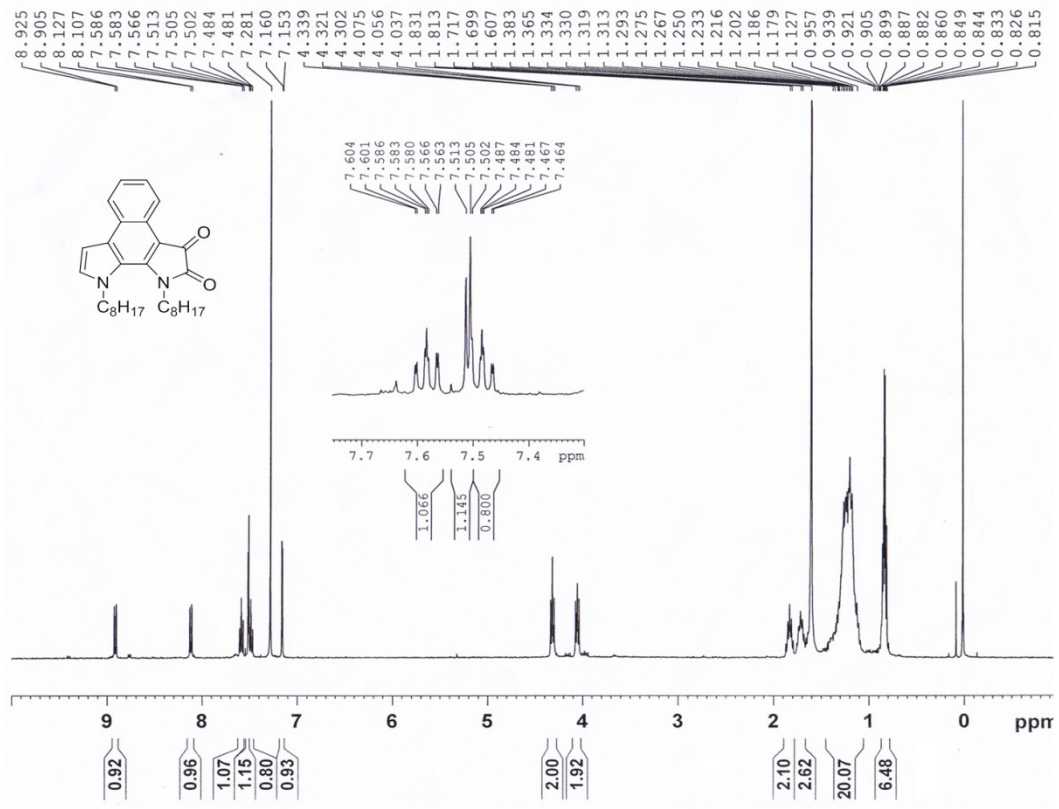

Figure 3.27 ^{1}H NMR spectrum of **DONBP-MIs**

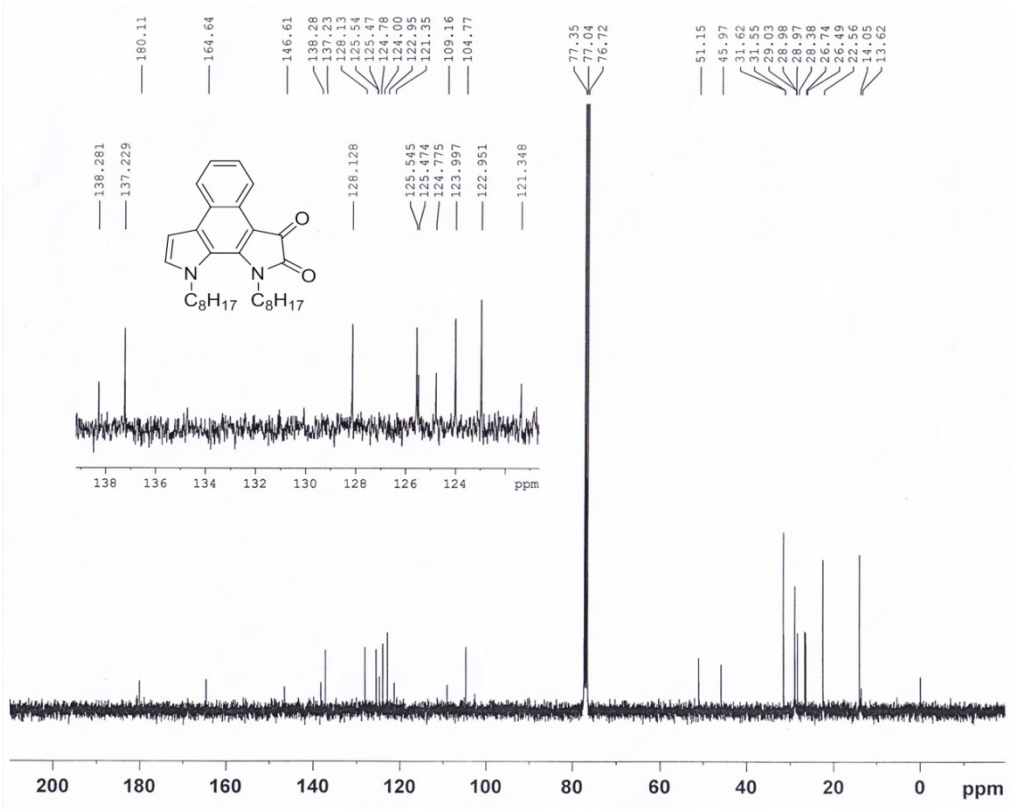

Figure 3.28 ^{13}C NMR spectrum of **DONBP-MIs**

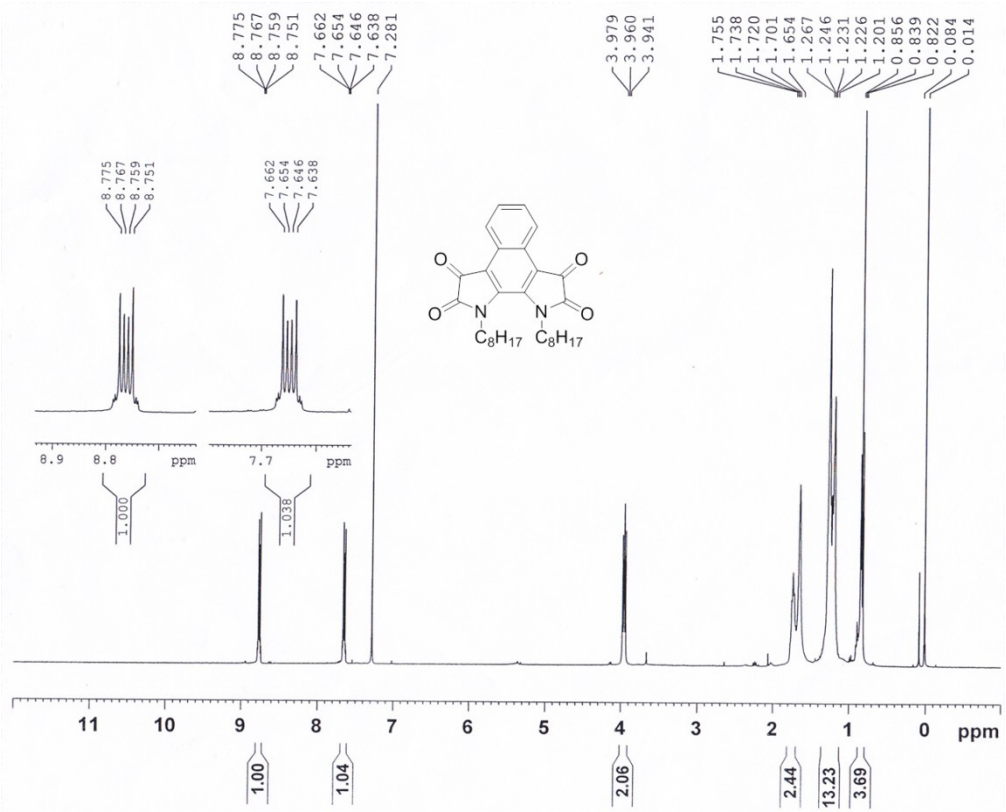

Figure 3.29 ^{1}H NMR spectrum of **DONBP-BIs**

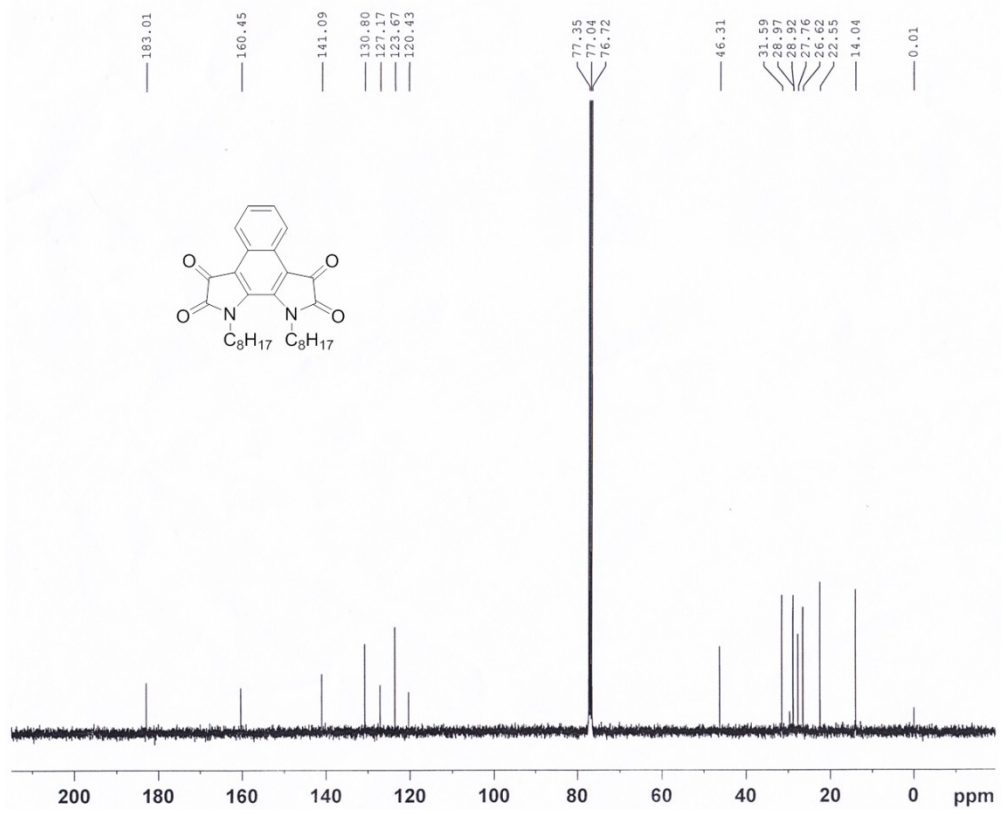

Figure 3.30 ^{13}C NMR spectrum of **DONBP-BIs**

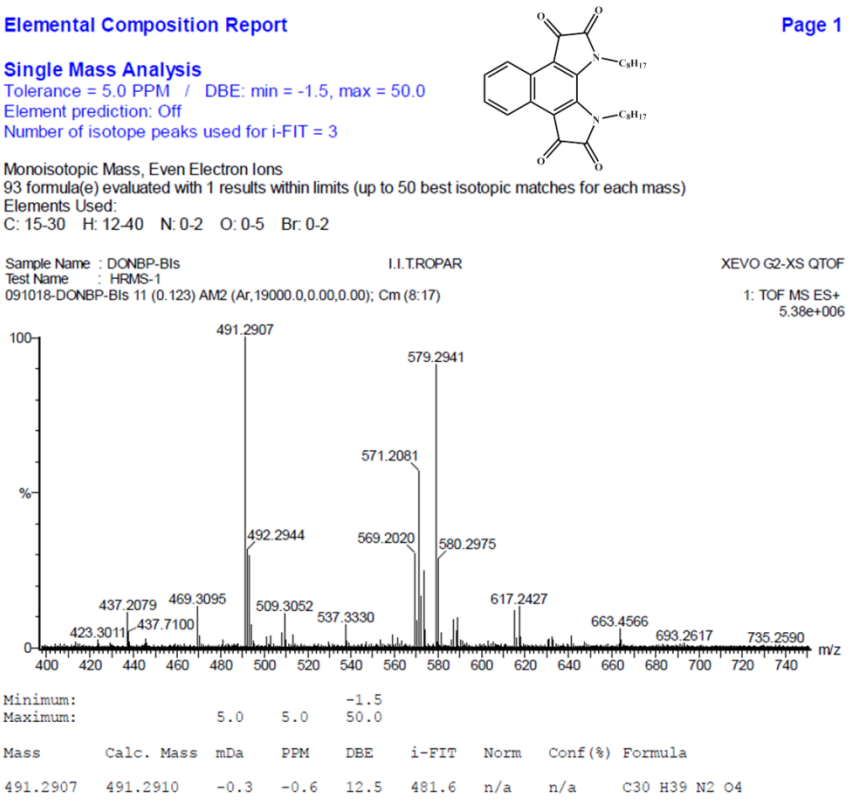

Figure 3.31 HRMS spectrum of **DONBP-BIs**

Part-B: Synthesis, characterization and electrochemical study of novel fused bi-isatyls and novel indophenine polymers

Results and discussion

Synthesis and characterization of fused bi-isatyl monomers DBr-DDBDP-BIs and DTNBP-BIs

The synthesized fused bi-isatyls, namely **DBr-DOBDP-BIs** and **DONBP-BIs**, were further explored for the synthesis of indophenine polymers by following the indophenine reaction conditions reported by Tormos *et al.*[99] The synthesized indophenine polymers based on **DBr-DOBDP-BIs** and **DONBP-BIs**, exhibited very low solubilities in the common organic solvents. Therefore, to improve the solubility of indophenine polymers, we have synthesized fused bi-isatyls, 4,5-dibromo-1,8-didodecyl-1,8-dihydropyrrolo[3,2-*g*]indole-2,3,6,7-tetraone (**DBr-DDBDP-BIs**) and 1,10-ditetradecyl-1,10-dihydrobenzo[*e*]pyrrolo[3,2-*g*]indole-2,3,8,9-tetraone (**DTNBP-BIs**), having longer *n*-dodecyl and *n*-tetradecyl alkyl chains, respectively.

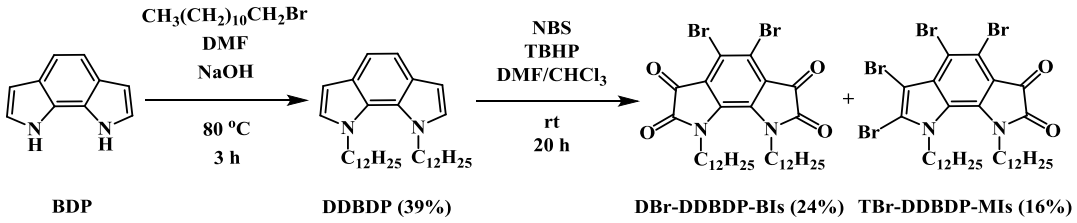

Scheme 3.12 Synthesis of di-oxidized **DBr-DDBDP-BIs** and mono-oxidized **TBr-DDBDP-MIs**

Both of the starting materials for the **DBr-DDBDP-BIs** and **DTNBP-BIs**, are 1,8-didodecyl-1,8-dihydropyrrolo[3,2-*g*]indole (**DDBDP**) and 1,10-ditetradecyl-1,10-dihydrobenzo[*e*]pyrrolo[3,2-*g*]indole derivative (**DTNBP**), respectively which are synthesized using the similar synthetic procedure described in Chapter 2. The synthesized **DDBDP** was subjected to the oxidation reaction by following the similar synthetic procedure for **DBr-DOBDP-BIs**, using NBS/*tert*-butyl hydroperoxide (TBHP) in DMF/chloroform at room temperature (Scheme 3.12).

The tetra-bromo mono-oxidized derivative, 4,5,6,7-tetrabromo-1,8-didodecyl-1,8-dihydropyrrolo[3,2-*g*]indole-2,3-dione (**TBr-DDBDP-MIs**), being formed during the reaction was also isolated and characterized by ^{1}H, ^{13}C, DEPT-135 NMR spectroscopy and High Resolution Mass Spectroscopy (HRMS). It was found that, after the addition of NBS to the reaction mixture, the formation of **TBr-DDBDP-MIs** takes place immediately, and the red coloration observed, immediately after the addition of NBS to the reaction mixture is due to the conversion of **DDBDP** to the **TBr-DDBDP-MIs**.

The initially formed tetra-bromo mono-oxidized **TBr-DDBDP-MIs** slowly gets converted into the di-oxidized **DBr-DDBDP-BIs**, over a period of time. However, the complete conversion of **TBr-DDBDP-MIs** into the **DBr-DDBDP-BIs** is not achieved at the end of the reaction and small amount of the **TBr-DDBDP-MIs (**16%**)** is always present along with the desired product **DBr-DDBDP-BIs**, no matter for how long the reaction has been continued or how much excess of oxidizing reagent is used. The synthesized **DBr-DDBDP-BIs** have been characterized by ^{1}H, ^{13}C, DEPT-135 NMR spectroscopy and High Resolution Mass Spectroscopy (HRMS).

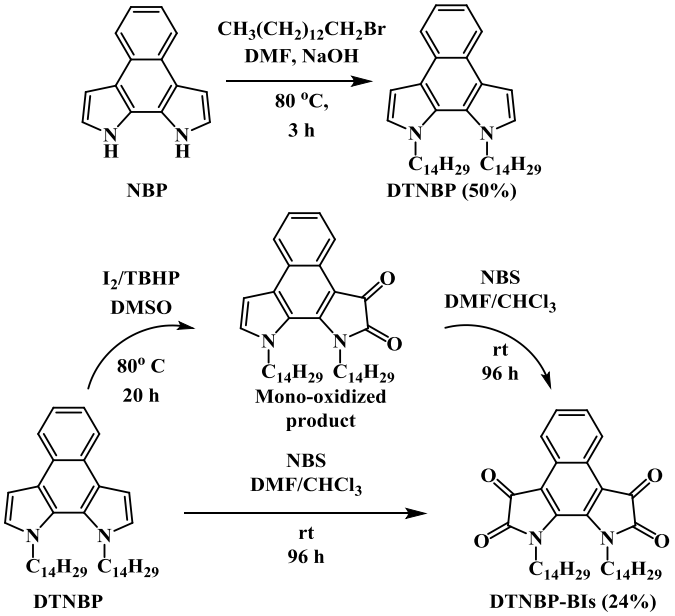

Scheme 3.13 Synthesis of alkylated **DTNBP** and synthesis of the di-oxidized **DTNBP-BIs** *via* single step oxidation reaction using NBS as an oxidizing agent

For the oxidation of the synthesized *N*-alkylated **DTNBP** to the fused bi-isatyl product **DTNBP-BIs**, a single step oxidation reaction methodology was developed to avoid the tedious and time consuming isolation of the intermediate mono-oxidized product (Scheme 3.13). The synthesized **DTNBP** was oxidized to the fused bi-isatyl

product, **DTNBP-BIs** by using NBS as an oxidizing reagent in DMF/chloroform at room temperature.

Synthesis of novel indophenine polymers DBr-BDP-INDPH and NBP-INDPH

The indophenine polymers, having highly planar, rigid and quinoidal bithiophene-based backbone, have been synthesized following the indophenine reaction conditions, reported by Tormos *et al.*[99] and Hwang *et al.*[94] The synthesized fused bi-isatyls, **DBr-DDBDP-BIs** and **DTNBP-BIs**, are reacted with thiophene in presence of concentrated sulphuric acid in toluene at 70 °C under nitrogen atmosphere to afford the two novel indophenine polymers, **DBr-BDP-INDPH** and **NBP-INDPH** (Scheme 3.14).

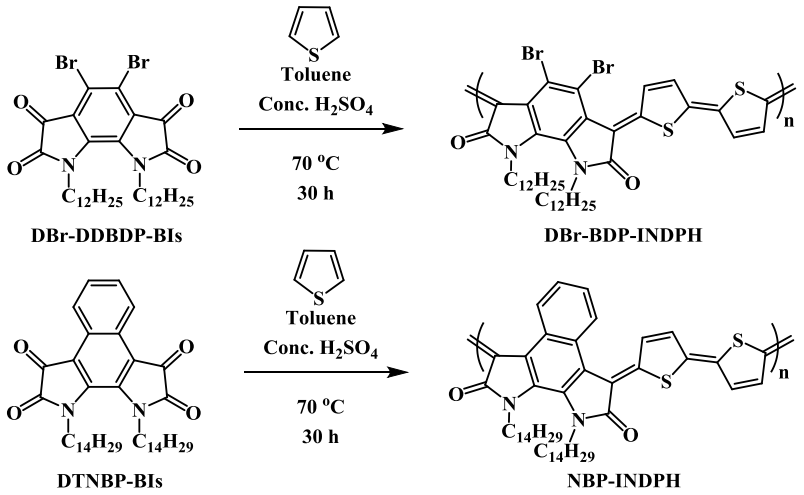

Scheme 3.14 Synthesis of indophenine polymers **DBr-BDP-INDPH** and **NBP-INDPH**

The sulphuric acid catalyzed polymerization reaction of fused bi-isatyls to afford indophenine polymers proceeds through the protonation of bi-isatyls, forming the dihyroxydication intermediate, **INT-A**, which undergoes nucleophilic attack by thiophene to afford dihydroxydithienyl intermediate, **INT-B**. **INT-B** undergoes acid catalyzed dehydration reaction to yield dithienyldication intermediate, **INT-C**, which undergoes nucleophilic addition reaction with **INT-B**, followed by the acid catalyzed dehydration reaction, forming indophenine polymer having quinoidal bi-thiophene backbone.[99] The proposed mechanism for indophenine polymerization is shown in Figure 3.32.

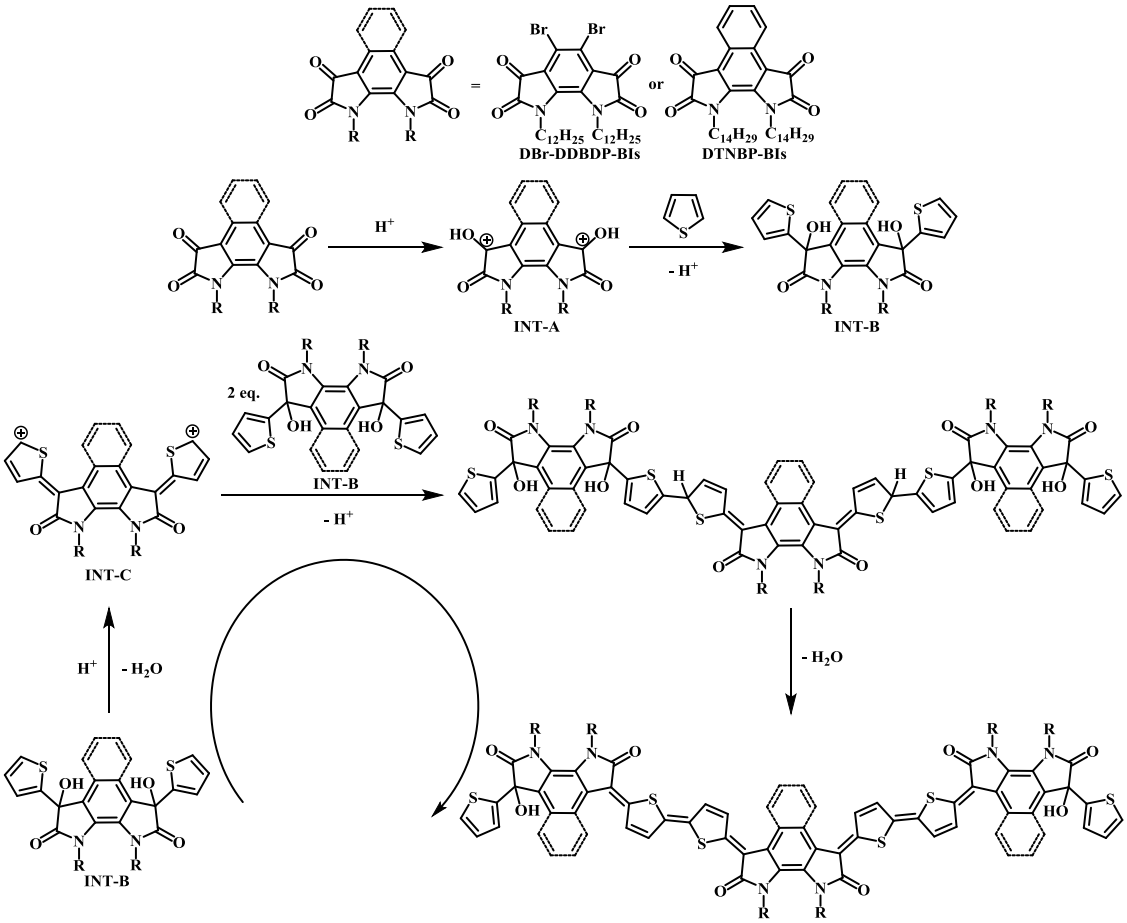

Figure 3.32 Proposed mechanism for synthesis of indophenine polymers **DBr-BDP-INDPH** and **NBP-INDPH**

The synthetic procedure followed to synthesize indophenine polymers neither required any costlier transition-metal catalysts nor harsh temperature and pressure conditions. Moreover, the concentrated sulphuric acid used for the polymerization can be easily removed by simple basic aqueous workup procedure. The obtained indophenine polymers are further purified by sequential soxhlet extraction using different solvents like methanol, acetone, petroleum ether and the pure polymer fraction was finally eluted using chloroform. The solvent was evaporated under reduced pressure and solids were further dried under vacuum at 50 ^{o}C.

Thermal properties of monomers and polymers, molecular weight and solubility of polymers

The quinoidal bi-thiophene based indophenine polymers, **DBr-BDP-INDPH** and **NBP-INDPH**, showed weight average molecular weight (M_w) of 13.9 kDa and 10.8 kDa, respectively measured by GPC analysis. Introduction of longer alkyl chains in the fused bi-isatyls, **DBr-DDBDP-BIs** and **DTNBP-BIs**, promoted the solubility of

the resulting quinoidal polymers. All the synthesized monomers and polymers showed moderate to good solubility properties in the common organic solvents, like dichloromethane, chloroform, 1,2-dichlorobenzene and THF.

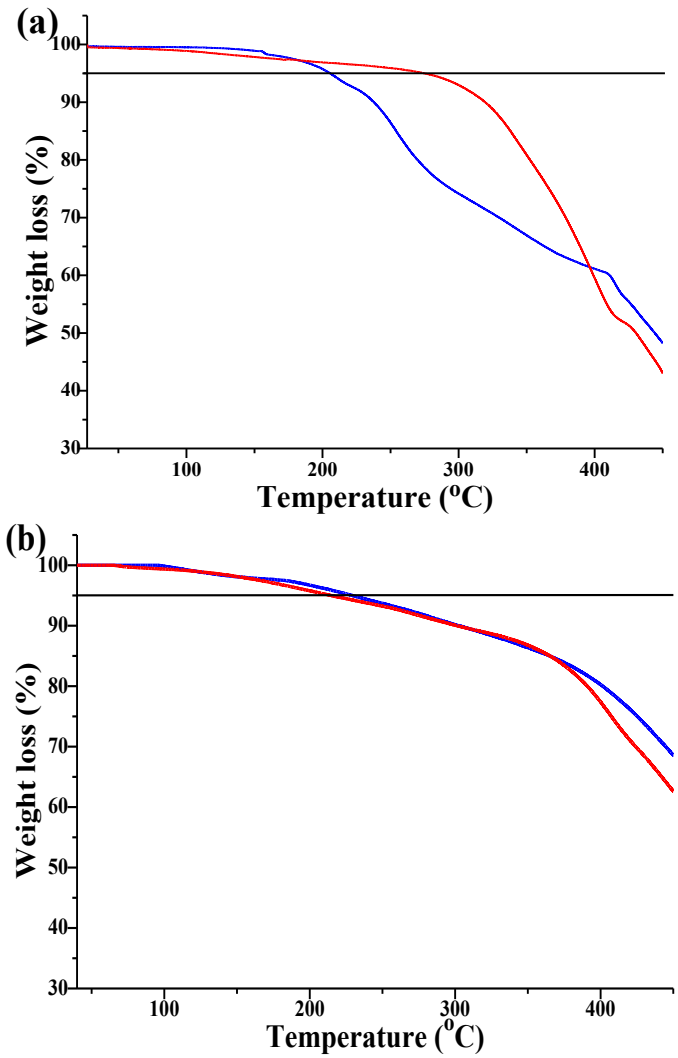

Figure 3.33 Thermogravimetric analysis (TGA) of (a) fused bi-isatyls **DBr-DDBDP-BIs** (blue line) and **DTNBP-BIs** (red line) and (b) BDP and NBP-based indophenine polymers; **DBr-BDP-INDPH** (blue line) and **NBP-INDPH** (red line)

Thermal properties of the synthesized **DBr-DDBDP-BIs**, **DTNBP-BIs** and indophenine polymers (**DBr-BDP-INDPH** and **NBP-INDPH**) were analyzed by thermogravimetric analysis (TGA) at a heating rate of 10 °C/min under nitrogen atmosphere (Figure 3.33a and b). The decomposition temperature (T_d) is defined as the temperature at which, the molecule or polymer loses 5% of its weight. Synthesized fused bi-isatyls **DBr-DDBDP-BIs** (Figure 3.33a; blue line) and **DTNBP-BIs** (Figure 3.33a; red line) exhibited decomposition temperatures (T_d) of 204 °C and 270 °C, respectively. The improved thermal stability of **DTNBP-BIs** compared to that of **DBr-DDBDP-BIs** can be correlated to the presence of central naphthalene ring unit. Both of

the synthesized polymers showed decomposition temperatures above 200 ^{o}C, which demonstrates their sufficiently high thermal stabilities for applications of organic electronic devices. BDP-based indophenine polymer **DBr-BDP-INDPH** (Figure 3.33b; blue line) exhibited slightly higher thermal decomposition temperature (T_d) of 229 ^{o}C, compared to the NBP-based indophenine polymer **NBP-INDPH** (Figure 3.33b; red line), whose decomposition temperature (T_d) is 214 ^{o}C. Weight average molecular weight (M_w), poly-dispersity index (PDI) and decomposition temperatures (T_d) of the DTPBT-based conjugated polymers are summarized in Table 3.1.

Photo-physical properties of monomers

The photo-physical properties of the synthesized novel fused bi-isatyls, **DBr-DDBDP-BIs** and **DTNBP-BIs**, have been studied by UV-visible spectroscopy of dilute chloroform solutions as well as thin films on quartz glass, casted from chloroform solutions. Both of the fused bi-isatyls exhibited dual band absorption spectra in solution state (Figure 3.34a). **DBr-DDBDP-BIs** (Figure 3.34a; blue solid line) showed first absorption band ranging from 300 nm to 425 nm, having an absorption maxima (λ_{max}) at 340 nm with a weak shoulder peak at 393 nm, which can be ascribed to the π–π^* transitions. The second broad absorption band ranging from 425 nm to 708 nm; having absorption maxima (λ_{max}) at 569 nm, can be correlated to the charge transfer transitions within bi-isatyl scaffold. However, the solution spectra of **DTNBP-BIs** (Figure 3.34a; red solid line) exhibited relatively blue shifted first absorption band extending up to 400 nm, having λ_{max} at 320 nm, with a very weak shoulder peak at 344 nm. The second broad absorption band, ranging from 400 nm to 722 nm, has an absorption maximum at 517 nm, which is blue shifted compared to that of **DBr-DDBDP-BIs**. The second absorption band has a shoulder peak at 550 nm. The charge transfer (CT) band of NBP-based fused bi-isatyl, **DTNBP-BIs**, is much broader and intense compared to the BDP-based fused bi-isatyl, **DBr-DDBDP-BIs**. The reason behind this may be the relatively improved charge transfer between the electron rich fused naphthalene ring and electron deficient fused pyrrole-2,3-dione and pyrrole-8,9-dione moieties. In case of BDP-based fused bi-isatyl, **DBr-DDBDP-BIs**, the central 4,5-dibromo substituted fused benzene ring is comparatively electron poor, and hence the resulting charge transfer between the central dibromo substituted fused benzene ring and the electron deficient fused pyrrole-2,3-dione and pyrrole-6,7-dione moieties is weaker.

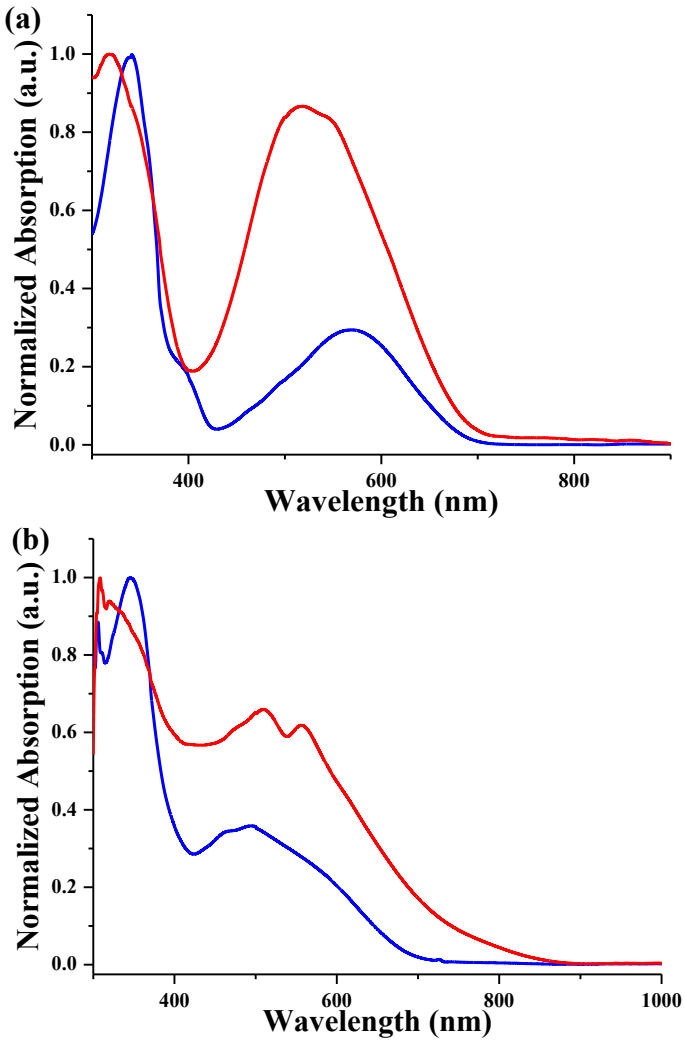

Figure 3.34 Absorption spectra of synthesized fused bi-isatyls **DBr-DDBDP-BIs** (blue solid line) and **DTNBP-BIs** (red solid line); (a) in chloroform solution and (b) in the film state.

In the film state, the absorption spectra of both of the fused bi-isatyls (Figure 3.34b) exhibited shifting of the absorption maximum of the CT bands compared to the absorption spectra in the solution state, however, the absorption behaviour exhibits the same trend as the absorption in solution. The bathochromic shift of ~85 nm is observed in the absorption edge of **DTNBP-BIs** (Figure 3.34b; red solid line) with a broadening of the CT band, while that in the case of **DBr-DDBDP-BIs** (Figure 3.34b; blue solid line) is much lesser (~10 nm). The CT band of the **DTNBP-BIs** in the film state exhibited slightly hypsochromically shifted absorption maximum of 510 nm, with a complex splitting pattern. Additionally, the shoulder peak present at 550 nm along with the CT band in the absorption spectrum of **DTNBP-BIs** in solution state, became resolved, enhanced and a little bathochromically shifted, appearing at 559 nm. The CT band of the **DBr-DDBDP-BIs** in the film state (Figure 3.34b; blue solid line), is more

hypsochromically shifted (~74 nm) with an absorption maximum at 495 nm compared to that of **DTNBP-BIs** in the film state (Figure 3.34b; red solid line). The CT band of the **DBr-DDBDP-BIs** in the film state exhibited complex band splitting with the shoulder peak appearing at 460 nm and a very weak shoulder peak at 580 nm.

It is hard to tell the exact type of the aggregation of the **DBr-DDBDP-BIs** molecules in the solid state, but considering the large hypsochromic shift in the absorption maximum of the CT band, a probable H-type aggregation is a likely cause.[94] The bathochromically shifted absorption edge and the broadening of the CT band implies that the highly coplanar **DTNBP-BIs**, is capable of exhibiting better π–π stacking between the molecules in the solid state, in consequence of the broader π-face, rendered by the centrally fused naphthalene ring. The optical band-gaps of the synthesized fused bi-isatyls were calculated from the absorption edges in the film state and were found to be in following order: **DTNBP-BIs** (1.58 eV) < **DBr-DDBDP-BIs** (1.78 eV). The photo-physical properties of the synthesized monomers are summarized in Table 3.1.

Photo-physical properties of polymers

The photo-physical properties of both of the quinoidal bithiophene-based indophenine polymers, **DBr-BDP-INDPH** and **NBP-INDPH**, were studied by UV-visible spectroscopy of dilute chloroform solutions of the polymers as well as thin films on quartz glass casted from chloroform solution. As shown in Figure 3.35a, the BDP-based indophenine polymer **DBr-BDP-INDPH** (Figure 3.35a; blue solid line) showed dual band absorption spectrum in chloroform solution; the first absorption band lies into the UV region and extending up to 425 nm, which can be ascribed to the π–π* transitions, while the second broad absorption band ranging from 426 nm and extending up to 1000 nm, with the absorption maxima (λ_{max}) of 566 nm, can be correlated to the charge transfer (CT) transitions between the donor thiophene units and acceptor lactam rings of the fused bi-isatyl units. This extended absorption up to the near IR region (~1000 nm) can be attributed to the quinoidal nature of the polymer backbone, which imparts superior delocalization of the π-electrons as well as the rigidity to the polymer architecture. On the other hand, NBP-based indophenine polymer **NBP-INDPH** (Figure 3.35a; red solid line) exhibited multiple bands with the complex band-splitting in the absorption spectrum of its chloroform solution. The first

absorption band is ranging from the UV region and extending up to 370 nm, which can be attributed to the $\pi-\pi^*$ transitions. The second absorption band, starting from 371 nm, is extending up to the 985 nm in the near IR region, with the absorption maxima of 541 nm and a distinct shoulder peak at 443 nm, can be ascribed to the CT band. The λ_{max} of the CT band of the solution of **NBP-INDPH** is hypsochromically shifted (~25 nm) compared to the λ_{max} of the CT band of the solution of **DBr-BDP-INDPH**.

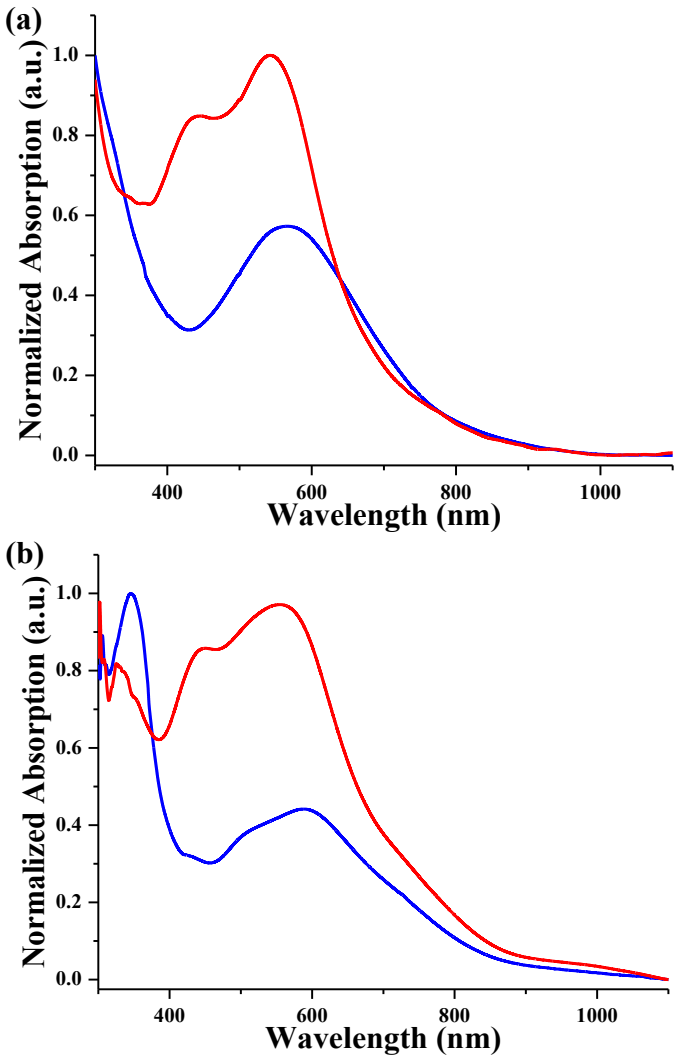

Figure 3.35 Absorption spectra of indophenine polymers **DBr-BDP-INDPH** (blue solid line) and **NBP-INDPH** (red solid line); (a) in chloroform solution and (b) in the film state.

In the film state, the absorption spectra of both of the quinoidal polymers (Figure 3.35b) exhibited bathochromic shifting of the absorption maxima of the CT bands compared to the absorption spectra in the solution state, however, the absorption behaviour exhibits the same trend as the absorption in solution. The bathochromic shift of ~58 nm is observed in the absorption edge of **NBP-INDPH** (Figure 3.35b; red solid

line) with a broadening of the CT band, while that in the case of **DBr-BDP-INDPH** (Figure 3.35b; blue solid line) is ~45 nm, compared to the solution absorption spectra. The bathochromic shifts in the λ_{max} of the CT bands and the absorption edges can be ascribed to the possible J-type aggregation of polymeric chains in the solid state.[94,113] The CT band of the **NBP-INDPH** (Figure 3.35b; red solid line) in the film state exhibited slightly bathochromically shifted (~17 nm) absorption maximum of 558 nm, with a shoulder peak appearing at 448 nm, compared to its solution state absorption spectrum.

The BDP-based indophenine polymer **DBr-BDP-INDPH** (Figure 3.33b; blue solid line) exhibited dual band absorption spectrum in the film state; first absorption band, corresponding to the π–π^* transitions, appeared at 345 nm and extending up to 450 nm, while the second band, corresponding to the charge transfer transitions, is ranging from 451 nm to 1000 nm, having the bathochromically shifted (~24 nm) absorption maxima of 590 nm, and a shoulder peak appearing at 510 nm. The optical band-gaps of the synthesized indophenine polymers were calculated from the absorption edges in the film state and were found to be in following order: **NBP-INDPH** (1.35 eV) < **DBr-BDP-INDPH** (1.37 eV). The photo-physical properties of the synthesized polymers are summarized in Table 3.1.

Table 3.1 Photo-physical properties of fused bi-isatyls and indophenine polymers, decomposition temperature T_d (obtained from TGA), Molecular weight M_w and poly-dispersity index (obtained from GPC analysis) of indophenine polymers; [a] calculated using equation $E_g^{opt} = 1240/\lambda_{edge}$.

Compound	λ_{max}^{soln} (nm)	λ_{max}^{film} (nm)	λ_{edge}^{film} (nm)	$E_g^{opt\ a}$ (eV)	T_d (°C)	M_w (Dalton)	PDI
DBr-DDBDP-BIs	340, 569	345, 460, 495	697	1.78	204	--	--
DTNBP-BIs	320, 517	310, 510, 559	785	1.58	270	--	--
DBr-BDP-INDPH	566	345, 510, 590	905	1.37	229	13973	2.76
NBP-INDPH	443, 541	448, 558	919	1.35	214	10819	1.30

Electrochemical properties of monomers

The frontier orbital energy levels of the synthesized novel fused bi-isatyls were measured using cyclic voltammetry (CV). CV experiments were performed in the dry

acetonitrile using TBAPC as a supporting electrolyte (~50 mM) using a three electrode system: a Pt disc electrode as the working electrode, a Pt wire electrode as the counter electrode and Ag/Ag^+ as the reference electrode. The synthesized fused bi-isatyls, **DBr-DDBDP-BIs** and **DTNBP-BIs**, were dissolved in dry acetonitrile (~5 mM), degassed with nitrogen gas and were subjected to the CV measurements.

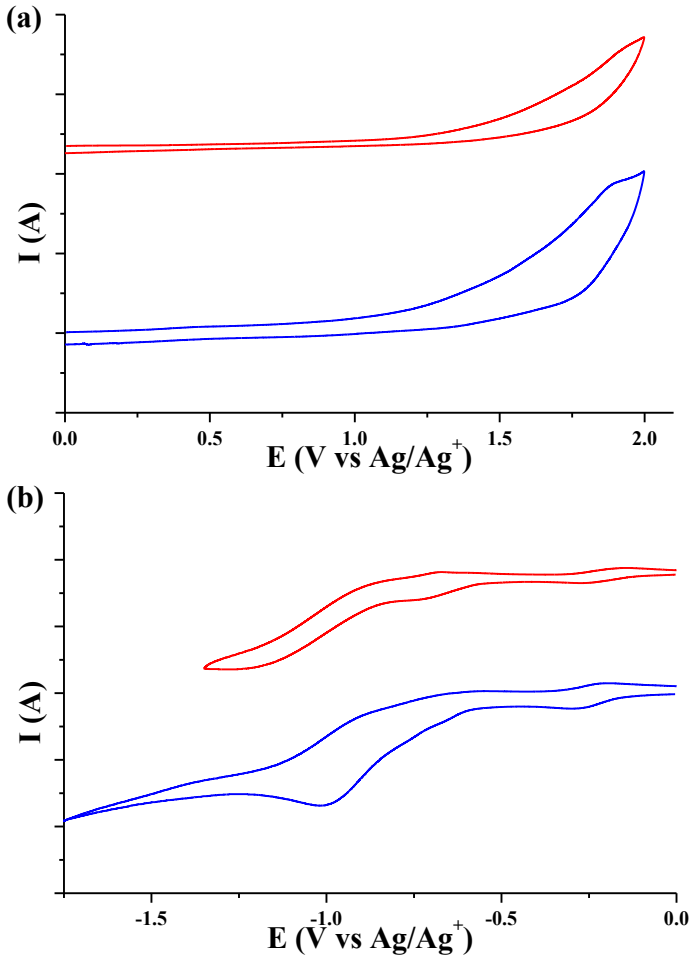

Figure 3.36 Cyclic voltammogram of **DBr-DDBDP-BIs** (blue solid line) and **DTNBP-BIs** (red solid line); (a) oxidation wave and (b) reduction wave; scanned at 50 mV/s in dry acetonitrile using TBAPC as a supporting electrolyte; $E_{onset\ (Fc/Fc+)}$ = 0.36 V

Both of the monomers showed irreversible oxidation and reduction waves in the cyclic voltammogram (Figure 3.36a and b). The oxidation potentials of **DBr-DDBDP-BIs** and **DTNBP-BIs** were measured from the oxidation wave and were found to be at +1.89 V and +1.91 V, respectively with onset oxidation potentials of +1.11 V and +1.16 V, respectively (Figure 3.36a). The corresponding HOMO energy levels were calculated from the onset oxidation potentials. The HOMO energy level of **DBr-DDBDP-BIs** was found to be at −5.55 eV, while that of **DTNBP-BIs** was found to be at −5.60 eV. The lowering of the HOMO energy level can be ascribed to the superior

electron withdrawing properties of fused pyrrolodione (pyrrole-2,3-dione and pyrrole-6,7-dione in case of **DBr-DDBDP-BIs** and pyrrole-2,3-dione and pyrrole-8,9-dione in case of **DTNBP-BIs**) rings. The reduction potentials of **DBr-DDBDP-BIs** and **DTNBP-BIs** were measured from the reduction wave and were found to be at −1.01 V and −0.71 V, respectively with onset reduction potentials of −0.60 V and −0.51 V, respectively (Figure 3.36b). The LUMO energy levels were calculated using equation: $E_{LUMO} = E_{HOMO} + E_{opt}$ and were found to be at −3.77 eV and −4.02 eV, respectively for **DBr-DDBDP-BIs** and **DTNBP-BIs**. The electrochemical properties of the synthesized fused bi-isatyls are summarized in Table 3.2.

Electrochemical properties of polymers

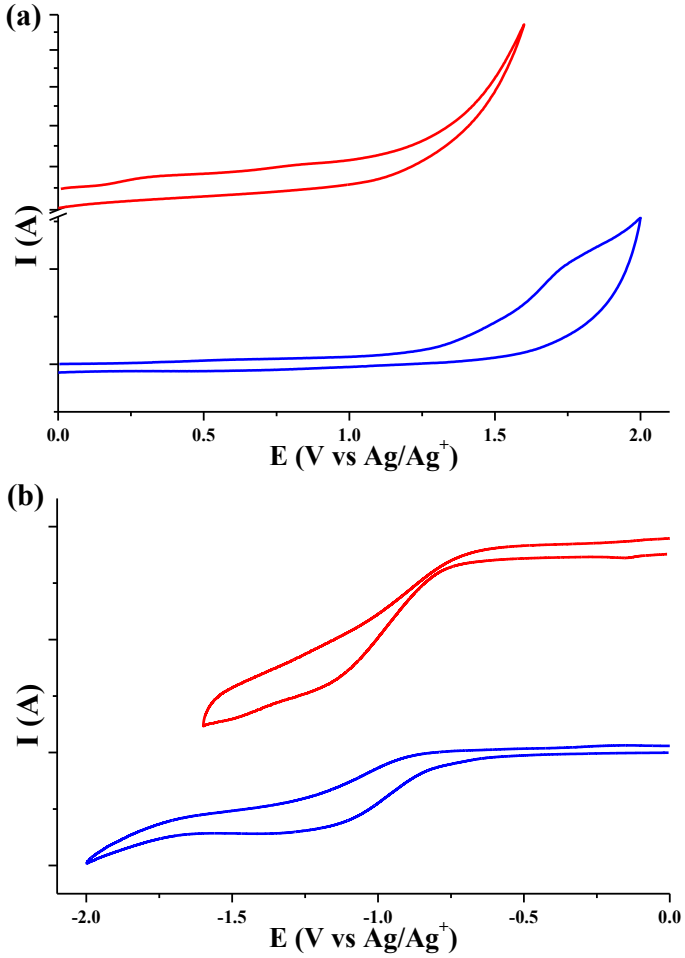

Figure 3.37 Cyclic voltammogram of **DBr-BDP-INDPH** (blue solid line) and **NBP-INDPH** (red solid line); (a) oxidation wave and (b) reduction wave; scanned at 50 mV/s in dry acetonitrile using TBAPC as a supporting electrolyte; $E_{onset\ (Fc/Fc+)}$ = 0.36 V

The frontier orbital energy levels of the synthesized indophenine polymers were measured using cyclic voltammetry (CV). CV experiments were performed in the dry acetonitrile using TBAPC as a supporting electrolyte (~50 mM) using a three electrode

system: a Pt disc electrode as the working electrode, a Pt wire electrode as the counter electrode and Ag/Ag^+ as the reference electrode. The BDP and NBP-based indophenine polymers, **DBr-BDP-INDPH** and **NBP-INDPH**, were dissolved in dry acetonitrile (~5 mM), degassed with nitrogen gas and were subjected to the CV measurements.

Both of the indophenine polymers showed irreversible oxidation and reduction waves in the cyclic voltammogram (Figure 3.37a and b). The oxidation potential of **DBr-BDP-INDPH** was measured from the oxidation wave and was found to be at +1.72 V, while the oxidation potential of the NBP-based indophenine polymer, **NBP-INDPH** was not obtained from its oxidation wave, due to the unresolved oxidation peak. However, the onset oxidation potentials of +1.21 V and +1.19 V, respectively for **DBr-BDP-INDPH** and **NBP-INDPH** were measured from the oxidation wave (Figure 3.37a). The corresponding HOMO energy levels were calculated from the onset oxidation potentials. The HOMO energy level of **DBr-BDP-INDPH** was found to be at −5.65 eV, while that of **NBP-INDPH** was found to be at −5.63 eV. The lowering of the HOMO energy level can be ascribed to the superior electron withdrawing properties of fused lactam rings of the bi-isatyl units. Moreover, the HOMO energy levels of indophenine polymers are elevated compared to the HOMO energy levels of the fused bi-isatyls, owing to the electron-rich quinoidal bithiophene units. The reduction potentials of **DBr-BDP-INDPH** and **NBP-INDPH** were measured from the reduction wave and were found to be at −1.16 V and −1.14 V, respectively with onset reduction potentials of −0.54 V and −0.65 V, respectively (Figure 3.37b). The LUMO energy levels were calculated using equation: $E_{LUMO} = E_{HOMO} + E_{opt}$ and were found to be at −4.28 eV, for both **DBr-BDP-INDPH** and **NBP-INDPH**. The electrochemical properties of the synthesized fused bi-isatyls are summarized in Table 3.2.

Table 3.2 Electrochemical properties of synthesized monomers and polymers; [a] potential v/s Ag/Ag^{+}; [b] calculated from equation $E_{HOMO} = -(E_{oxi,onset} + 4.8 - E_{onset\ (Fc/Fc+)})$; [c] calculated from equation $E_g^{el} = E_{LUMO} - E_{HOMO}$; [d] unresolved peak.

Compound	E_{oxi} [a] (V)	$E_{oxi,onset}$ [a] (V)	E_{HOMO} [b] (eV)	E_{red} [a] (V)	$E_{red,onset}$ [a] (V)	E_{LUMO} [b] (eV)	E_g^{el} [c] (eV)
DBr-DDBDP-BIs	+ 1.89	+ 1.12	− 5.55	− 1.01	− 0.60	− 3.84	1.71
DTNBP-BIs	+ 1.91	+ 1.18	− 5.60	− 0.71	− 0.51	− 3.93	1.67
DBr-BDP-INDPH	+ 1.72	+ 1.06	− 5.65	− 1.16	− 0.54	− 3.90	1.75
NBP-INDPH	--[d]	+ 0.97	− 5.63	− 1.14	− 0.65	− 3.79	1.84

Organic Field Effect Transistor (OFET) device characterization of polymers

To study the field effect transistor performance of quinoidal indophenine polymers, organic field-effect transistors (OFETs) with bottom-gate/top-contact (BG/TC) configurations were fabricated by spin coating. The active polymer films were coated onto the polyvinyl alcohol (PVA) dielectric layer, supported on bottom FTO gate electrode using 15 mg/mL dichlorobenzene solution of **DBr-BDP-INDPH** as well as 15 mg/mL THF solution of **NBP-INDPH** using spin coater at 1000 rpm for 30 s. The films were dried at room temperature under nitrogen atmosphere. The aluminium (Al) source and drain contacts were deposited onto the active layer *via* thermal deposition. The device architecture is shown in Figure 3.38.

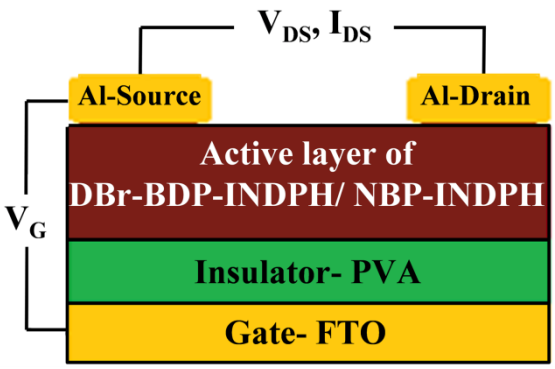

Figure 3.38 Indophenine polymers-based OFET device architecture with bottom-gate/top-contact (BG/TC) configuration

The field effect mobilities were calculated at the saturation region using the gradual channel approximation equations

$$I_{DS} = ({}^{W}/_{2L})\mu C_i(V_G - V_{th})^2$$

Where L is the channel length, W is the channel width, C_i is the capacitance per unit area of the gate dielectric layer, and V_{th} is the threshold voltage. The transfer characteristics of the as-spun films of **DBr-DDBDP-INDPH** and **NBP-INDPH** at room temperature are shown in Figure 3.38. The output characteristics showed a linear regime at low voltage and a current saturation regime at high voltage. Additionally, in good accordance with the low band gap and amphoteric redox properties of the quinoidal polymers discussed above, the OFETs based on both **DBr-DDBDP-INDPH** and **NBP-INDPH** films showed the V-shaped transfer characteristics of typical ambipolar transistors as illustrated in Figure 3.38.

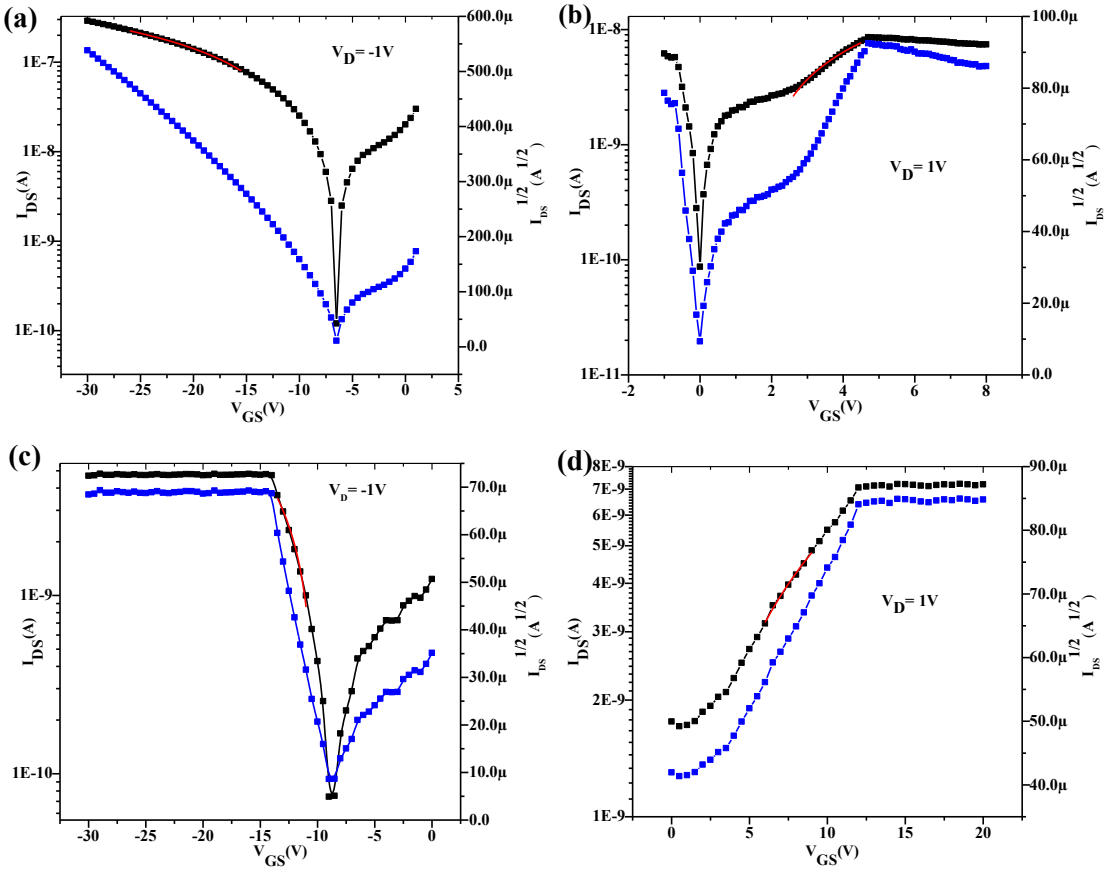

Figure 3.39 Transfer characteristics of OFETs based on as-spun films of (a, b) **DBr-BDP-INDPH** and (c, d) **NBP-INDPH**; (a) and (c) showing transfer characteristics of p-type OFET device while (b) and (d) showing transfer characteristics of n-type OFET device

The hole and electron mobilities were extracted from the saturation regime of the transfer curve, as shown in Figure 3.38. The as-spun film of the **DBr-DDBDP-INDPH** exhibited p-channel dominant ambipolar semiconducting behaviour with high hole and moderate electron mobilities of 0.02 and 0.004 $cm^2V^{-1}s^{-1}$, respectively while **NBP-INDPH** film showed moderate but balanced ambipolar semiconducting behaviour with hole and electron mobilities of 0.001 and 0.0009 $cm^2V^{-1}s^{-1}$, respectively. Such enhanced mobilities of as-spun polymer films were considered to be due to an improved delocalisation of π-electrons and quinoidal backbone formation, providing mobilities comparable or slightly higher than common dicyanomethylene (DCM) containing quinoidal molecules. As mentioned above in the CV results, the two polymers showed almost identical energy levels and electron densities of the HOMO and LUMO frontier molecular orbitals. Therefore, lower mobilities of **NBP-INDPH** polymer can be ascribed to the presence of bulkier central naphthalene ring unit, causing steric hindrance to the adjacent thiophenes, which in turn leads to the twisting of the polymer backbone.

Conclusion

The famous indophenine reaction is mimicked with our synthesized BDP and NBP-based novel fused bi-isatyls 4,5-dibromo-1,8-didodecyl-1,8-dihydropyrrolo[3,2-*g*]indole-2,3,6,7-tetraone (**DBr-DDBDP-BIs**) and 1,10-ditetradecyl-1,10-dihydrobenzo[*e*]pyrrolo[3,2-*g*]indole-2,3,8,9-tetraone (**DTNBP-BIs**) by exploring β-keto positions to form BDP and NBP-based novel indophenine polymers **DBr-BDP-INDPH** and **NBP-INDPH** (*via* cationic polymerization) having quinoidal backbone. The synthesized indophenine polymers showed moderate to good solubility properties in the common organic solvents, sufficiently high thermal stabilities and good film forming properties. Both of the synthesized polymers were characterized and studied photophysically and electrochemically. Both indophenine polymers showed good absorptivities in the visible and near IR region of the solar spectrum and very low optical band-gaps. Moreover, in the solid state, the polymers exhibited bathchromically shifted absorption edges due to the π-π stacking between the polymer chains. Electrochemical studies revealed that the indophenine polymers exhibits lowered HOMO (below −5.40 eV) and LUMO (below −4.00 eV) energy levels and low electrochemical band-gaps compared to the synthesized fused bi-isatyl monomers owing to the extended delocalisation of π-electrons and quinoidal backbone formation.

The synthesized indophenine polymer **DBr-BDP-INDPH** exhibited p-channel dominant ambipolar semiconducting behaviour with hole and electron mobilities of 0.02 and 0.004 $cm^2V^{-1}s^{-1}$ for its as-spun films while NBP-INDPH showed somewhat lowered but balanced ambipolar semiconducting behaviour with hole and electron mobilities of 0.001 and 0.0009 $cm^2V^{-1}s^{-1}$ for its as-spun films in consequence of the twisted quinoidal polymer backbone.

Experimental procedures

General procedures

All the chemicals were reagent grade and used as purchased. Moisture-sensitive reactions were performed under an inert atmosphere of dry nitrogen with dried solvents. Reactions were monitored by thin-layer chromatography (TLC) using Merck 60 F_{254} aluminium-coated plates and the spots were visualized under ultraviolet (UV) light. Column chromatography was carried out on silica gel (60–120 mesh). NMR spectra were recorded on a Bruker Avance-III 400 spectrometer in $CDCl_3$ and DMSO-D_6. The high resolution mass spectra were recorded on Xevo G2-XS QTOF Mass Spectrometer. UV-Visible absorption spectra were recorded on Jasco V-630 spectrophotometer using quartz cuvette. CV data were obtained with CH Instruments model of CHI 600E with three electrode (Glassy carbon as the working electrode, platinum as the counter electrode, and nonaqueous $Ag/AgNO_3$ as the reference electrode) cells in anhydrous acetonitrile solution containing 50 mM tetra-*n*-butylammoniumperchlorate at a scan rate of 50 mV/s. Molecular weights of the polymer samples were measured with Agilent 1260 Infinity GPC instrument, equipped with RI detector. Polystyrene was used as a calibration standard. Polymer samples (~5 mg) were dissolved in THF (~5 mL) and were filtered through a 0.2 μ filter. The analysis was done using THF as an eluent at a flow rate of 1-2 mL/min. Thermo-Gravimmetric Analysis (TGA) of the polymer was done on Exstar SII TG/DTA 6300 using N_2 as inert gas.

Synthesis of monomers

The synthesis and characterization of the polycyclic fused aromatic pyrrole-based building block 1,8-dihydropyrrolo[3,2-*g*]indole (**BDP**) has been discussed thoroughly in the Chapter 2. Its *N*-alkylated derivative 1,8-didodecyl-1,8-

dihydropyrrolo[3,2-*g*]indole (**DDBDP**) has been synthesized according to the similar procedure for *N*-alkylation of BDP, discussed in Chapter 2.

Synthesis of 1,8-didodecyl-1,8-dihydropyrrolo[3,2-*g*]indole (**DDBDP**): The **BDP** (1.64 g, 10.51 mmol) was dissolved in DMF (50 mL). To this was added sodium hydroxide flakes (4.20 g, 105.12 mmol) and the resulting suspension was stirred at room temperature for 10 min. To this stirred solution was added, *n*-dodecyl bromide (16.4 mL, 68.33 mmol) dropwise over a period of 5 min. After the complete addition, reaction mixture was stirred at 80 ^{o}C for 3 h and monitored by TLC. After completion of the reaction, as indicated by TLC, 200 mL of water was added to it and extracted with aliquots of dichloromethane (2 X 50 mL). Combined organic layers are washed with saturated brine solution, finally with water and dried over $MgSO_4$. Crude product is obtained after evaporation of solvent which is subjected to the column chromatography over silica gel using petroleum ether as eluent. The pure product **DDBDP** is separated by column chromatography, yielding yellowish oil from the later fractions from the column.

1,8-didodecyl-1,8-dihydropyrrolo[3,2-*g*]indole (**DDBDP**): Yellowish oil (2.02 g, 39%); ^{1}H NMR (400 MHz, $CDCl_3$): 7.37 (s, 1H), 7.01−7.02 (d, J = 2.8 Hz, 1H), 6.63−6.64 (d, J = 3.2 Hz, 1H), 4.34−4.38 (t, J = 7.6 Hz, 2H), 1.85−1.90 (m, 2H), 1.26−1.36 (m, 18H), 0.91−0.94 (t, J = 7.2 Hz, 3H). ^{13}C NMR (100 MHz, $CDCl_3$): 127.6, 127.0, 124.3, 114.4, 103.6, 50.9, 32.0, 31.3, 29.7, 29.6, 29.5, 29.4, 29.3, 26.7, 22.8, 14.2. HRMS (ES+): $C_{34}H_{57}N_2$ requires 493.4522, found 493.4528. IR (NaCl plate, cm^{-1}): 3020.6, 2927.9, 2855.1, 2400.7, 1599.9, 1524.1, 1424.0, 1215.6, 1019.9, 928.5, 759.2, 669.5, 451.8.

Synthesis of 4,5-dibromo-1,8-didodecyl-1,8-dihydropyrrolo[3,2-*g*]indole-2,3,6,7-tetraone (**DBr-DDBDP-BIs**) and 4,5,6,7-tetrabromo-1,8-didodecyl-1,8-dihydropyrrolo[3,2-*g*]indole-2,3-dione (**TBr-DDBDP-MIs**): The **DDBDP** (0.14 g; 0.29 mmol) was dissolved in the mixture of chloroform (3 mL) and DMF (20 mL) and stirred at room temperature. To this stirred solution, *tert*-butyl hydroperoxide (~70% aqueous solution, 0.6 mL; 2.92 mmol) was added and reaction mixture was allowed to stir at room temperature for 5 min. NBS (0.52 g; 2.92 mmol) was added to this stirred reaction mixture and up on addition of NBS, reaction mixture immediately turned into deep red coloured solution. After stirring the reaction mixture for 2 h, additional *tert*-butyl hydroperoxide (~70% aqueous solution, 0.3 mL; 1.46 mmol) and NBS (0.26 g;

1.46 mmol) was added and reaction was allowed to continue for 20 h. After completion, the reaction mixture was poured into the 400 mL of aqueous sodium thiosulphate solution and was stirred for about 30 min at room temperature. The resulting dark red-purple precipitates were filtered and washed with water for several times to remove traces of DMF and *tert*-butanol. The pure product **DBr-DDBDP-BIs** was obtained by washing the crude material with copious amounts of petroleum ether, leaving behind deep purple-black solid product. The combined petroleum ether washings were evaporated to dryness and the deep reddish brown solid product was subjected to the column chromatography over silica gel and eluting the pure product **TBr-DDBDP-MIs** as a red coloured band in 15% ethyl acetate-petroleum ether.

4,5-dibromo-1,8-didodecyl-1,8-dihydropyrrolo[3,2-*g*]indole-2,3,6,7-tetraone (**DBr-DDBDP-BIs**): Dark purple-black solids (0.05 g, 24%); ^{1}H NMR (400 MHz, $CDCl_3$): 3.94−3.97 (t, J = 7.2 Hz, 2H), 1.70 (br s, 2H), 1.23−1.28 (m, 18H), 0.87−0.90 (t, J = 7.2 Hz, 3H). ^{13}C NMR (100 MHz, $CDCl_3$): 179.8, 158.4, 136.0, 125.5, 122.5, 46.0, 31.9, 29.6, 29.6, 29.5, 29.3, 29.0, 27.6, 26.6, 22.7, 14.2. HRMS (ES+): $C_{34}H_{51}N_2O_4Br_2$ requires 709.2216, found 709.2210. IR (KBr, cm^{-1}): 3432.6, 2921.2, 2851.8, 1734.9, 1599.9, 1566.9, 1468.1, 1396.8, 1366.0, 1217.2, 771.9, 433.8.

4,5,6,7-tetrabromo-1,8-didodecyl-1,8-dihydropyrrolo[3,2-*g*]indole-2,3-dione (**TBr-DDBDP-MIs**): Dark red-brown solids (0.04 g, 16%); ^{1}H NMR (400 MHz, $CDCl_3$): 4.26−4.30 (t, J = 7.6 Hz, 2H), 3.92−3.96 (t, J = 8.0 Hz, 2H), 1.62−1.67 (m, 2H), 1.46−1.53 (p, J = 7.6 Hz, 2H), 1.20−1.30 (m, 34H), 1.09−1.11 (m, 2H), 0.87−0.90 (t, J = 7.2 Hz, 6H). ^{13}C NMR (100 MHz, $CDCl_3$): 178.0, 162.5, 141.3, 135.4, 130.7, 125.1, 118.1, 115.5, 112.6, 100.1, 50.9, 47.4, 31.9, 29.8, 29.6, 29.6, 29.5, 29.4, 29.4, 29.3, 29.3, 28.9, 28.9, 28.0, 26.7, 26.3, 22.7, 14.2. HRMS (ES+): $C_{34}H_{51}N_2O_2Br_4$ requires 835.0684, found 835.0670.

The synthesis and the characterization of the polycyclic fused aromatic pyrrole-based building block 1,10-dihydrobenzo[*e*]pyrrolo[3,2-*g*]indole (**NBP**) has been discussed thoroughly in the Chapter 2. Its *N*-alkylated derivative 1,10-ditetradecyl-1,10-dihydrobenzo[*e*]pyrrolo[3,2-*g*]indole (**DTNBP**) has been synthesized according to the similar procedure for *N*-alkylation of NBP, discussed in Chapter 2.

Synthesis of 1,10-ditetradecyl-1,10-dihydrobenzo[*e*]pyrrolo[3,2-*g*]indole (**DTNBP**): The **NBP** (1.10 g, 5.34 mmol) was dissolved in DMF (107 mL). To this was

added sodium hydroxide flakes (1.49 g, 37.4 mmol) and the resulting suspension was stirred at room temperature for 10 min. To this stirred solution was added, *n*-tetradecylbromide (8 mL, 26.7 mmol) dropwise over a period of 5 min. After the complete addition, reaction mixture was stirred at 80 ^{o}C for 3 h and monitored by TLC. After completion of the reaction, as indicated by TLC, 400 mL of water was added to it and extracted with aliquots of dichloromethane (2 X 50 mL). Combined organic layers are washed with saturated brine solution, finally with water and dried over $MgSO_4$. Crude product is obtained after evaporation of solvent which is subjected to the column chromatography over silica gel using 1% ethyl acetate-petroleum ether as eluent. The pure product **DTNBP** was obtained as off white crystalline solids.

1,10-ditetradecyl-1,10-dihydrobenzo[*e*]pyrrolo[3,2-*g*]indole (**DTNBP**): Off white solids (1.60 g, 50%); ^{1}H NMR (400 MHz, $CDCl_3$): 8.20−8.23 (dd, J_1 = 6.4 Hz, J_2 = 3.6 Hz, 1H), 7.44−7.46 (dd, J_1 = 6.0 Hz, J_2 = 3.2 Hz, 1H), 7.11−7.12 (d, J = 2.8 Hz, 1H), 7.05−7.06 (d, J = 3.2 Hz, 1H), 4.36-4.40 (t, J = 7.6 Hz, 2H), 1.82-1.89 (m, 2H), 1.22-1.30 (m, 22H), 0.89-0.92 (t, J = 6.8 Hz, 3H). ^{13}C NMR (100 MHz, CDCl3): 126.6, 125.2, 123.8, 123.5, 123.2, 122.8, 102.6, 51.0, 31.9, 31.2, 29.7, 29.6, 29.6, 29.5, 29.4, 29.4, 29.2, 26.7, 22.7, 14.1. HRMS (ES+): $C_{42}H_{67}N_2$ requires 599.5304, found 599.5302. IR (KBr, cm^{-1}): 3433.5, 2950.1, 2916.6, 2850.8, 1580.8, 1471.1, 1375.0, 1353.8, 1289.7, 754.8, 721.7, 599.2.

Synthesis of 1,10-ditetradecyl-1,10-dihydrobenzo[*e*]pyrrolo[3,2-*g*]indole-2,3,8,9-tetraone (**DTNBP-BIs**): The **DTNBP** (0.52 g, 0.87 mmol) was dissolved in the mixture of DMF (240 mL) and chloroform (80 mL) and was allowed to stir for 5 min. To this stirred solution, was added NBS (3.09 g, 17.4 mmol) in a single portion and resulting reddish-brown reaction mixture was allowed to stir at room temperature for 96 h. After completion of the reaction, the reaction mixture was poured into 800 mL of de-ionized water and resulting mixture was stirred at room temperature for 2 h. The crude product was extracted using chloroform (2 X 50 mL) and combined organic extracts were washed with water (2 X 100 mL), brine (1 X 100 mL), dried over anhydrous sodium sulphate and evaporated to dryness under reduced pressure to yield dark red-brown precipitates. Finally the crude precipitates were washed with small amounts of petroleum ether to remove the by-products and impurities, leaving behind the pure product **DTNBP-BIs** as dark purple-black amorphous solids.

1,10-ditetradecyl-1,10-dihydrobenzo[*e*]pyrrolo[3,2-*g*]indole-2,3,8,9-tetraone (**DTNBP-BIs**): Dark purple-black amorphous solids (0.13 g; 24%); ^{1}H NMR (400 MHz, $CDCl_3$): 8.75−8.78 (dd, J_1 = 6.4 Hz, J_2 = 3.2Hz, 1H), 7.64−7.66 (dd, J_1 = 6.8 Hz, J_2 = 3.6 Hz, 1H), 3.94−3.98 (t, J = 7.6 Hz, 2H), 1.74 (br s, 2H), 1.20−1.27 (m, 22H), 0.87−0.90 (t, J = 6.8 Hz, 3H). ^{13}C NMR (100 MHz, $CDCl_3$): 183.0, 160.5, 141.1, 130.8, 127.2, 123.7, 120.4, 46.3, 31.9, 29.7, 29.6, 29.6, 29.6, 29.4, 29.4, 29.3, 29.0, 27.8, 26.6, 22.7, 14.2. HRMS (ES+): $C_{42}H_{63}N_2O_4$ requires 659.4788, found 659.4787. IR (KBr, cm^{-1}): 3431.5, 2921.1, 2851.5, 1753.5, 1716.2, 1617.2, 1570.9, 1468.6, 1403.1, 1373.8, 1187.8, 1114.9, 752.9, 601.9, 436.2.

General procedure for the synthesis of indophenine polymers

The BDP and NBP-based indophenine polymers **DBr-BDP-INDPH** and **NBP-INDPH** were synthesized following the modification of the literature procedure reported by Tormos *et al*.[99] and Hwang *et al*.[94] The fused bi-isatyl (0.17 mmol, 1 eq.) was dissolved in 20 mL of anhydrous toluene and was allowed to stir at room temperature under nitrogen atmosphere for 5 min. To this stirred solution, thiophene (0.35 mmol, 2.1 eq.) was added dropwise and reaction mixture was stirred vigorously at room temperature for 5 min under nitrogen atmosphere. Concentrated sulphuric acid (0.5 mL) was added drop wise to this vigorously stirred reaction mixture at room temperature under inert atmosphere and resulting reaction mixture was stirred at 70 ^{o}C for 30 h. After completion of the reaction, the reaction mixture was poured into 200 mL of 0.2 M aqueous sodium hydroxide solution and was allowed to stir vigorously for 1 h. The crude polymer was extracted using chloroform (3 X 100 mL) and combined organic extracts were washed with water (2 X 100 mL), brine (1 X 100 mL), dried over the anhydrous sodium sulphate and evaporated to dryness under reduced pressure to afford dark purple-black solids. The sticky solids were triturated with petroleum ether and were filtered, washed with small amounts of petroleum ether and were subjected to the soxhlet extraction using petroleum ether, methanol and the pure polymer fraction was eluted using chloroform. The pure indophenine polymer was obtained by evaporating chloroform under reduced pressure and further dried under vacuum at 50 ^{o}C to yield dark purple-black solids.

BDP-based indophenine polymer **DBr-BDP-INDPH**: Dark purple-black solids (0.06 g, 42%); ^{1}H NMR (400 MHz, $CDCl_3$) δ: 7.15 (br s, 2H), 3.94 (br s, 2H), 2.34 (br s, 2H),

1.23 (br, 18H), 0.86 (br s, 3H). IR (KBr, cm^{-1}): 3405.4, 2956.8, 2925.2, 2856.1, 1726.3, 1685.5, 1596.7, 1555.8, 1456.2, 1304.4, 1179.4, 1118.8, 808.8, 771.2, 724.2.

NBP-based indophenine polymer **NBP-INDPH**: Dark purple-black solids (0.07 g, 52%); ^{1}H NMR (400 MHz, $CDCl_3$) δ: 8.63−8.85 (m, 1H), 8.06−8.50 (m, 1H), 7.39−8.05 (m, 2H), 7.13 (br, 1H), 3.94 (br s, 2H), 1.68 (br s, 2H), 1.23−1.38 (m, 22H), 0.88 (br s, 3H). IR (KBr, cm^{-1}): 3406.0, 2922.4, 2851.1, 1682.7, 1653.1, 1564.6, 1461.6, 1305.8, 1183.9, 1106.5, 756.7.

Spectral data

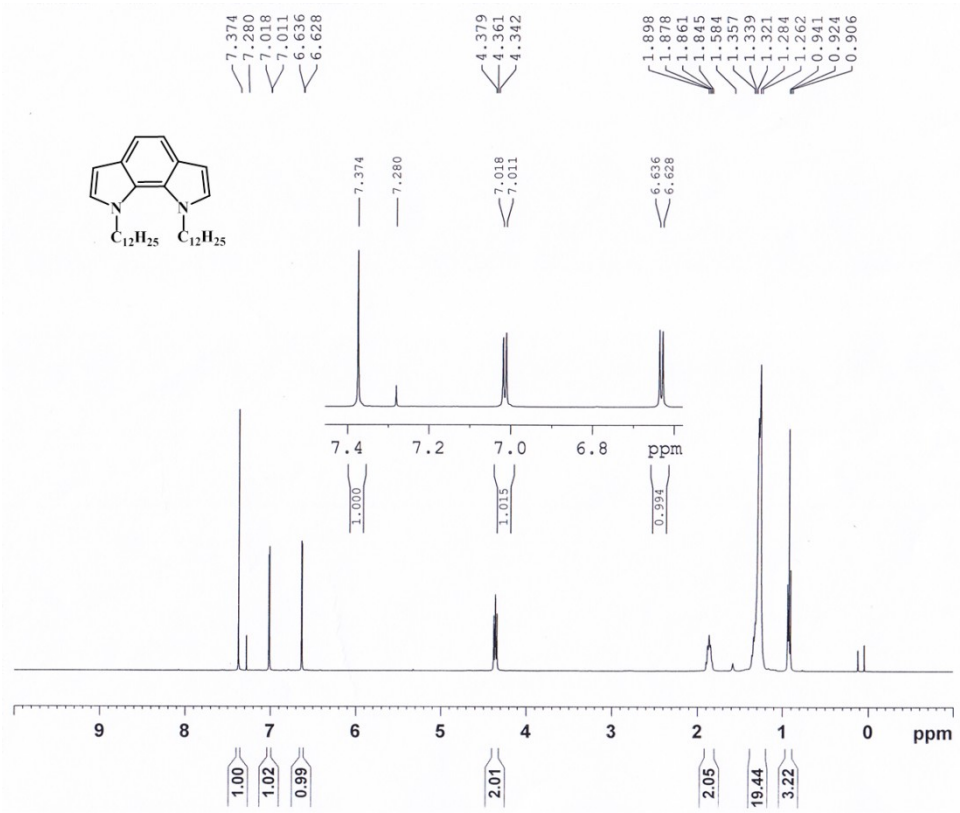

Figure 3.40 ^{1}H NMR spectrum of **DDBDP**

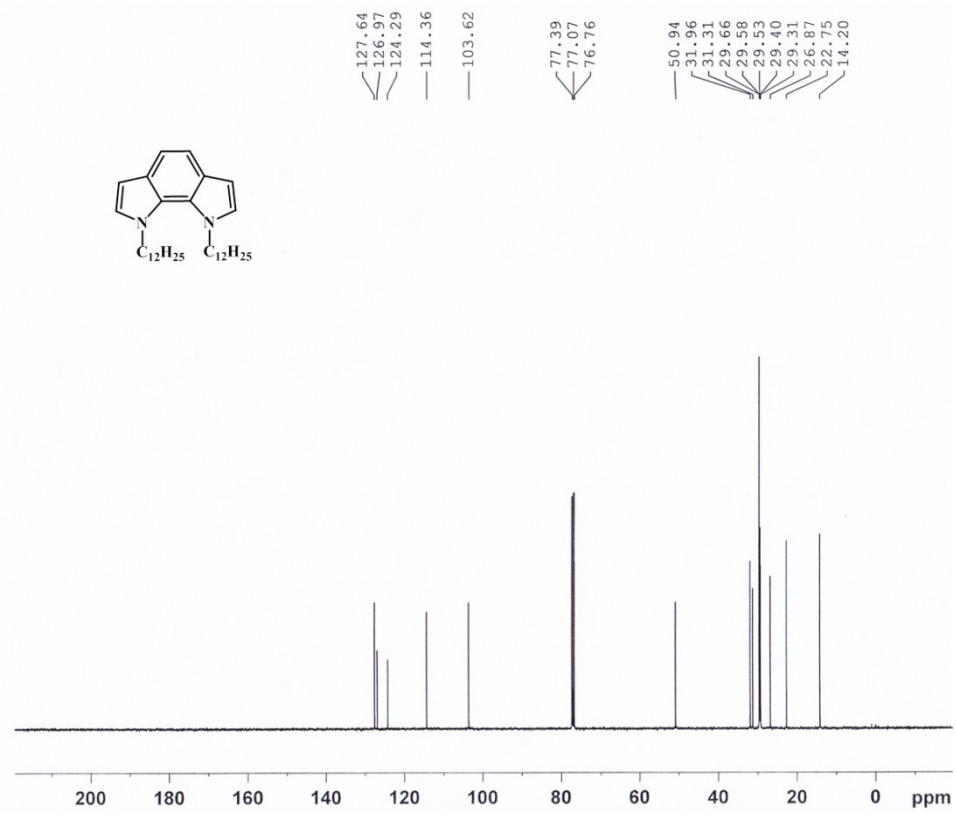

Figure 3.41 ^{13}C NMR spectrum of **DDBDP**

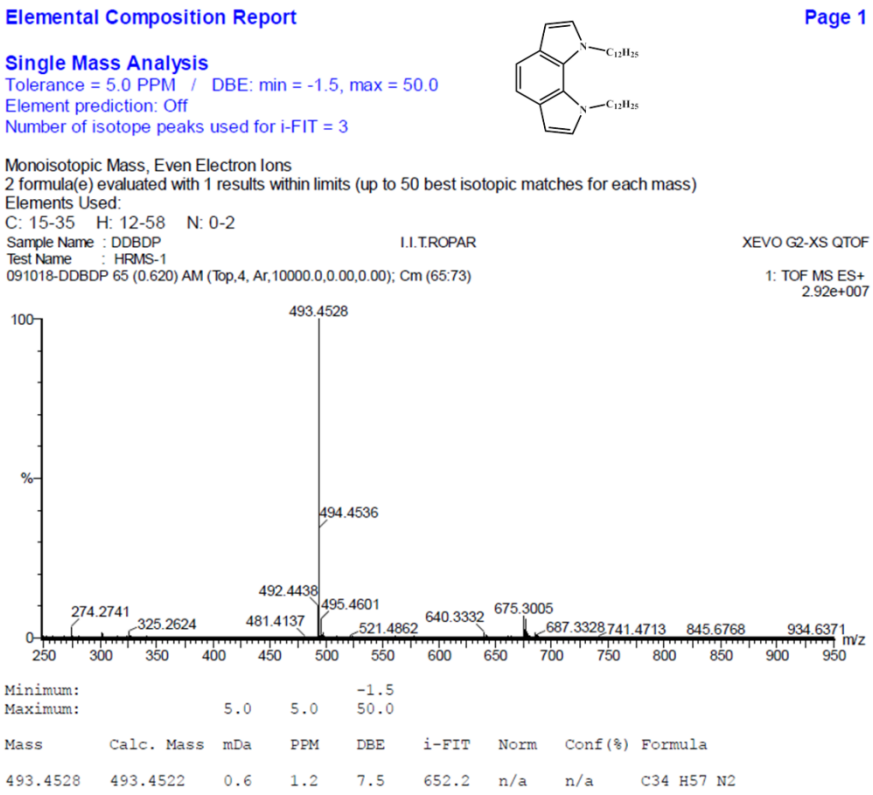

Figure 3.42 HRMS spectrum of **DDBDP**

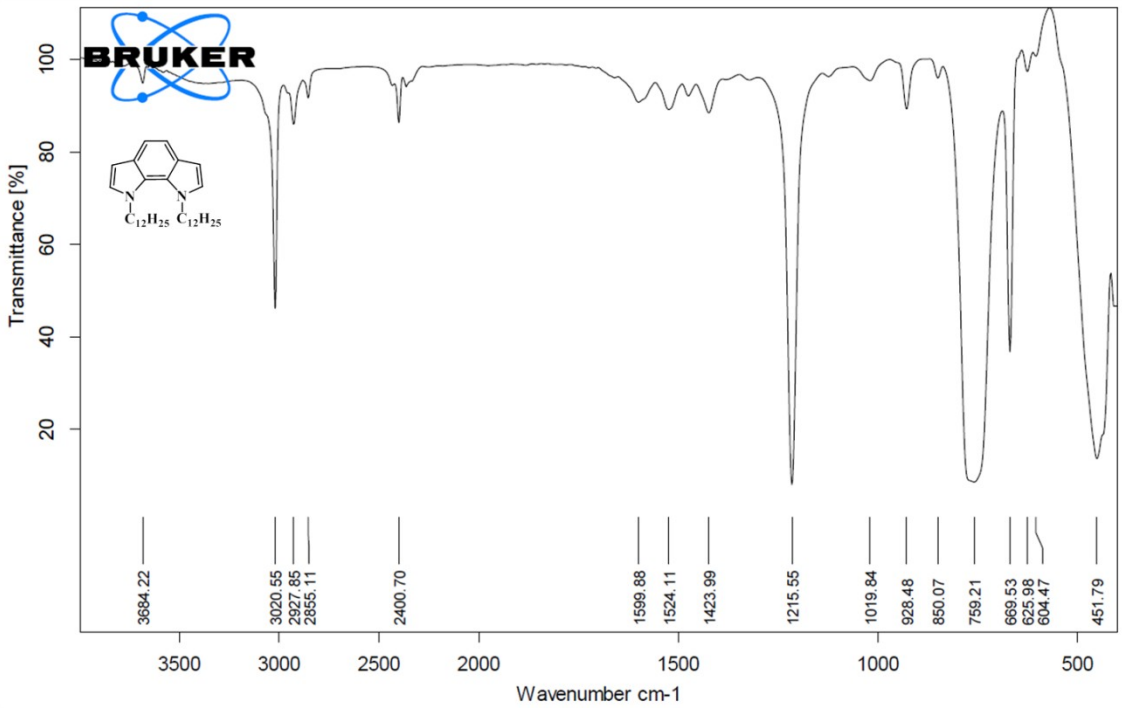

Figure 3.43 IR spectrum (NaCl plate) of **DDBDP**

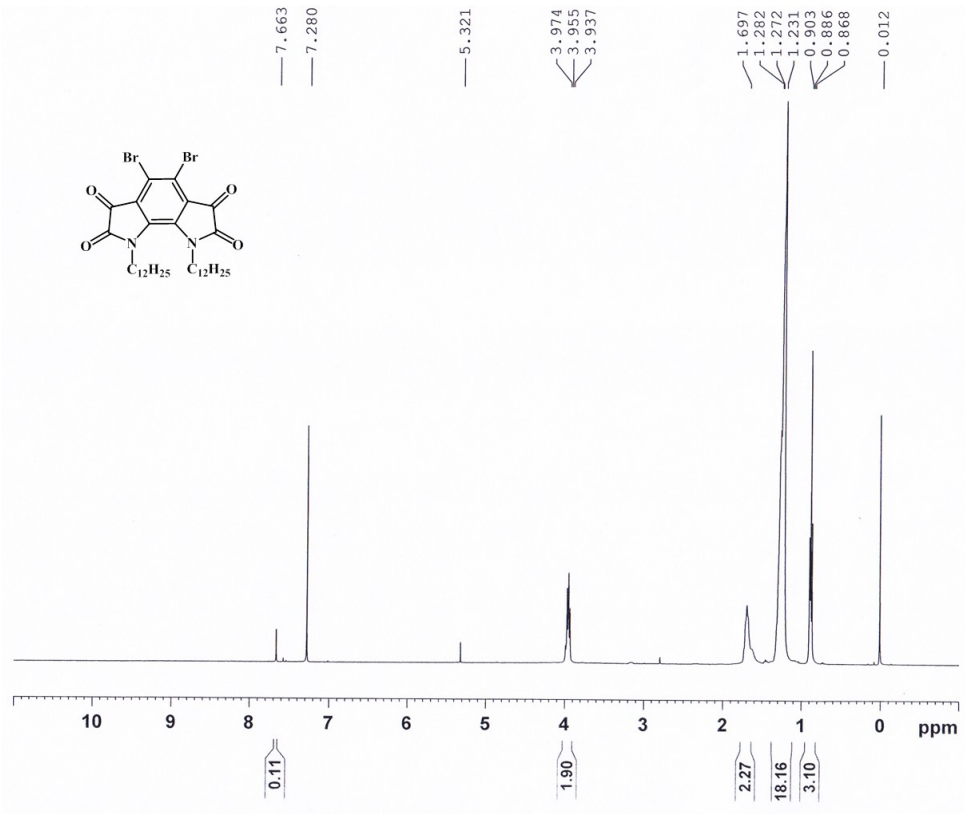

Figure 3.44 ^{1}H NMR spectrum of **DBr-DDBDP-BIs**

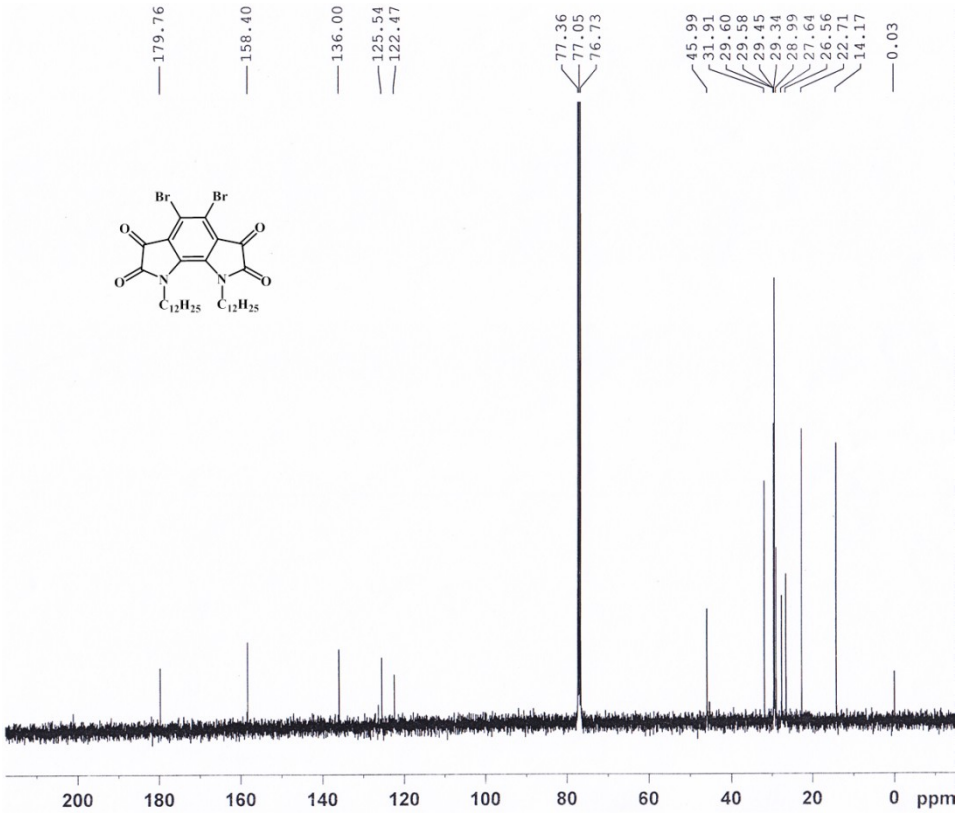

Figure 3.45 ^{13}C NMR spectrum of **DBr-DDBDP-BIs**

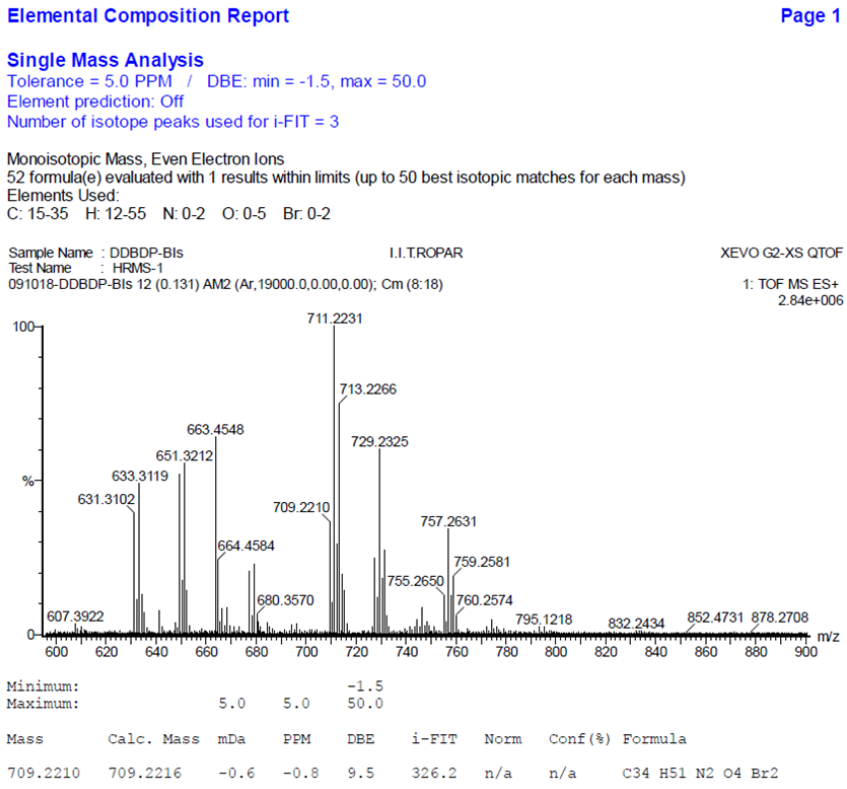

Elemental Composition Report Page 1

Single Mass Analysis
Tolerance = 5.0 PPM / DBE: min = -1.5, max = 50.0
Element prediction: Off
Number of isotope peaks used for i-FIT = 3

Monoisotopic Mass, Even Electron Ions
52 formula(e) evaluated with 1 results within limits (up to 50 best isotopic matches for each mass)
Elements Used:
C: 15-35 H: 12-55 N: 0-2 O: 0-5 Br: 0-2

Sample Name : DDBDP-BIs I.I.T.ROPAR XEVO G2-XS QTOF
Test Name : HRMS-1
091018-DDBDP-BIs 12 (0.131) AM2 (Ar,19000.0,0.00,0.00); Cm (8:18) 1: TOF MS ES+ 2.84e+006

Minimum:				-1.5				
Maximum:		5.0	5.0	50.0				
Mass	Calc. Mass	mDa	PPM	DBE	i-FIT	Norm	Conf(%)	Formula
709.2210	709.2216	-0.6	-0.8	9.5	326.2	n/a	n/a	C34 H51 N2 O4 Br2

Figure 3.46 HRMS spectrum of **DBr-DDBDP-BIs**

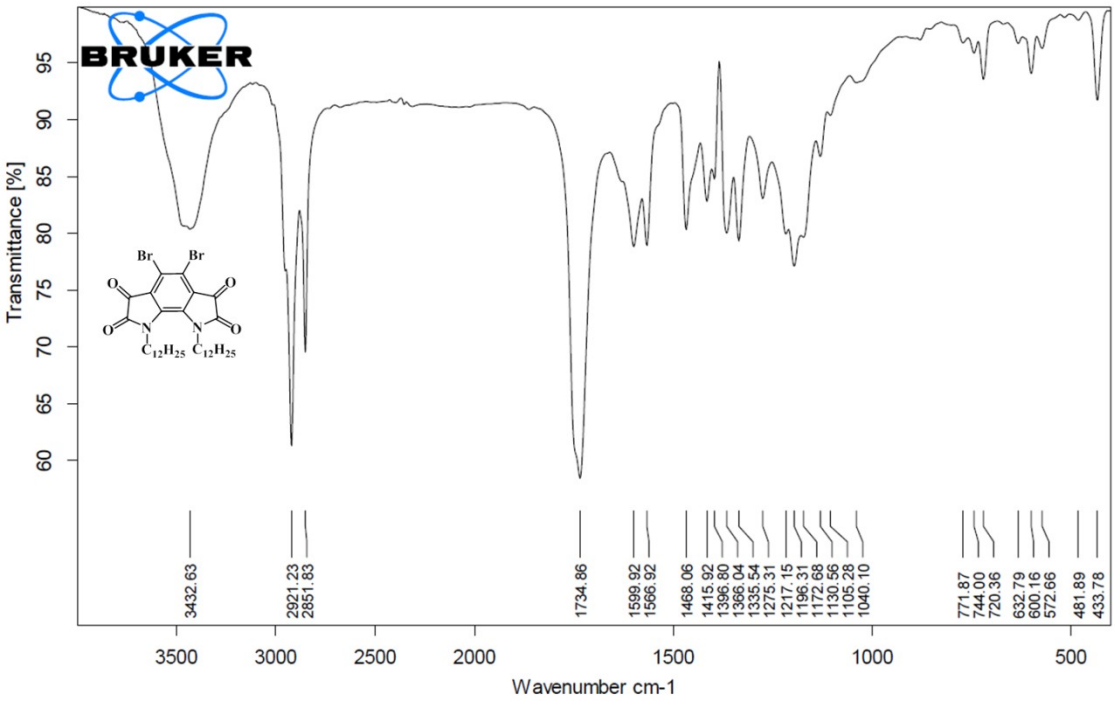

Figure 3.47 IR spectrum (KBr pellet) of **DBr-DDBDP-BIs**

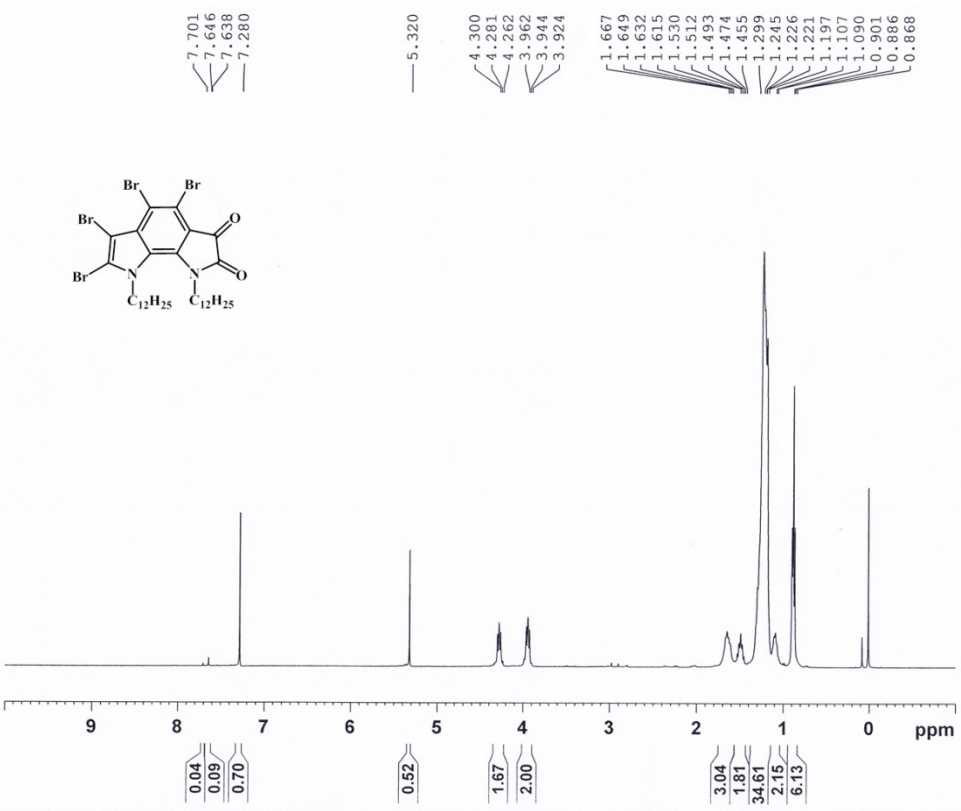

Figure 3.48 ^{1}H NMR spectrum of **TBr-DDBDP-MIs**

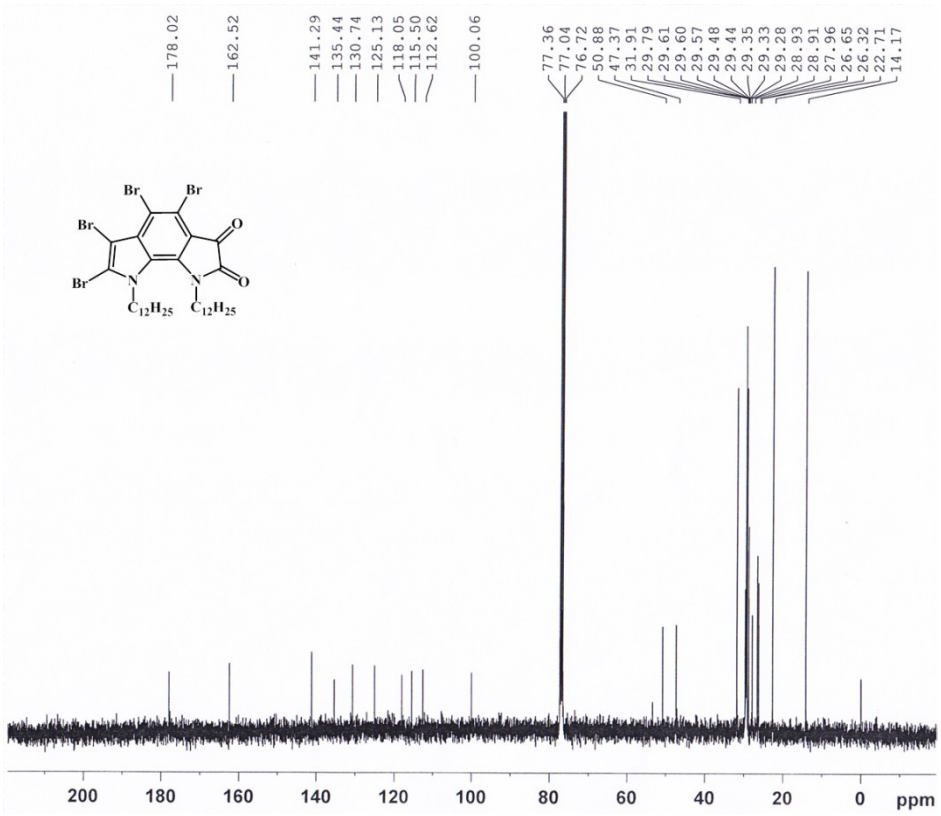

Figure 3.49 ^{13}C NMR spectrum of **TBr-DDBDP-MIs**

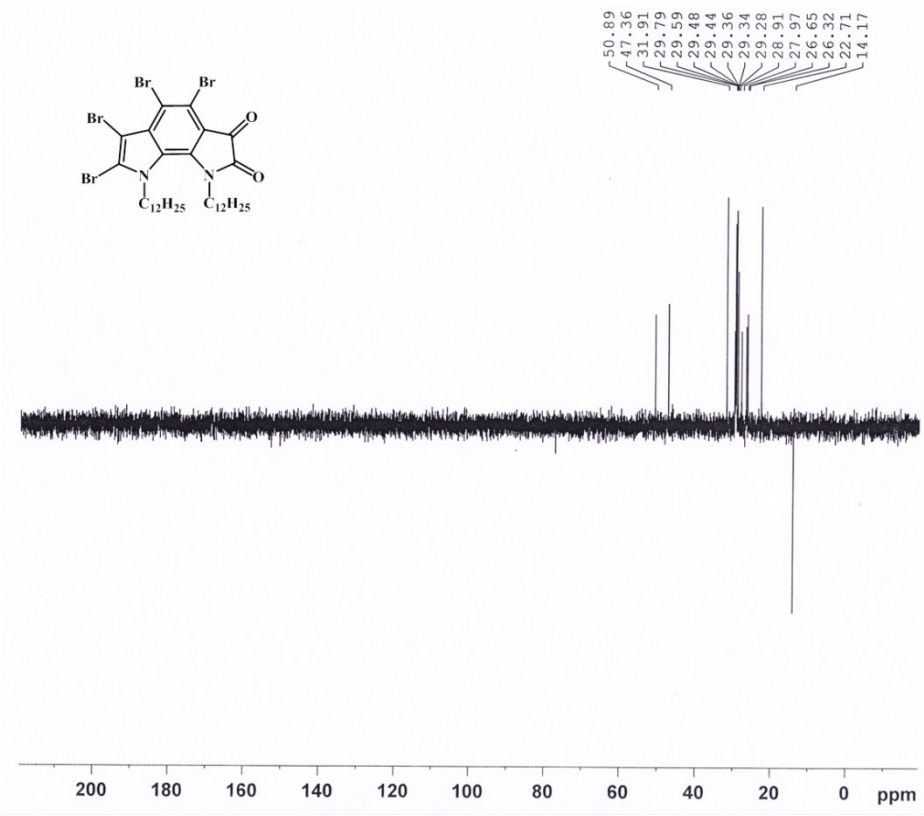

Figure 3.50 DEPT-135 NMR spectrum of **TBr-DDBDP-MIs**

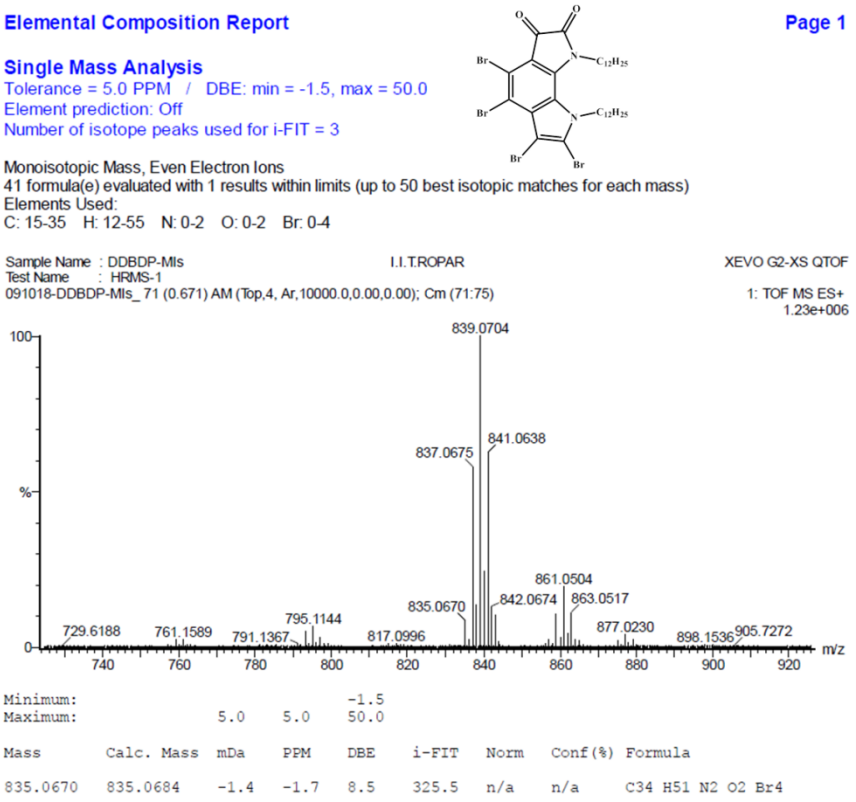

Figure 3.51 HRMS spectrum of **TBr-DDBDP-MIs**

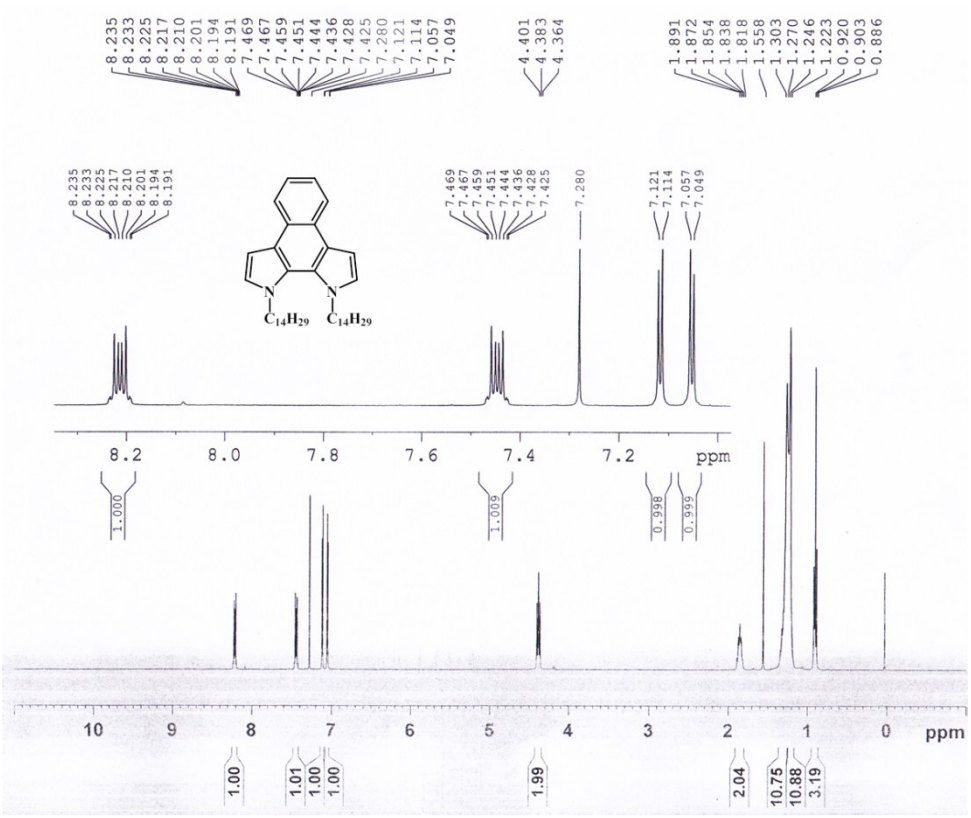

Figure 3.52 ^{1}H NMR spectrum of **DTNBP**

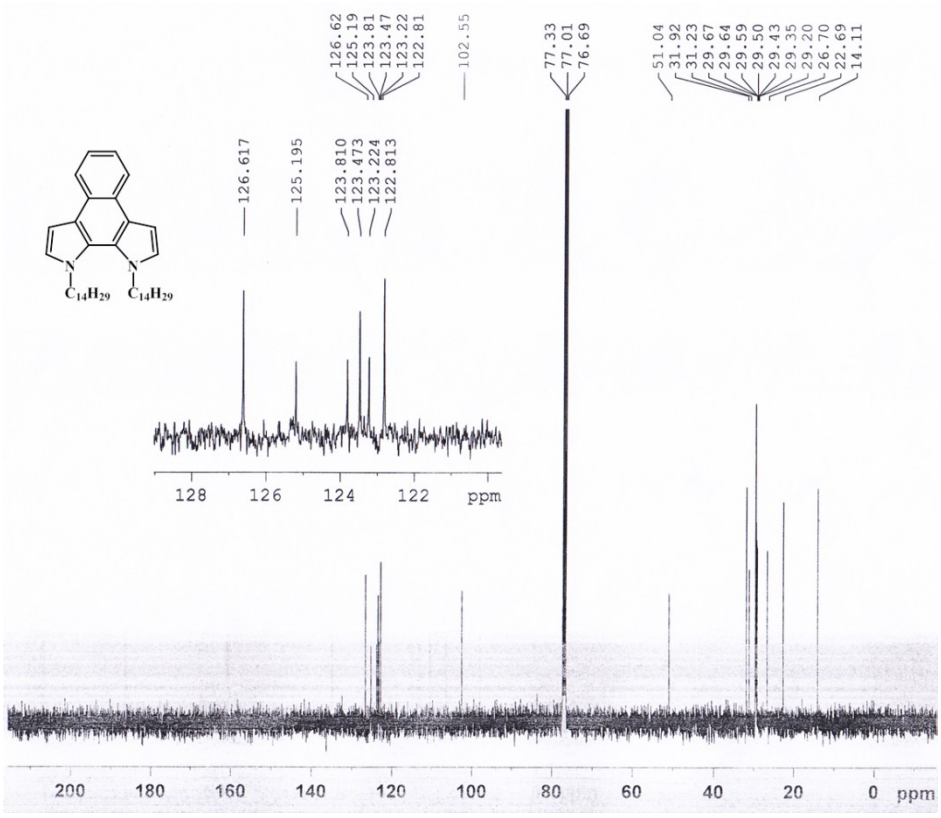

Figure 3.53 ^{13}C NMR spectrum of **DTNBP**

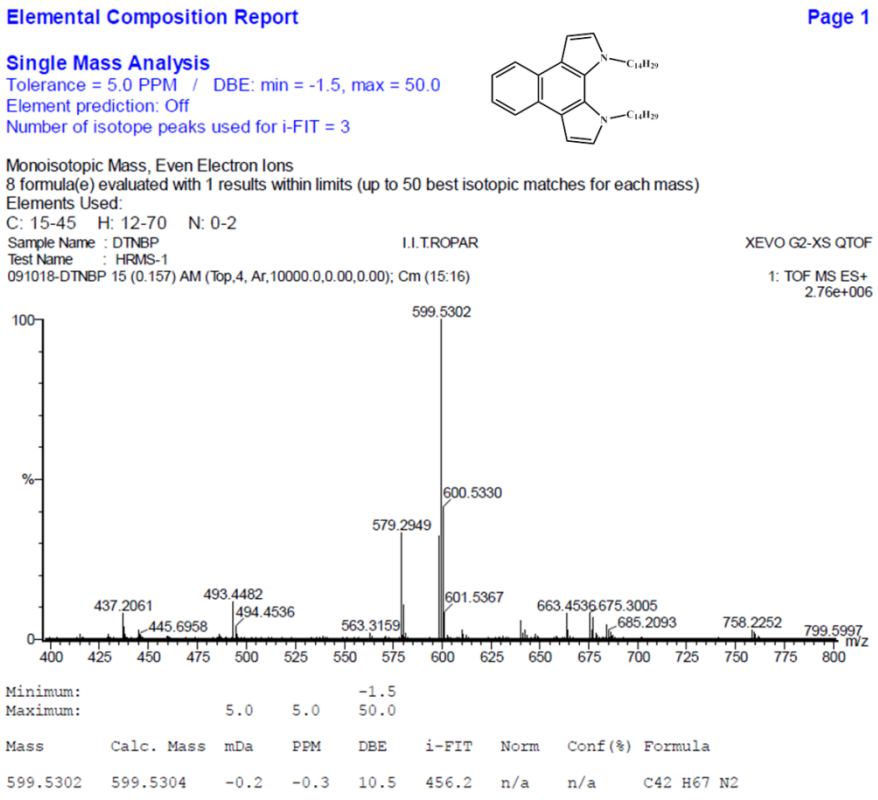

Figure 3.54 HRMS spectrum of **DTNBP**

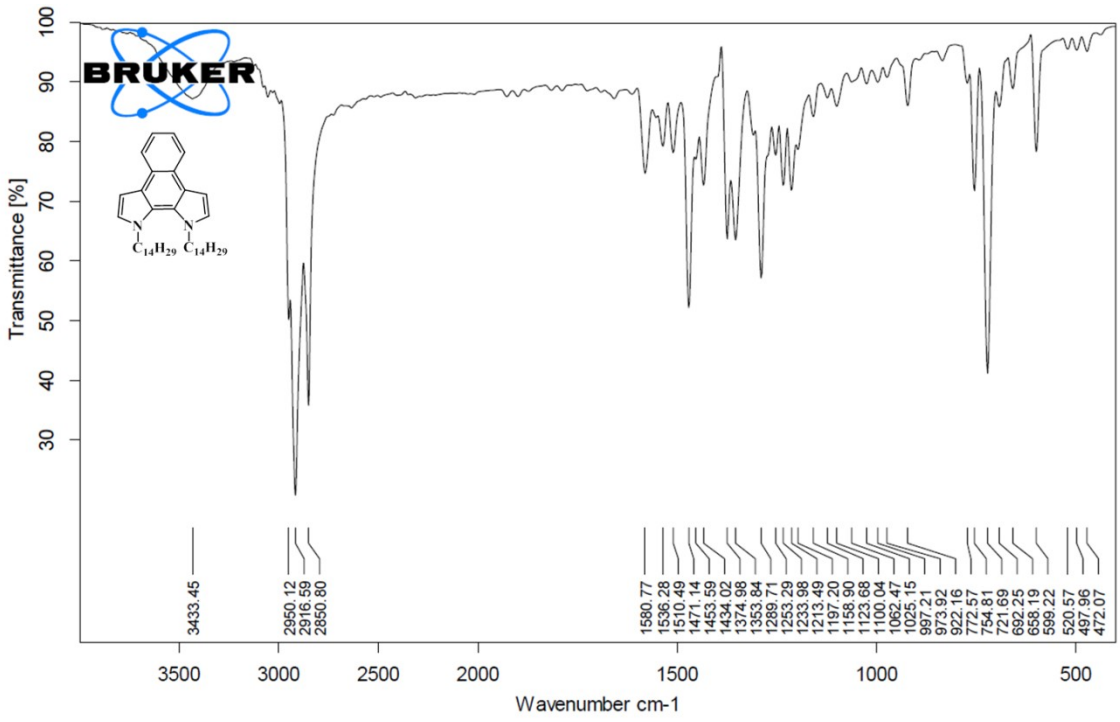

Figure 3.55 IR spectrum (KBr pellet) of **DTNBP**

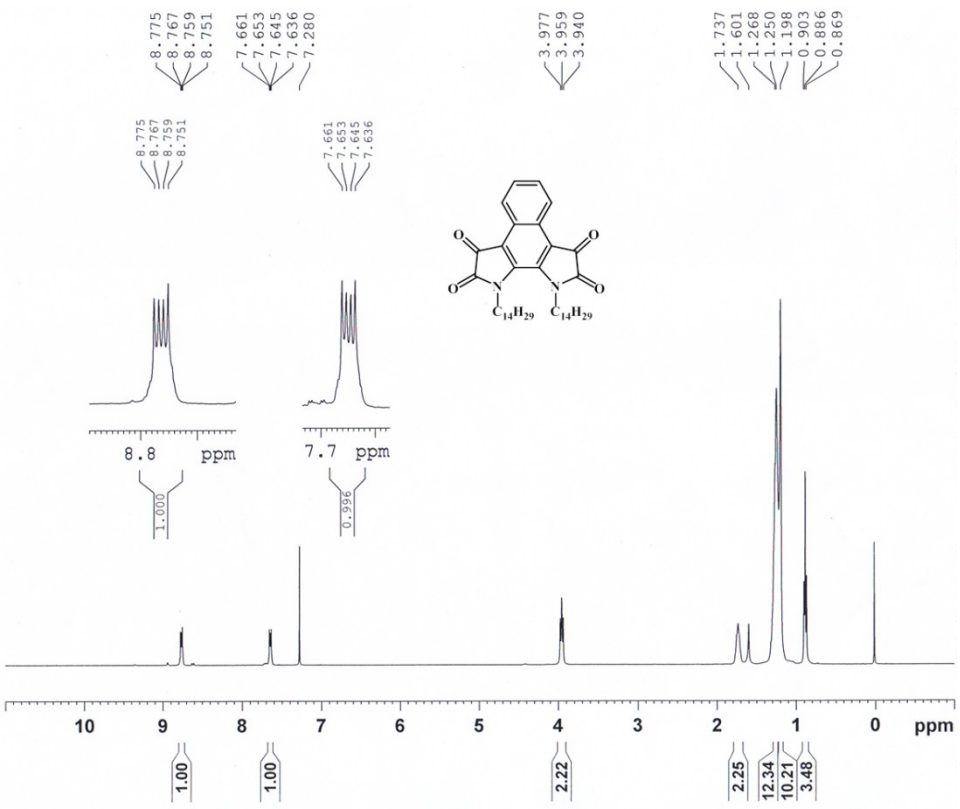

Figure 3.56 ^{1}H NMR spectrum of **DTNBP-BIs**

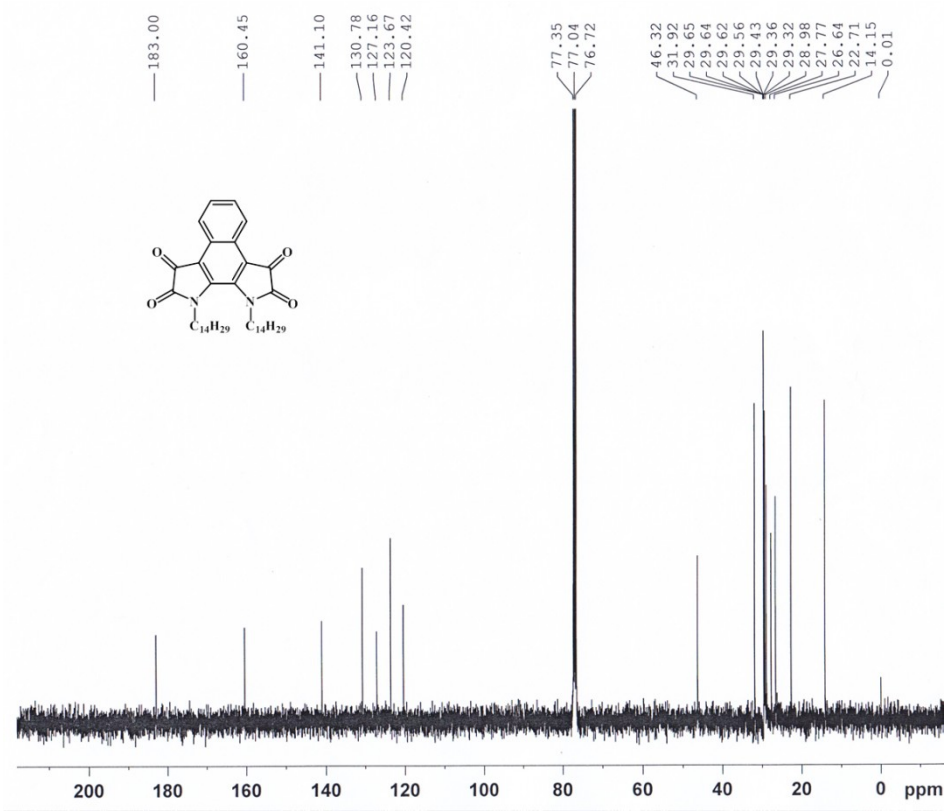

Figure 3.57 ^{13}C NMR spectrum of **DTNBP-BIs**

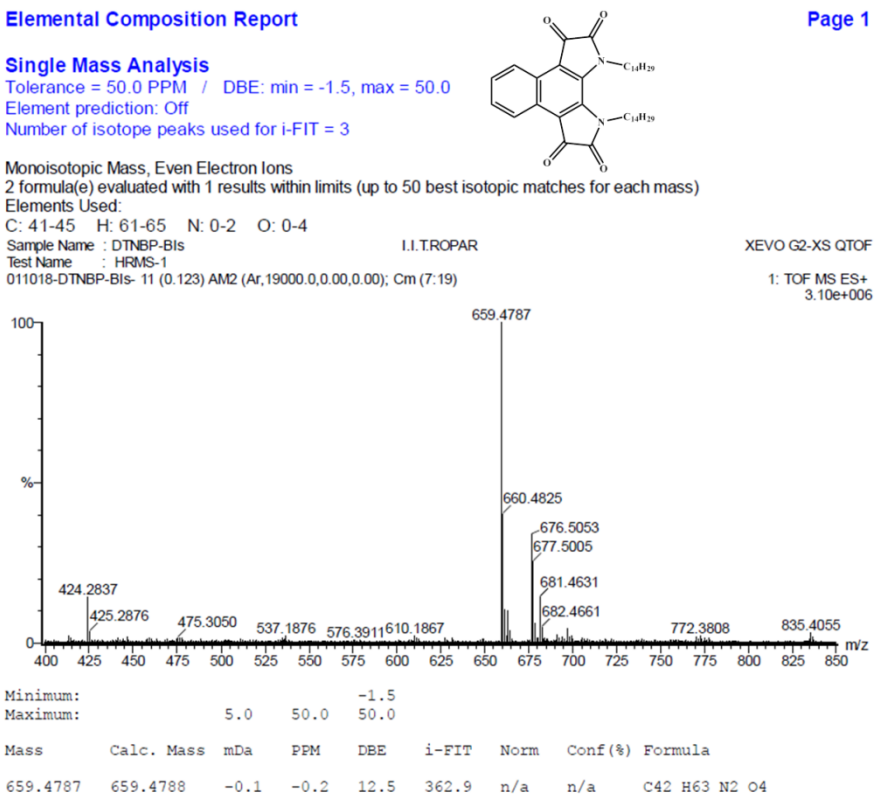

Figure 3.58 HRMS spectrum of **DTNBP-BIs**

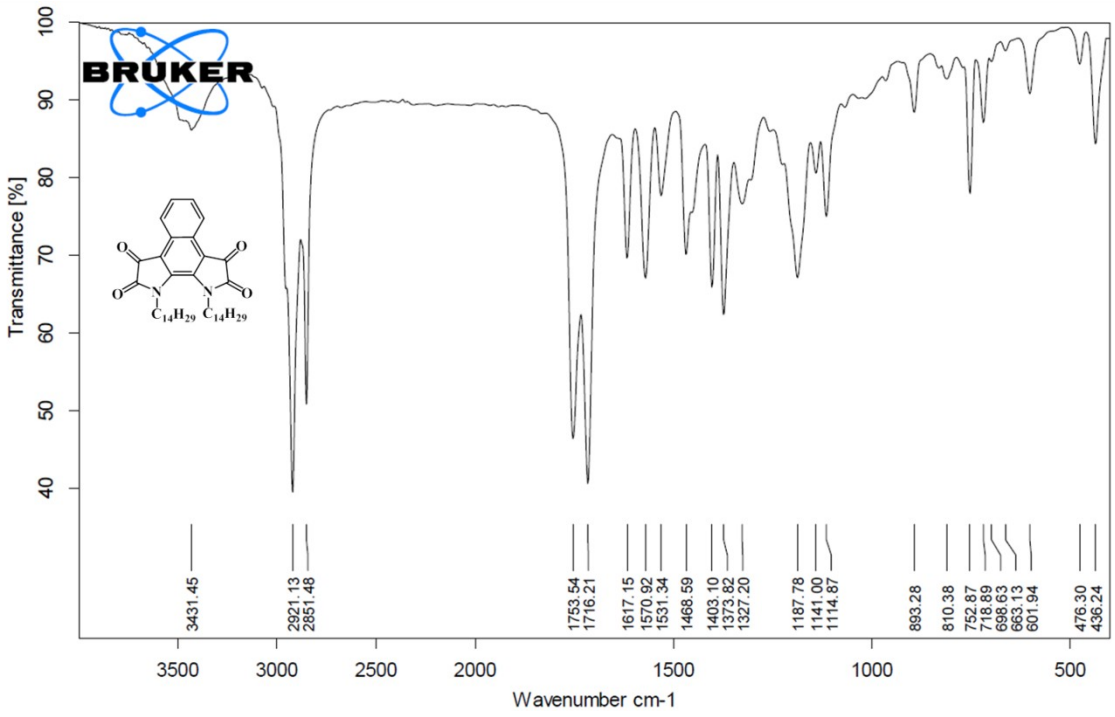

Figure 3.59 IR spectrum (KBr pellet) of **DTNBP-BIs**

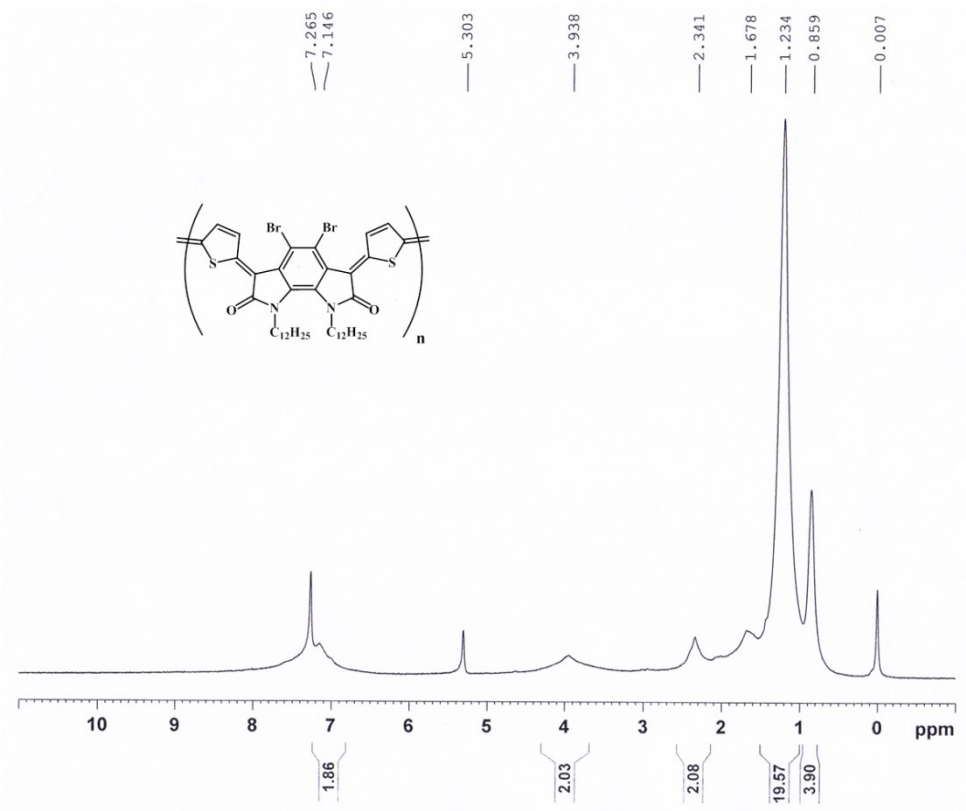

Figure 3.60 ^{1}H NMR spectrum of **DBr-BDP-INDPH**

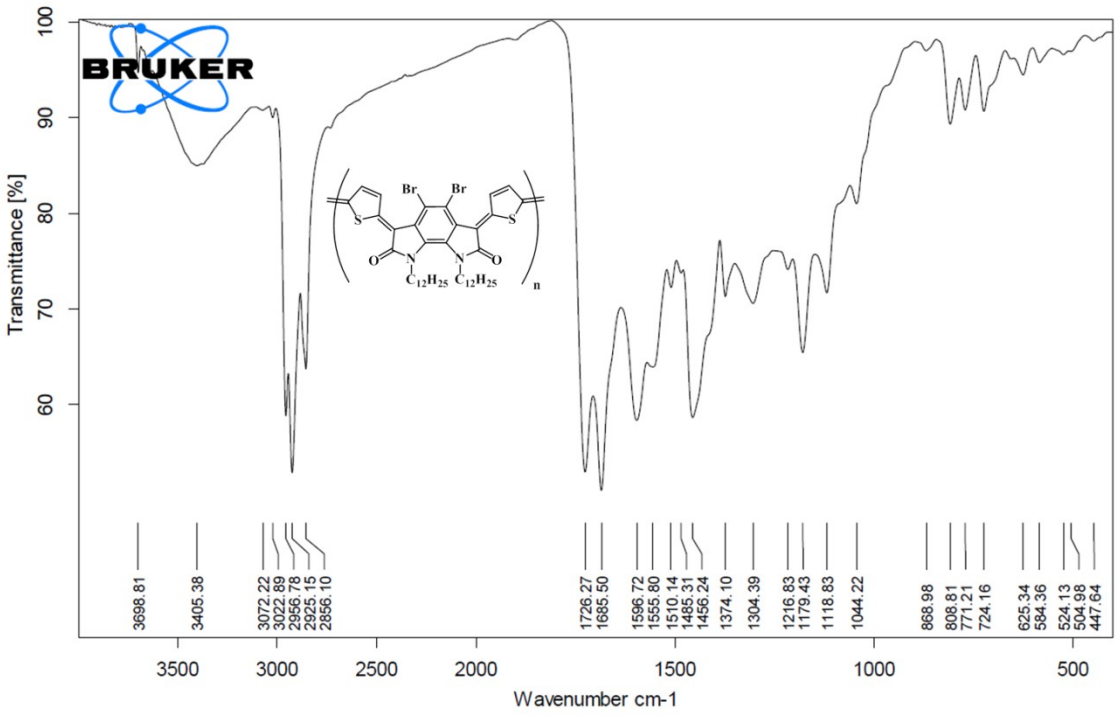

Figure 3.61 IR spectrum (KBr pellet) of **DBr-BDP-INDPH**

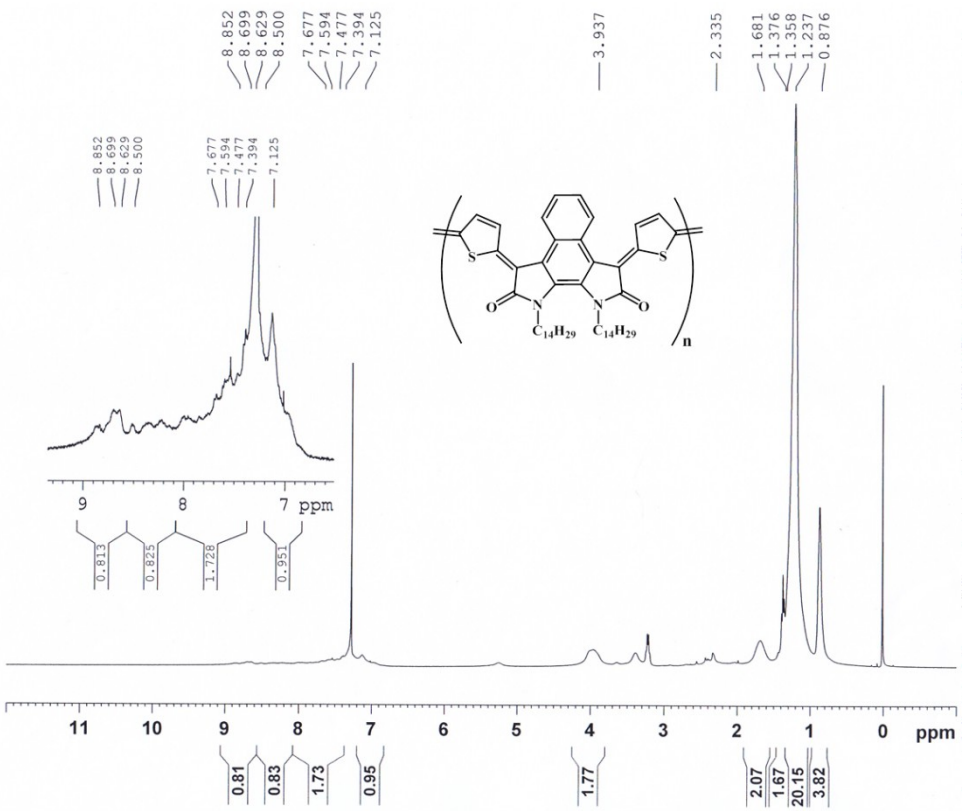

Figure 3.62 ^{1}H NMR spectrum of **NBP-INDPH**

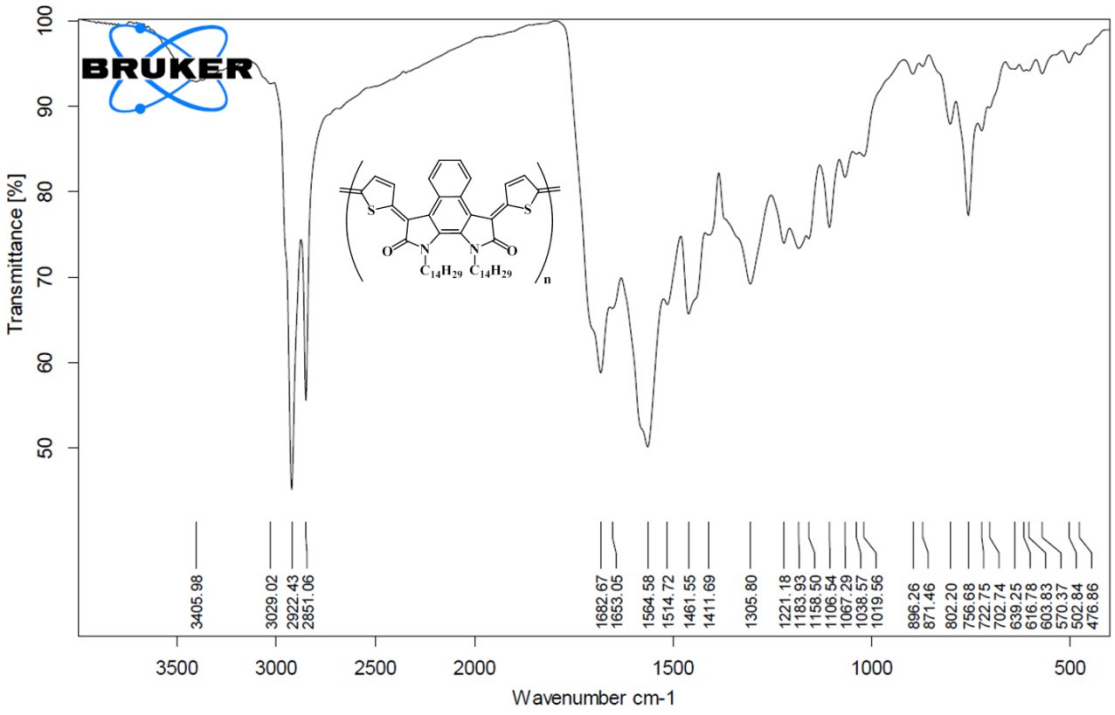

Figure 3.63 IR spectrum (KBr pellet) of **NBP-INDPH**

Agilent GPC/SEC Software
MS University GPC Report

Agilent Technologies

Distribution Plot

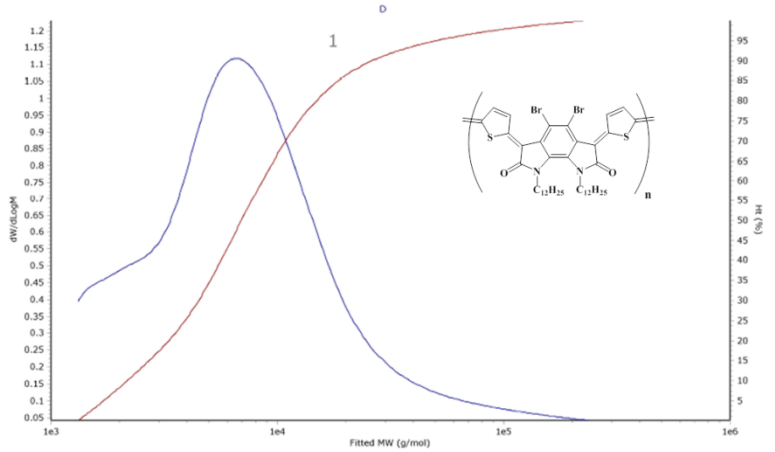

Results

Analysed by
Comments

Applied Chem at 17:06:15 on 05 June 2018

Molecular Weight Averages

Peak	Mp (g/mol)	Mn (g/mol)	Mw (g/mol)	Mz (g/mol)	Mz+1 (g/mol)	Mv (g/mol)	PD
Peak 1	6773	5066	13973	59383	130276	49711	2.758

Figure 3.64 GPC analysis report of BDP-based indophenine polymer **DBr-BDP-INDPH**

Agilent GPC/SEC Software
MS University GPC Report

Agilent Technologies

Distribution Plot

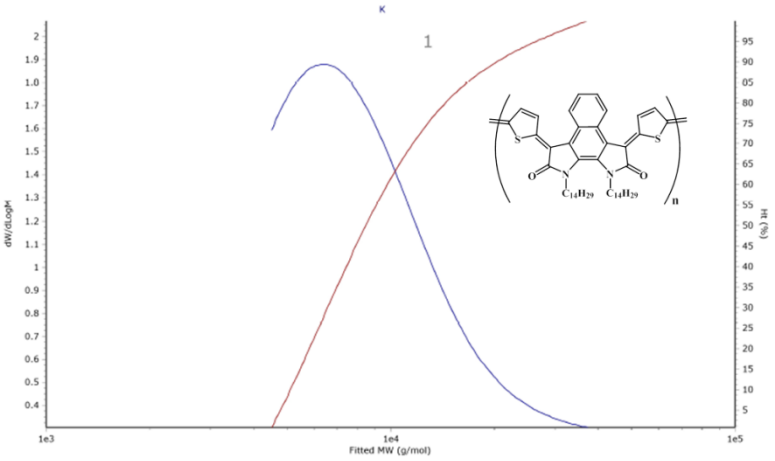

Results

Analysed by
Comments

Applied Chem at 17:11:30 on 05 June 2018

Molecular Weight Averages

Peak	Mp (g/mol)	Mn (g/mol)	Mw (g/mol)	Mz (g/mol)	Mz+1 (g/mol)	Mv (g/mol)	PD
Peak 1	6561	8300	10819	15034	20254	14307	1.303

Figure 3.65 GPC analysis report of NBP-based indophenine polymer **NBP-INDPH**

References

1 R. A. Street, *Adv. Mater.*, 2009, **21**, 2007–2022.

2 J. Mei, Y. Diao, A. L. Appleton, L. Fang and Z. Bao, *J. Am. Chem. Soc.*, 2013, **135**, 6724–6746.

3 D. Venkateshvaran, M. Nikolka, A. Sadhanala, V. Lemaur, M. Zelazny, M. Kepa, M. Hurhangee, A. J. Kronemeijer, V. Pecunia, I. Nasrallah, I. Romanov, K. Broch, I. McCulloch, D. Emin, Y. Olivier, J. Cornil, D. Beljonne and H. Sirringhaus, *Nature*, 2014, **515**, 384–388.

4 G. Horowitz, *Adv. Mater.*, 1999, **10**, 365–377.

5 C. D. Dimitrakopoulos and P. R. L. Malenfant, *Adv. Mater.*, 2002, **14**, 99–117.

6 H. Sirringhaus, *Adv. Mater.*, 2014, **26**, 1319–1335.

7 K. Fukuda, Y. Takeda, Y. Yoshimura, R. Shiwaku, L. T. Tran, T. Sekine, M. Mizukami, D. Kumaki and S. Tokito, *Nat. Commun.*, 2014, **5**, 4147.

8 M. Kaltenbrunner, T. Sekitani, J. Reeder, T. Yokota, K. Kuribara, T. Tokuhara, M. Drack, R. Schwödiauer, I. Graz, S. Bauer-Gogonea, S. Bauer and T. Someya, *Nature*, 2013, **499**, 458–463.

9 T. Sekitani, U. Zschieschang, H. Klauk and T. Someya, *Nat. Mater.*, 2010, **9**, 1015–1022.

10 K. Myny, S. Steudel, S. Smout, P. Vicca, F. Furthner, B. van der Putten, A. K. Tripathi, G. H. Gelinck, J. Genoe, W. Dehaene and P. Heremans, *Org. Electron.*, 2010, **11**, 1176–1179.

11 M. E. Roberts, S. C. B. Mannsfeld, N. Queraltó, C. Reese, J. Locklin, W. Knoll and Z. Bao, *Proc. Natl. Acad. Sci.*, 2008, **105**, 12134 LP-12139.

12 H. T. Nicolai, M. Kuik, G. A. H. Wetzelaer, B. de Boer, C. Campbell, C. Risko, J. L. Brédas and P. W. M. Blom, *Nat. Mater.*, 2012, **11**, 882–887.

13 S. B. and R. R. and U. Z. and M. J. K. and K. T. and H. K. and S. P. Tiwari, *Semicond. Sci. Technol.*, 2016, **31**, 25011.

14 S. Holliday, J. E. Donaghey and I. McCulloch, *Chem. Mater.*, 2014, **26**, 647–663.

15 X. Guo, A. Facchetti and T. J. Marks, *Chem. Rev.*, 2014, **114**, 8943–9021.

16 C. B. Nielsen, M. Turbiez and I. McCulloch, *Adv. Mater.*, 2012, **25**, 1859–1880.

17 B. S. Ong, Y. Wu, Y. Li, P. Liu and H. Pan, *Chem. – A Eur. J.*, 2008, **14**, 4766–4778.

18 J. Takeya, M. Yamagishi, Y. Tominari, R. Hirahara, Y. Nakazawa, T. Nishikawa, T. Kawase, T. Shimoda and S. Ogawa, *Appl. Phys. Lett.*, 2007, **90**, 102120.

19 J. Liu, H. Zhang, H. Dong, L. Meng, L. Jiang, L. Jiang, Y. Wang, J. Yu, Y. Sun, W. Hu and A. J. Heeger, *Nat. Commun.*, 2015, **6**, 10032.

20 Y. Yuan, G. Giri, A. L. Ayzner, A. P. Zoombelt, S. C. B. Mannsfeld, J. Chen, D. Nordlund, M. F. Toney, J. Huang and Z. Bao, *Nat. Commun.*, 2014, **5**, 3005.

21 C. Luo, A. K. K. Kyaw, L. A. Perez, S. Patel, M. Wang, B. Grimm, G. C. Bazan, E. J. Kramer and A. J. Heeger, *Nano Lett.*, 2014, **14**, 2764–2771.

22 J. Li, Y. Zhao, H. S. Tan, Y. Guo, C.-A. Di, G. Yu, Y. Liu, M. Lin, S. H. Lim, Y. Zhou, H. Su and B. S. Ong, *Sci. Rep.*, 2012, **2**, 754.

23 I. Kang, H.-J. Yun, D. S. Chung, S.-K. Kwon and Y.-H. Kim, *J. Am. Chem. Soc.*, 2013, **135**, 14896–14899.

24 G. Kim, S.-J. Kang, G. K. Dutta, Y.-K. Han, T. J. Shin, Y.-Y. Noh and C. Yang, *J. Am. Chem. Soc.*, 2014, **136**, 9477–9483.

25 Y.-Q. Zheng, T. Lei, J.-H. Dou, X. Xia, J.-Y. Wang, C.-J. Liu and J. Pei, *Adv. Mater.*, 2016, **28**, 7213–7219.

26 D. Zhang, L. Zhao, Y. Zhu, A. Li, C. He, H. Yu, Y. He, C. Yan, O. Goto and H. Meng, *ACS Appl. Mater. Interfaces*, 2016, **8**, 18277–18283.

27 W.-Y. Lee, J. H. Oh, S.-L. Suraru, W.-C. Chen, F. Würthner and Z. Bao, *Adv. Funct. Mater.*, 2011, **21**, 4173–4181.

28 X. Gao, C. Di, Y. Hu, X. Yang, H. Fan, F. Zhang, Y. Liu, H. Li and D. Zhu, *J. Am. Chem. Soc.*, 2010, **132**, 3697–3699.

29 Y. Fukutomi, M. Nakano, J.-Y. Hu, I. Osaka and K. Takimiya, *J. Am. Chem. Soc.*, 2013, **135**, 11445–11448.

30 H. Yan, Z. Chen, Y. Zheng, C. Newman, J. R. Quinn, F. Dotz, M. Kastler and A. Facchetti, *Nature*, 2009, **457**, 679–686.

31 X. Guo and M. D. Watson, *Org. Lett.*, 2008, **10**, 5333–5336.

32 R. Kim, P. S. K. Amegadze, I. Kang, H.-J. Yun, Y.-Y. Noh, S.-K. Kwon and Y.-H. Kim, *Adv. Funct. Mater.*, 2013, **23**, 5719–5727.

33 Z. Zhao, F. Zhang, Y. Hu, Z. Wang, B. Leng, X. Gao, C. Di and D. Zhu, *ACS Macro Lett.*, 2014, **3**, 1174–1177.

34 A. Lv, S. R. Puniredd, J. Zhang, Z. Li, H. Zhu, W. Jiang, H. Dong, Y. He, L. Jiang, Y. Li, W. Pisula, Q. Meng, W. Hu and Z. Wang, *Adv. Mater.*, 2012, **24**, 2626–2630.

35 W. Zhou, Y. Wen, L. Ma, Y. Liu and X. Zhan, *Macromolecules*, 2012, **45**, 4115–4121.

36 H. Li, F. S. Kim, G. Ren and S. A. Jenekhe, *J. Am. Chem. Soc.*, 2013, **135**, 14920–14923.

37 C. Di, J. Li, G. Yu, Y. Xiao, Y. Guo, Y. Liu, X. Qian and D. Zhu, *Org. Lett.*,

2008, **10**, 3025–3028.

38 G. Gruntz, H. Lee, L. Hirsch, F. Castet, T. Toupance, A. L. Briseno and Y. Nicolas, *Adv. Electron. Mater.*, 2015, **1**, 1500072.

39 S. Jung, M. Albariqi, G. Gruntz, T. Al-Hathal, A. Peinado, E. Garcia-Caurel, Y. Nicolas, T. Toupance, Y. Bonnassieux and G. Horowitz, *ACS Appl. Mater. Interfaces*, 2016, **8**, 14701–14708.

40 Y. Yamaguchi, Y. Maruya, H. Katagiri, K. Nakayama and Y. Ohba, *Org. Lett.*, 2012, **14**, 2316–2319.

41 Y. Yamaguchi, M. Takubo, K. Ogawa, K. Nakayama, T. Koganezawa and H. Katagiri, *J. Am. Chem. Soc.*, 2016, **138**, 11335–11343.

42 H. Xin, C. Ge, X. Yang, H. Gao, X. Yang and X. Gao, *Chem. Sci.*, 2016, **7**, 6701–6705.

43 Z. Yuan, B. Fu, S. Thomas, S. Zhang, G. DeLuca, R. Chang, L. Lopez, C. Fares, G. Zhang, J.-L. Bredas and E. Reichmanis, *Chem. Mater.*, 2016, **28**, 6045–6049.

44 B. Sun, W. Hong, Z. Yan, H. Aziz and Y. Li, *Adv. Mater.*, 2014, **26**, 2613,2636-2642.

45 Y. Li, B. Sun, P. Sonar and S. P. Singh, *Org. Electron.*, 2012, **13**, 1606–1613.

46 P. Sonar, S. P. Singh, Y. Li, M. S. Soh and A. Dodabalapur, *Adv. Mater.*, 2010, **22**, 5409–5413.

47 W. Hong, B. Sun, H. Aziz, W.-T. Park, Y.-Y. Noh and Y. Li, *Chem. Commun.*, 2012, **48**, 8413–8415.

48 S. Xu, N. Ai, J. Zheng, N. Zhao, Z. Lan, L. Wen, X. Wang, J. Pei and X. Wan, *RSC Adv.*, 2015, **5**, 8340–8344.

49 J.-H. Dou, Y.-Q. Zheng, Z.-F. Yao, Z.-A. Yu, T. Lei, X. Shen, X.-Y. Luo, J. Sun, S.-D. Zhang, Y.-F. Ding, G. Han, Y. Yi, J.-Y. Wang and J. Pei, *J. Am. Chem. Soc.*, 2015, **137**, 15947–15956.

50 T. Lei, J. H. Dou, Z. J. Ma, C. H. Yao, C. J. Liu, J. Y. Wang and J. Pei, *J. Am. Chem. Soc.*, 2012, **134**, 20025–20028.

51 J. Huang, Z. Mao, Z. Chen, D. Gao, C. Wei, W. Zhang and G. Yu, *Chem. Mater.*, 2016, **28**, 2209–2218.

52 X. Zhou, N. Ai, Z.-H. Guo, F.-D. Zhuang, Y.-S. Jiang, J.-Y. Wang and J. Pei, *Chem. Mater.*, 2015, **27**, 1815–1820.

53 C. Lu, H.-C. Chen, W.-T. Chuang, Y.-H. Hsu, W.-C. Chen and P.-T. Chou, *Chem. Mater.*, 2015, **27**, 6837–6847.

54 R. S. Ashraf, A. J. Kronemeijer, D. I. James, H. Sirringhaus and I. McCulloch, *Chem. Commun.*, 2012, **48**, 3939–3941.

55 W. Yue, R. S. Ashraf, C. B. Nielsen, E. Collado-Fregoso, M. R. Niazi, S. A.

Yousaf, M. Kirkus, H.-Y. Chen, A. Amassian, J. R. Durrant and I. McCulloch, *Adv. Mater.*, 2015, **27**, 4702–4707.

56 T. Lei, Y. Cao, Y. Fan, C.-J. Liu, S.-C. Yuan and J. Pei, *J. Am. Chem. Soc.*, 2011, **133**, 6099–6101.

57 Z. Yan, B. Sun and Y. Li, *Chem. Commun.*, 2013, **49**, 3790–3792.

58 W. Yue, M. Nikolka, M. Xiao, A. Sadhanala, C. B. Nielsen, A. J. P. White, H.-Y. Chen, A. Onwubiko, H. Sirringhaus and I. McCulloch, *J. Mater. Chem. C*, 2016, **4**, 9704–9710.

59 N. R. Krishnaswamy and C. N. Sundaresan, *Reson. Sci. Educ.*, 2012, **17**, 1022–1033.

60 R. Robinson, *J. Soc. Dye. Colour.*, 2018, **37**, 77–81.

61 J. Weinstein and G. M. Wyman, *J. Am. Chem. Soc.*, 1956, **78**, 2387–2390.

62 W. Lüttke and M. Klessinger, *Chem. Ber.*, 1964, **97**, 2342–2357.

63 M. Klessinger and W. Lüttke, *Chem. Ber.*, 1966, **99**, 2136–2145.

64 E. D. Głowacki, G. Voss, L. Leonat, M. Irimia-Vladu, S. Bauer and N. S. Sariciftci, *Isr. J. Chem.*, 2012, **52**, 540–551.

65 M. Irimia-Vladu, E. D. Głowacki, P. A. Troshin, G. Schwabegger, L. Leonat, D. K. Susarova, O. Krystal, M. Ullah, Y. Kanbur, M. A. Bodea, V. F. Razumov, H. Sitter, S. Bauer and N. S. Sariciftci, *Adv. Mater.*, 2011, **24**, 375–380.

66 E. D. Głowacki, L. Leonat, G. Voss, M.-A. Bodea, Z. Bozkurt, A. M. Ramil, M. Irimia-Vladu, S. Bauer and N. S. Sariciftci, *AIP Adv.*, 2011, **1**, 42132.

67 Y. Kanbur, M. Irimia-Vladu, E. D. Głowacki, G. Voss, M. Baumgartner, G. Schwabegger, L. Leonat, M. Ullah, H. Sarica, S. Erten-Ela, R. Schwödiauer, H. Sitter, Z. Küçükyavuz, S. Bauer and N. S. Sariciftci, *Org. Electron.*, 2012, **13**, 919–924.

68 C. Guo, B. Sun, J. Quinn, Z. Yan and Y. Li, *J. Mater. Chem. C*, 2014, **2**, 4289–4296.

69 C. Guo, J. Quinn, B. Sun and Y. Li, *J. Mater. Chem. C*, 2015, **3**, 5226–5232.

70 C. W. Greenhalgh, J. L. Carey and D. F. Newton, *Dye. Pigment.*, 1980, **1**, 103–120.

71 W. Cui, J. Yuen and F. Wudl, *Macromolecules*, 2011, **44**, 7869–7873.

72 W. Hong, C. Guo, Y. Li, Y. Zheng, C. Huang, S. Lu and A. Facchetti, *J. Mater. Chem.*, 2012, **22**, 22282–22289.

73 P. Deng, L. Liu, S. Ren, H. Li and Q. Zhang, *Chem. Commun.*, 2012, **48**, 6960–6962.

74 M. Miller, W. Tsang, A. Merritt and D. J. Procter, *Chem. Commun.*, 2007, 498–

500.

75 M. Miller, J. C. Vogel, W. Tsang, A. Merrit and D. J. Procter, *Org. Biomol. Chem.*, 2009, **7**, 589–597.

76 J. W. Rumer, M. Levick, S.-Y. Dai, S. Rossbauer, Z. Huang, L. Biniek, T. D. Anthopoulos, J. R. Durrant, D. J. Procter and I. McCulloch, *Chem. Commun.*, 2013, **49**, 4465–4467.

77 W. Cui and F. Wudl, *Macromolecules*, 2013, **46**, 7232.

78 J. W. Rumer, S.-Y. Dai, M. Levick, L. Biniek, D. J. Procter and I. McCulloch, *J. Polym. Sci. Part A Polym. Chem.*, 2012, **51**, 1285–1291.

79 J. W. Rumer, S.-Y. Dai, M. Levick, Y. Kim, M.-B. Madec, R. S. Ashraf, Z. Huang, S. Rossbauer, B. Schroeder, L. Biniek, S. E. Watkins, T. D. Anthopoulos, R. A. J. Janssen, J. R. Durrant, D. J. Procter and I. McCulloch, *J. Mater. Chem. C*, 2013, **1**, 2711–2716.

80 S. Kola, J. Sinha and H. E. Katz, *J. Polym. Sci. Part B Polym. Phys.*, 2012, **50**, 1090–1120.

81 C. Wang, H. Dong, W. Hu, Y. Liu and D. Zhu, *Chem. Rev.*, 2012, **112**, 2208–2267.

82 D. E. Janzen, M. W. Burand, P. C. Ewbank, T. M. Pappenfus, H. Higuchi, D. A. da Silva Filho, V. G. Young, J.-L. Brédas and K. R. Mann, *J. Am. Chem. Soc.*, 2004, **126**, 15295–15308.

83 J. Casado, T. M. Pappenfus, K. R. Mann, E. Ortí, P. M. Viruela, B. Milián, V. Hernández and J. T. López Navarrete, *ChemPhysChem*, 2004, **5**, 529–539.

84 J. L. Brédas, *J. Chem. Phys.*, 1985, **82**, 3808–3811.

85 Y.-J. Cheng, S.-H. Yang and C.-S. Hsu, *Chem. Rev.*, 2009, **109**, 5868–5923.

86 T. M. Pappenfus, R. J. Chesterfield, C. D. Frisbie, K. R. Mann, J. Casado, J. D. Raff and L. L. Miller, *J. Am. Chem. Soc.*, 2002, **124**, 4184–4185.

87 R. J. Chesterfield, C. R. Newman, T. M. Pappenfus, P. C. Ewbank, M. H. Haukaas, K. R. Mann, L. L. Miller and C. D. Frisbie, *Adv. Mater.*, 2003, **15**, 1278–1282.

88 S. Handa, E. Miyazaki, K. Takimiya and Y. Kunugi, *J. Am. Chem. Soc.*, 2007, **129**, 11684–11685.

89 C. Zhang, Y. Zang, E. Gann, C. R. McNeill, X. Zhu, C. Di and D. Zhu, *J. Am. Chem. Soc.*, 2014, **136**, 16176–16184.

90 Q. Wu, R. Li, W. Hong, H. Li, X. Gao and D. Zhu, *Chem. Mater.*, 2011, **23**, 3138–3140.

91 Y. Xiong, J. Tao, R. Wang, X. Qiao, X. Yang, D. Wang, H. Wu and H. Li, *Adv. Mater.*, 2016, **28**, 5949–5953.

92 H. D. Hartough and S. L. Meisel, Eds., in *Chemistry of Heterocyclic Compounds*, INTERSCIENCE PUBLISHERS, INC., Newyork, 2008, p. p-206.

93 A. Baeyer, *Berichte der Dtsch. Chem. Gesellschaft*, 1879, **12**, 1309–1319.

94 H. Hwang, D. Khim, J. M. Yun, E. Jung, S. Y. Jang, Y. H. Jang, Y. Y. Noh and D. Y. Kim, *Adv. Funct. Mater.*, 2015, **25**, 1146–1156.

95 N. M. Randell, P. C. Boutin and T. L. Kelly, *J. Mater. Chem. A*, 2016, **4**, 6940–6945.

96 G. Kossmehl and G. Menecke, *Die Makromol. Chemie*, 1975, **176**, 333–340.

97 A. Onwubiko, W. Yue, C. Jellett, M. Xiao, H. Y. Chen, M. K. Ravva, D. A. Hanifi, A. C. Knall, B. Purushothaman, M. Nikolka, J. C. Flores, A. Salleo, J. L. Bredas, H. Sirringhaus, P. Hayoz and I. McCulloch, *Nat. Commun.*, 2018, **9**, 416:1-9.

98 Y. Jiang, Y. Gao, H. Tian, J. Ding, D. Yan, Y. Geng and F. Wang, *Macromolecules*, 2016, **49**, 2135–2144.

99 G. V Tormos, K. A. Belmore and M. P. Cava, *J. Am. Chem. Soc.*, 1993, **115**, 11512–11515.

100 Z. J. Allan, *Collect. Czechoslov. Chem. Commun.*, 1953, **18**, 231–242.

101 R. Sriram, C. N. S. S. Pavan Kumar, N. Raghunandan, V. Ramesh, M. Sarangapani and V. Jayathirtha Rao, *Synth. Commun.*, 2012, **42**, 3419–3428.

102 C. N. S. S. Pavan Kumar, C. L. Devi, V. Jayathirtha Rao and S. Palaniappan, *synlett*, 2008, **13**, 2023–2027.

103 S. Messaoudi, M. Sancelme, V. Polard-housset, B. Aboab, P. Moreau and M. Prudhomme, *Eur. J. Med. Chem.*, 2004, **39**, 453–458.

104 M. Sassatelli, F. Bouchikhi, S. Messaoudi, F. Anizon, E. Debiton, C. Barthomeuf, M. Prudhomme and P. Moreau, *Eur. J. Med. Chem.*, 2006, **41**, 88–100.

105 Y. Zi, Z. Cai, S. Wang and S. Ji, *Org. Lett.*, 2014, **16**, 3094–3097.

106 J. S. Yadav, B. V. S. Reddy, C. S. Reddy and A. D. Krishna, *Tetrahedron Lett.*, 2007, **48**, 2029–2032.

107 J. Parrick, A. Yahya, A. S. Ijaz and J. Yizun, *J. Chem. Soc., Perkin Trans. 1*, 1989, **0**, 2009–2015.

108 J. Parrick, A. Yahya and Y. Jin, *Tetrahedron Lett.*, 1984, **25**, 3099–3100.

109 D. N. Do Amaral, F. R. De Sá Alves, E. J. Barreiro, S. A. Laufer and L. M. Lima, *J. Braz. Chem. Soc.*, 2017, **28**, 1874–1878.

110 H. O. Stumpf, Y. Pei, O. Kahn, J. Sletten and J. P. Renard, *J. Am. Chem. Soc.*, 1993, **115**, 6738–6745.

111 G. P. Souza, C. Konzen, T. R. G. Simões, B. L. Rodrigues, A. F. C. Alcântara and H. O. Stumpf, *J. Mol. Struct.*, 2012, **1016**, 13–21.

112 F. A. S. Alasmari, N. A. Aljaber and M. M. S. Korrah, *Int. J. Adv. Res. Chem. Sci.*, 2015, **2**, 14–23.

113 J. M. W. Chan, J. R. Tischler, S. E. Kooi, V. Bulovic and T. M. Swager, *J. Am. Chem. Soc.*, 2009, **131**, 5659–5666.